Benemérita Universidad Autónoma de Puebla
Facultad de Ciencias Físico-Matemáticas

Anomalous couplings in the Standard Model and beyond at the LHC

Tesis presentada al

Posgrado en Física

para obtener el título de

Doctorado en Ciencias (Física Aplicada)

presenta

Alan Ignacio Hernández Juárez

asesorado por

Gilberto Tavares Velasco

Agustín Moyotl Acuahuitl

Puebla, Pue.
Diciembre 2021

Anomalous couplings in the Standard Model and beyond at the LHC

Tesis

Alan Ignacio Hernández Juárez

Gilberto Tavares Velasco

Agustín Moyotl Acuahuitl

Título: Anomalous couplings in the Standard Model and beyond at the LHC.

Estudiante: Alan Ignacio Hernández Juárez

COMITÉ

Dr. J. Jesús Toscano Chávez
Presidente

Dr. Héctor Novales Sánchez
Secretario

Dr. Arturo Fernández Téllez
Vocal

Dr. Ricardo Gaitán Lozano
Vocal externo

Dr. Pablo Roig Garcés
Vocal externo

Dr. Ricardo Sánchez Vélez
Suplente

Dr. Agustín Moyotl Acuahuitl
Co-asesor

Dr. Gilberto Tavares Velasco
Asesor

Publications related to this thesis

Refereed publications:

- A.I Hernández-Juárez, A. Moyotl, G. Tavares-Velasco, *New estimate of the chromomagnetic dipole moment of quarks in the standard model*, Eur. Phys. JPlus 136 (2021) 2, 262, arXiv:2009.11955 [hep-ph].
- A.I Hernández-Juárez, A. Moyotl, G. Tavares-Velasco, *Contributions to ZZV^* ($V = \gamma$, Z, Z') couplings from CP violating flavor changing couplings*, Eur. Phys. J. C 81 (2021) 4, 304, arXiv:2102.02197 [hep-ph].
- A.I Hernández-Juárez, A. Moyotl, G. Tavares-Velasco, *Cromomagnetic and Chromoelectric dipole moments of quarks in the reduced 331 model*, Chinese Phys. C 45 113101, arXiv:2012.09883 [hep-ph].

Preprints:

- A.I Hernández-Juárez, A. Moyotl, G. Tavares-Velasco, *Bounds on the absortpive parts of the chromomagnetic and chromoelectric dipole moments of the top quark from LHC data*, arXiv:2109.09978 [hep-ph].

Can't you hear it calling?
Everybody's dancing
Tonight everything is over
I feel too young

Para mi abuelo Vicente, la persona más extraordinaria que he conocido. Te voy a extrañar toda la vida.

Gracias

A mis padres Juanita y Nacho, todo lo que soy se lo debo a ellos. Gracias por su amor y apoyo en este camino que llega a su fin, este logro no hubiera sido posible sin ustedes. Los amo.

A mis hermanos, Caro, Ángel y Luis, mis compañeros de toda la vida. Gracias por su apoyo, siempre vamos a estar juntos.

A mis abuelos Vicente y Sofía, gracias por su amor infinito y todas las enseñanzas. Ojalá fueran eternos.

A mi familia, tíos y primos que han sido compañeros en este largo viaje. Siempre los llevo presentes.

A Gabriela, gracias por tu apoyo y por hacer muy divertido estos últimos meses de trabajo. Hiciste mejor el final de este viaje.

A mi amigo y asesor el Dr. Gilberto Tavares, gracias por su paciencia y enseñanzas en estos 8 años. Mejor padre académico no me pudo haber tocado, espero ser algún día tan GRAN-de como usted.

A mi asesor el Dr. Agustín, gracias por sus enseñanzas y consejos en esas tardes de viernes en Cholula y Puebla. Su apoyo fue fundamental para este logro.

A mis amigos de la Tropa y el equipo sangría en todas sus versiones, todas esos días de diversión fueron importantes para mantenerme cuerdo estos últimos 6 años.

Contents

Abstract

This work is divided in four parts. In chapter one a new estimate of the one loop contributions of the standard model to the chromomagnetic dipole moment (CMDM) $\hat{\mu}_q(q^2)$ of quarks is presented with the aim to address a few disagreements arising in previous calculations. The most general case with arbitrary q^2 is considered and analytical results are obtained in terms of Feynman parameter integrals and Passarino-Veltman scalar functions, which are then expressed in terms of closed form functions when possible. It is found that while the QCD contribution to the static CMDM ($q^2 = 0$) is infrared divergent, which agrees with previous evaluations and stems from the fact that this quantity has no sense in perturbative QCD, the off-shell CMDM ($q^2 \neq 0$) is finite and gauge independent, which is verified by performing the calculation for arbitrary gauge parameter ξ via both a renormalizable linear R_ξ gauge and the background field method. It is thus argued that the off-shell $\hat{\mu}_q(q^2)$ can represent a valid observable quantity. For the numerical analysis we consider the region 30 GeV$< \|q\| <$ 1000 GeV and analyze the behavior of $\hat{\mu}_q(q^2)$ for all the standard model quarks. It is found that the CMDM of light quarks is considerably smaller than that of the top quark as it is directly proportional to the quark mass. In the considered energy interval, both the real and imaginary parts of $\hat{\mu}_t(q^2)$ are of the order of $10^{-2} - 10^{-3}$, with the largest contribution arising from the QCD induced diagrams, though around the threshold $q^2 = 4m_t^2$ there are also important contributions from diagrams with Z gauge boson and Higgs boson exchange.

Further, in chapter two the effects of the absorptive (imaginary) parts of the top quark chromomagnetic $\hat{\mu}_t$ and chromoelectric $\hat{d}_t$ dipole moments on top quark production at the LHC are studied and the allowed area in the $\mathrm{Im}[\hat{\mu}_t] - \mathrm{Im}[\hat{d}_t]$ plane is obtained using the experimental data at $\sqrt{s} = 14$ TeV, with the limits on $\mathrm{Im}[\hat{\mu}_t]$ being of the order of $10^{-1} - 10^{-2}$, which are consistent with the standard model prediction. The most recent limits on the real parts of $\hat{\mu}_t$ and $\hat{d}_t$ reported by the CMS collaboration are then used to assess the potential impact of their corresponding imaginary parts on top quark production via the study of some kinematic distributions, but no significant deviation from the standard model at leading order contribution is observed.

In chapter three the one-loop contributions to the chromomagnetic dipole moment $\hat{\mu}_t(q^2)$ and electric dipole moment $\hat{d}_t(q^2)$ of the top quark are calculated within the reduced 331 model (RM331) for non-zero q^2. It is argued that the results are gauge independent and thus represent valid observable quantities. In the RM331 $\hat{\mu}_t(q^2)$ receives new contributions from two heavy gauge bosons Z' and $V^\pm$ and one neutral scalar boson h_2, along with a new contribution from the standard model Higgs boson via flavor changing neutral currents. The latter, which are also mediated by the Z' gauge boson and the scalar boson h_2, can give a non-vanishing $\hat{d}_t(q^2)$ provided that there is a CP-violating phase. The analytical results are presented in terms of both Feynman parameter integrals and Passarino-Veltman scalar functions, which are useful to cross-check the numerical results. Both $\hat{\mu}_t(q^2)$ and $\hat{d}_t(q^2)$ are numerically evaluated for parameter

values still allowed by the constraints from experimental data. It is found that the new one-loop contributions of the RM331 to the real (imaginary) part of $\hat{\mu}_t(q^2)$ are of the order of 10^{-5} (10^{-6}), which are at least three orders of magnitude smaller than the standard model prediction, but are larger than the predictions of other models of new physics. In the RM331 the dominant contribution arising from the $V^{\pm}$ gauge boson for $\|q\|$ in the 30-1000 GeV interval and a mass m_V of the order of a few hundreds of GeVs. As for $\hat{d}_t(q^2)$, it receives its largest contribution from h_2 exchange and can reach values of the order of 10^{-19}, which is smaller than the contributions predicted by other standard model extensions.

And finally, in chapter four the one-loop contributions to the trilinear neutral gauge boson couplings ZZV^* ($V = \gamma, Z, Z'$), parametrized in terms of one CP-conserving f_5^V and one CP-violating f_4^V form factors, are calculated in models with CP-violating flavor changing neutral current couplings mediated by the Z gauge boson and an extra neutral gauge boson Z'. Analytical results are presented in terms of Passarino-Veltman scalar functions. Constraints on the vector and axial couplings of the Z gauge boson $\left|g_{VZ}^{tu}\right| < 0.0096$ and $\left|g_{VZ}^{tc}\right| < 0.011$ are obtained from the current experimental data on the $t \to Zq$ decays. It is found that in the case of the $ZZ\gamma^*$ vertex the only non-vanishing form factor is f_5^{γ}, which can be of the order of 10^{-3}, whereas for the ZZZ^* vertex both form factors f_5^Z and f_4^Z are non-vanishing and can be of the order of 10^{-6} and 10^{-5}, respectively. Our estimates for f_5^{γ} and f_5^Z are smaller than those predicted by the standard model, where f_4^Z is absent up to the one loop level. We also estimate the ZZZ'^* form factors arising from both diagonal and non-diagonal Z' couplings within a few extension models. It is found that in the diagonal case $f_5^{Z'}$ is the only non-vanishing form factor and its real and imaginary parts can be of the order of $10^{-1} - 10^{-2}$ and $10^{-2} - 10^{-3}$, respectively, with the dominant contributions arising from the light quarks and leptons. In the non-diagonal case $f_5^{Z'}$ can be of the order of 10^{-4}, whereas $f_4^{Z'}$ can reach values as large as $10^{-7} - 10^{-8}$, with the largest contributions arising from the $Z'tq$ couplings.

Chapter 1

Chromomagnetic dipole moment of quarks in the standard model

The anomalous magnetic dipole moment (MDM) of fermions has been a fertile field of study, giving rise to a plethora of theoretical work within the context of the standard model (SM) [1, 2, 3, 4], as well as beyond the SM (BSM) theories [5]. Furthermore, the fermion electric dipole moment (EDM) has also been analyzed in several models [6, 7, 8, 9, 10, 11, 12]. More recently, the calculation of radiative corrections to the gluon-quark-quark $\bar{q}qg$ vertex has also become a topic of considerable interest. Radiative corrections to the $\bar{t}tg$ coupling are expected to be considerably larger than those of lighter quarks due to the large top quark mass [13]. In particular the top quark chromomagnetic dipole moment (CMDM) and chromoelectric dipole moment (CEDM) have been studied within the framework of the SM [14], two-Higgs doublet models (THDMs) [15], the four-generation THDM (4GTHDM) [13], little Higgs models [16, 17], the minimal supersymmetric standard model (MSSM) [18], unparticle model [19], vector like multiplet models [20], etc.

The anomalous $\bar{q}qg$ coupling can be written as

$$\mathscr{L} = \frac{g_s}{2}\bar{q}T^a\sigma_{\mu\nu}\left(\frac{a_q}{2m_q} + id_q\gamma^5\right)qG_a^{\mu\nu}, \tag{1.1}$$

where a_q and d_q are the CMDM and CEDM, respectively, whereas $G_a^{\mu\nu}$ is the gluon field strength tensor and T^a are the $SU(3)$ color generators. The CMDM and CEDM are usually defined in the literature as dimensionless parameters [21]

$$\begin{aligned}\hat{\mu}_q &\equiv \frac{m_q}{g_s}\widetilde{\mu}_q,\\ \hat{d}_q &\equiv \frac{m_q}{g_s}\widetilde{d}_q,\end{aligned} \tag{1.2}$$

where $\hat{\mu}_q = a_q/2$ and $\hat{d}_q = m_q d_q$.

In the SM, the CMDM is induced at the one-loop level or higher orders via electroweak (EW) and QCD contributions. On the other hand, the CEDM is induced up to the three-loop level [22, 23] since all the partial contributions exactly cancel out at the two-loop level [24]. The lowest order SM contributions to the CMDM of the top quark have been studied in [14] and more recently in [25, 26]. However, there are some disagreement between those calculations (see

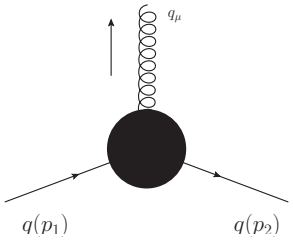

Figure 1.1: Notation for the quark-gluon vertex.

section 2.1 of [25] and section 3.D of [26]). In particular, authors of Ref. [14] only focus on the static CMDM, which they claim it receives an infrared finite QCD contribution, whereas authors of Ref. [25] argue that the on-shell CMDM ($q^2 = 0$) has no sense in perturbative QCD as this contribution diverge, so they consider the off-shell CMDM ($q^2 \neq 0$). Even more, the analytical results presented in [14], [25] and [26] disagree.

In the experimental side, the advent of the LHC has triggered the interest on the anomalous $\bar{t}tg$ couplings, which have become an important area of study in experimental particle physics. Searches for any deviation to the SM $\bar{t}t$ production has made it possible to set constraints on the top quark CMDM and CEDM, which are regularly improved [27, 21, 28]. In fact, the current upper bounds have been enhanced by one order of magnitude as compared to the previous ones [21]. Hopefully, more tight constraints on these top quark properties, closer to the SM predictions, would be achieved in the future, and thus a more precise and unambiguous prediction of the SM contributions to the top quark CMDM is mandatory. Also, since contributions to the CMDM in extension theories could give rise to a sizeable enhancement, a precise determination of such contributions is in order.

In this chapter we present a new calculation of the SM one-loop contributions to the quark CMDM, which is aimed to address some ambiguities of previous results. Our calculation is done via both a renormalizable linear R_ξ gauge and the background field method (BFM), which allows one to verify that the off-shell CMDM of a quark is gauge independent, which in turn is a necessary condition for a valid observable quantity. The rest of the chapter is organized as follows. In Sec. 1.1, we present the main steps of the analytical calculation, stressing any disagreement with previous results. The corresponding loop functions are presented in terms of Feynman parameter integrals, Passarino-Veltman scalar functions and closed form results in A.1, which may be useful for a numerical cross-check. In Sec. 1.2, we present a numerical analysis and discussion of the behavior of the CMDM of SM quarks, with emphasis on the top quark one. The conclusions of this chapter are presented in Sec. 1.3.

1.1 Analytical results

1.1.1 Quark-gluon vertex function

For off-shell quarks and gluon, the most general CP conserving quark-gluon vertex function can be cast as [29]

$$\Gamma^a_\mu = g_s T^a \Gamma_\mu = g_s T^a (\Gamma^L_\mu + \Gamma^T_\mu), \tag{1.3}$$

where the longitudinal Γ^L_μ (transverse Γ^T_μ) vertex function can be decomposed into four (eight) independent form factors λ_i (τ_i), which depend on q^2, p_1^2 and p_2^2, where we follow the notation

of Fig. 1.1. When $p_1^2 = p_2^2$, only the following linear independent terms survive:

$$\Gamma^{L\mu} = \lambda_1 \gamma^\mu + \lambda_2 p^\mu \not{p} + \lambda_3 p^\mu, \tag{1.4}$$

and

$$\begin{aligned}\Gamma^{T\mu} =& \tau_3 \left(q^2 \gamma^\mu - q^\mu \not{q} \right) + i\tau_5 q^\nu \sigma^\mu{}_\nu - i\tau_7\, p^\mu p_1^\nu p_2^\lambda \sigma_{\lambda\nu} \\ &+ \tau_8 \left(-i p_1^\nu p_2^\lambda \gamma^\mu \sigma_{\nu\lambda} + p_2^\mu \not{p}_1 - p_1^\mu \not{p}_2 \right),\end{aligned} \tag{1.5}$$

where $p = p_1 + p_2$. For on-shell quarks Γ_μ is enclosed by Dirac spinors and we arrive at the standard form

$$\begin{aligned}\overline{u}(p_2)\Gamma^\mu u(p_1) =& F_1(q^2)\overline{u}(p_2)\gamma^\mu u(p_1) \\ &- iF_2(q^2)\overline{u}(p_2)\left(\sigma^{\mu\nu} q_\nu\right) u(p_1),\end{aligned} \tag{1.6}$$

where the static CMDM can be obtained from the Pauli form factor as follows $a_q = -2m_q F_2(0)$, but in this work we are interested in the case with $q^2 \neq 0$. At the one-loop level, $a_q(q^2)$ receives QCD and EW contributions from the SM via the Feynman diagrams depicted in Figs. 1.2 and 1.3, respectively. We will address below the issue of the gauge independence of $a_q(q^2)$, which is necessary to have a valid observable quantity.

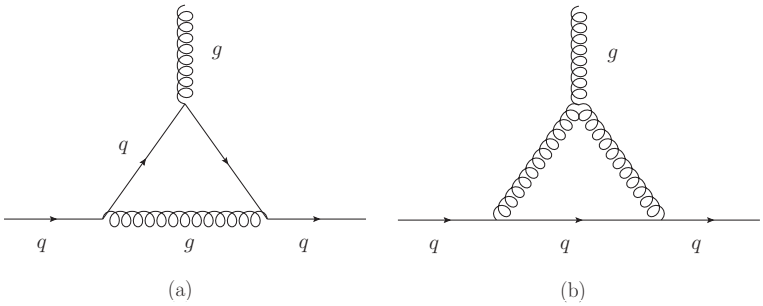

Figure 1.2: One-loop Feynman diagrams for the QCD contributions to the CMDM of quarks: (a)QED-like diagram and (b)three-gluon diagram. For the BFM the external gluon is replaced by its background field g_B.

1.1.2 The off-shell CMDM of quarks

While on-shell Green functions are gauge invariant and gauge independent, this is not necessarily true for off-shell Green functions as they do not correspond to a physical process but just to an amputated set of Feynman diagrams. The first systematic approach to obtain well-behaved off-shell Green functions out of which valid observable quantities can be extracted was the so-called pinch technique (PT) [30, 31, 32], which is based on a diagrammatic method that combines self-energy, vertex and box diagrams associated to a physical process to remove any gauge dependent term. It was later shown that at the one-loop level the results obtained via the PT coincide with those obtained by the BFM via the Feynman-'t Hooft gauge ($\xi_Q = 1$) [33, 34]. In this work we use the later approach to obtain a gauge independent quark CMDM as it is simpler in computational grounds.

Since we are interested in the CMDM of quarks for an off-shell gluon, we need to verify that the contributions of Figs. 1.2 and 1.3 are gauge independent and thus provide an observable quan-

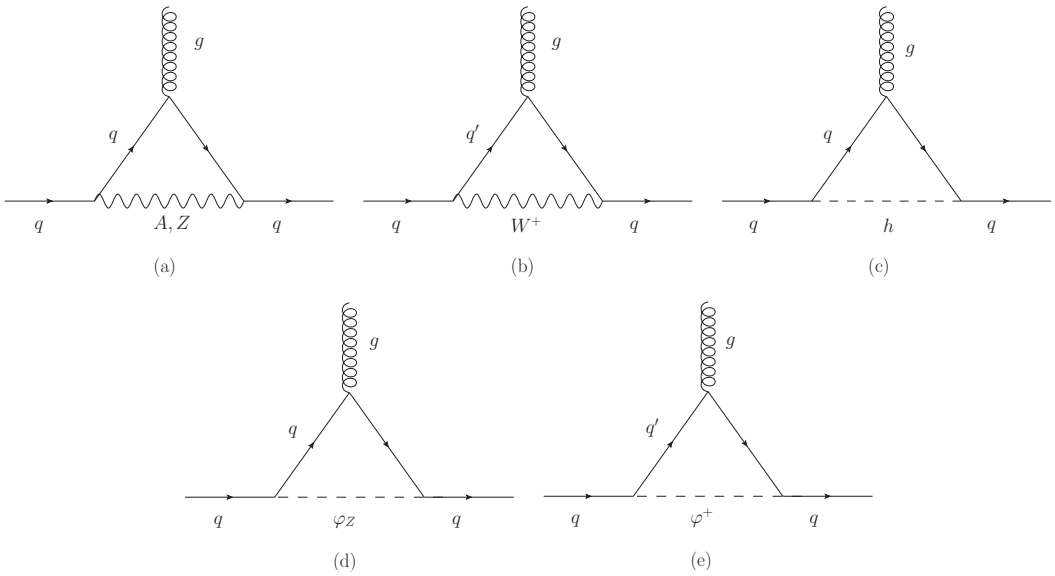

Figure 1.3: Feynman diagrams for the SM electroweak contributions to the CMDM of quarks at the one-loop level in a renormalizable linear R_ξ gauge: (a) and (b)gauge boson exchange, (d) and (e) Goldstone boson exchange, and (c)Higgs boson exchange. For the BFM the gluon is replaced by its background field g_B.

tity. With this aim, to cross-check our result, for our calculation we use both the conventional renormalizable linear R_ξ gauge and the BFM [33] with arbitrary gauge parameters. Indeed, both computations are technically identical except for the contribution of the three-gluon diagram of Fig. 1.2 as for the remaining diagrams the only dependence on the gauge parameters arises from the gauge boson propagators. The main outline of our calculation is as follows. We first wrote out the amplitude for each contributing Feynman diagram for arbitrary ξ (ξ_Q) and then used the Passarino-Veltman reduction scheme to perform the integration over the four-momentum space. Once the gauge parameter independence of $\hat{\mu}_q(q^2)$ was verified, we used Feynman parameter integration in the unitary gauge to obtain an alternate result, which can be used for a numerical cross-check. The loop functions are thus presented in terms of Feynman parameter integrals and Passarino-Veltman scalar functions. For the latter we include the results in terms of closed form functions if possible. The Dirac algebra and tensor reduction was done with the help of FeynCalc [35] and Package-X [36], which prove very helpful to verify explicitly that the gauge parameter drops out from the calculation.

Below, p_1 (p_2) denotes the four-momentum of the ingoing (outgoing) quark, whereas q is the gluon four-momentum as shown in Fig. 1.1. It is understood that in the D-dimensional integrals, the volume element d^Dk is accompanied by a factor of μ^{4-D}, with μ the scale of dimensional regularization, that drops out from the final results as they are ultraviolet finite. Also, a small imaginary part $i\epsilon$ must be added to the propagators. Below, the gauge parameters are indistinctly denoted by ξ as they cancel out for each partial contribution.

The CMDM is defined in a similar fashion to the electromanetic case. We thus write the S-matrix element for $\bar{q}qg$ coupling as

$$i\mathscr{M} = ig_s T^a \overline{u}(p_2)\Gamma^\mu u(p_1), \tag{1.7}$$

where, from Lagrangian (1.1), the corresponding vertex function Γ^{μ} can be written as

$$\Gamma^{\mu} = i\sigma_{\mu\nu}q^{\nu}\left(\frac{a_q}{2m_q} + id_q\gamma^5\right). \tag{1.8}$$

We now turn to outline the main steps of the calculation.

1.1.3 QCD contribution

The contribution to the vertex function Γ^{μ} from diagram 1.2(a) is

$$\Gamma^{\mu}_{\mathrm{QCD}_1} = \frac{ig_s^2}{6}\int\frac{d^Dk}{(2\pi)^D}\frac{\gamma_\beta\left(\not{q}_2 + m_q\right)\gamma^\mu\left(\not{q}_1 + m_q\right)\gamma_\alpha}{\left(q_2^2 - m_q^2\right)\left(q_1^2 - m_q^2\right)\left(k^2\right)} \times P^{\alpha\beta}(k), \tag{1.9}$$

where $P^{\lambda\rho}(p) = \left(g^{\lambda\rho} + (\xi - 1)\frac{p^\lambda p^\rho}{p^2}\right)$, $q_i = k + p_i$, and m_q is the quark mass. In this case we have three color generators T^a, which simplifies as follows

$$T^b_{jn}T^a_{nm}T^b_{mi} = \frac{1}{2}\delta_{ji}T^a_{nn} - \frac{1}{2N}T^a_{ji} = -\frac{1}{6}T^a_{ji}, \tag{1.10}$$

where we used $T^b_{jn}T^b_{mi} = \frac{1}{2}\left(\delta_{ji}\delta_{nm} - \frac{1}{N}\delta_{jn}\delta_{mi}\right)$ and $\mathrm{Tr}\left[T^a\right] = 0$, whereas N stands for the quark color number.

After four-momentum integration, the ξ parameter drops out and the following contribution to the CMDM is obtained:

$$a_q^{\mathrm{QCD}_1}\left(q^2\right) = \frac{\alpha_s}{6\pi}\mathscr{F}_q^{\mathrm{QCD}_1}\left(q^2\right), \tag{1.11}$$

where the function $\mathscr{F}_q^{\mathrm{QCD}_1}$ is presented in A.1.[1] When $q^2 = 0$, it is straightforward to obtain

$$a_q^{\mathrm{QCD}_1}(0) = -\frac{\alpha_s}{12\pi}, \tag{1.12}$$

which agrees with the well-known QED result after the replacement of the electric charge e by the strong coupling constant α_s and the insertion of the color factor of Eq. (1.10).

The non-abelian contribution to the quark CMDM from diagram 1.2(a) can be obtained from the following vertex function:

$$\Gamma^{\mu}_{\mathrm{QCD}_2} = -\frac{i3g_s^2}{2}\int\frac{d^Dk}{(2\pi)^D}\frac{\gamma_\rho\left(-\not{k} + m_q\right)\gamma_\lambda\Sigma^{\lambda\rho\mu}}{\left(q_2^2\right)\left(k^2 - m_q^2\right)\left(q_1^2\right)}, \tag{1.13}$$

[1] From now on, all the corresponding loop functions appearing in the contributions to $a_q\left(q^2\right)$, denoted by calligraphy letters, will be presented in terms of Feynman parameter integrals, Passarino-Veltman scalar functions and closed form results in appendices A.3.1, A.3.2, and A.1.3, respectively, including the results for $q^2 = 0$.

with

$$\Sigma^{\lambda\rho\mu} = \Big(g^{\alpha\mu}\left(p_2 - k - 2p_1\right)^{\beta} + g^{\beta\mu}\left(p_1 - k - 2p_2\right)^{\alpha} + g^{\alpha\beta}\left(2k + p_1 + p_2\right)^{\mu} + \frac{1}{\xi}\left(g^{\alpha\mu}q_2^{\beta} + g^{\beta\mu}q_1^{\alpha}\right)\Big) \times P_{\alpha}^{\lambda}(q_1)P_{\beta}^{\rho}(q_2), \tag{1.14}$$

for the BFM, whereas for the linear R_ξ gauge we must drop the $\frac{1}{\xi}$ term between the parenthesis.

As for the corresponding color factor, it was worked out as follows

$$T_{jb}^{m}T_{bi}^{n}f^{anm} = -2i\mathrm{Tr}\left[T^{m}\left[T^{n},T^{a}\right]\right]T_{jb}^{m}T_{bi}^{n} = -\frac{i3}{2}T_{ji}^{a}. \tag{1.15}$$

After four-momentum integration, our result for the quark CMDM is given as

$$a_q^{\mathrm{QCD}_2}\left(q^2\right) = \frac{3\alpha_s}{2\pi}\mathscr{F}_q^{\mathrm{QCD}_2}\left(q^2\right), \tag{1.16}$$

which disagrees with the result obtained in [25] as there is a disagreement with the color factor used by those authors.

When $q^2 = 0$, Eq. (1.16) yields an infrared divergent result for $q^2 = 0$:

$$\mathscr{F}_q^{\mathrm{QCD}_2}(0) = \frac{1}{2}\left(\frac{1}{\epsilon} + \log\left(\frac{\mu^2}{m_q^2}\right) + 3\right), \tag{1.17}$$

where ϵ is the pole of dimensional regularization. Therefore, the contribution of the three-gluon diagram is not well defined when $q^2 = 0$ as it was also pointed out in [25]. Since QCD contributions to the CMDM are proportional to the strong running coupling constant $\alpha_s\left(q^2\right)$, such contributions have not perturbative sense at $q^2 = 0$ but at a scale where a perturbative calculation is valid.

1.1.4 Electroweak contribution

We now present the calculation of the contributions to the quark CMDM induced through the Feynman diagrams of Fig. 1.3. We note that the diagrams with photon, Z gauge boson, φ_Z Goldstone boson, and Higgs boson exchange are similar to those inducing a lepton anomalous MDM [2, 37], but with the external photon replaced by a gluon. Therefore, the CMDM just differ by the coupling constants g_s and the $SU(3)$ generators T_{ij}^a instead of the electric charge. Thus our result must reproduce that of the anomalous MDM of a lepton. As far as the diagrams with $W^{\pm}$ gauge boson and G_W Goldstone boson exchange are concerned, the lepton anomalous MDM has no analogous contributions.

Photon exchange

The corresponding contribution to the $\bar{q}qg$ vertex function can be written as

$$\Gamma_A^\mu = -ie^2Q_q^2 \int \frac{d^Dk}{(2\pi)^D} \frac{\gamma_\beta \left(\not{q}_2 + m_q\right) \gamma^\mu \left(\not{q}_1 + m_q\right) \gamma_\alpha}{\left(q_2^2 - m_q^2\right)\left(q_1^2 - m_q^2\right)\left(k^2\right)} \times \left(g^{\alpha\beta} + (\xi - 1)\frac{k^\alpha k^\beta}{k^2}\right), \tag{1.18}$$

with Q_q the quark electric charge in units of e. After a straightforward calculation, we arrive at a gauge-parameter independent result for an on-shell gluon. It reads

$$a_q^A\left(q^2\right) = -\frac{e^2Q_q^2}{4\pi^2}\mathscr{F}_q^A\left(q^2\right), \tag{1.19}$$

which gives a result similar to that of the lepton anomalous MDM for $q^2 = 0$:

$$a_q^A(0) = \frac{\alpha Q_q^2}{2\pi}. \tag{1.20}$$

We note that the electric charge factor Q_q^2 is missing in the corresponding result of [25]. However, since the internal photon of diagram 1.3(a) is attached to two quark lines, such a factor must appear in this contribution.

Z gauge boson and φ_Z Goldstone boson exchange

We now present the calculation for the contributions of the loops with the neutral Z gauge boson and its associated Goldstone boson φ_Z [diagrams (a) and (d) of Fig. 1.3]. The corresponding contributions need to be added up to cancel out the dependence on the gauge parameter ξ. As far as the diagram with Z gauge boson exchange is concerned, the $\bar{q}qg$ vertex function in terms of the axial (vector) g_A^q (g_V^q) couplings reads:

$$\Gamma_Z^\mu = \frac{-ig^2}{c_W^2} \int \frac{d^Dk}{(2\pi)^D} \frac{\Xi^\mu}{\left(q_2^2 - m_q^2\right)\left(q_1^2 - m_q^2\right)\left(k^2 - m_Z^2\right)}, \tag{1.21}$$

where

$$\Xi^\mu = \gamma^\beta \left(g_V^q - g_A^q\gamma^5\right)\left(\not{q}_2 + m_q\right)\gamma^\mu\left(\not{q}_1 + m_q\right)\gamma^\lambda \times \left(g_V^q - g_A^q\gamma^5\right)\left(g_{\beta\lambda} + (\xi - 1)\frac{k_\beta k_\lambda}{k^2 - \xi m_Z^2}\right), \tag{1.22}$$

the vector and axial vector couplings are defined as

$$g_V^q = \frac{1}{2}T_{3_q} - Q_q s_W^2, \quad g_A^q = \frac{1}{2}T_{3_q}, \tag{1.23}$$

with T_{3_q} the weak isospin ($T_{3_u} = \frac{1}{2}$, $T_{3_d} = -\frac{1}{2}$). On the other hand, the contribution from the diagram with φ_Z Goldstone boson exchange is

$$\Gamma^{\mu}_{\varphi_Z} = \frac{-ig^2 m_q^2}{4m_W^2} \int \frac{d^D k}{(2\pi)^D} \gamma^5 \left(\not{q}_2 + m_q\right) \gamma^{\mu} \left(\not{q}_1 + m_q\right) \gamma^5 \times \frac{1}{\left(q_2^2 - m_q^2\right)\left(q_1^2 - m_q^2\right)\left(k^2 - \xi m_Z^2\right)}. \tag{1.24}$$

The explicit integration in the four-momentum space shows that the dependence on the ξ gauge parameter cancels out after adding up the contributions of the Z and φ_Z exchange diagrams. The total contribution is thus given by

$$a_q^Z\left(q^2\right) = \frac{\sqrt{2} G_F m_q^2}{\pi^2} \left(\left(g_A^q\right)^2 \mathscr{A}_q^Z\left(q^2\right) + \left(g_V^q\right)^2 \mathscr{V}_q^Z\left(q^2\right) \right), \tag{1.25}$$

whereas the result for $q^2 = 0$ is analogue to the Z contribution to the anomalous MDM of a lepton [2]. There is agreement with the calculation presented in [26], but there is no agreement with the result of [25] as those authors use the Feynman-'t Hooft gauge propagator for the Z gauge boson but seem to omit the φ_Z Goldstone boson exchange contribution.

$W^{\pm}$ gauge boson and $\varphi^{\pm}$ Goldstone boson exchange

We now calculate the contribution from the Feynman diagrams (b) and (e) of Fig. 1.3 as both contributions must be added up in order to drop out the dependence on the gauge parameter ξ. For the diagram with W gauge boson exchange, the $\bar{q}qg$ vertex function can be written as

$$\Gamma^{\mu}_{W} = \sum_{q'} \frac{-ig^2 \left|V_{qq'}\right|^2}{2} \int \frac{d^D k}{(2\pi)^D} \Pi^{\mu} \times \frac{1}{\left(q_2^2 - m_{q'}^2\right)\left(q_1^2 - m_{q'}^2\right)\left(k^2 - m_W^2\right)}, \tag{1.26}$$

with

$$\Pi^{\mu} = \gamma^{\beta} P_L \left(\not{q}_2 + m_{q'}\right) \gamma^{\mu} \left(\not{q}_1 + m_{q'}\right) \gamma^{\lambda} P_L \times \left(g_{\beta\lambda} + (\xi - 1) \frac{k_{\beta} k_{\lambda}}{k^2 - \xi m_W^2} \right), \tag{1.27}$$

whereas the contribution of the $\varphi^{\pm}$ Goldstone boson reads

$$\Gamma^{\mu}_{\varphi^{\pm}} = \sum_{q'} \frac{ig^2 \left|V_{qq'}\right|^2}{2m_W} \int \frac{d^D k}{(2\pi)^D} \Pi^{'\mu} \times \frac{1}{\left(q_2^2 - m_{q'}^2\right)\left(q_1^2 - m_{q'}^2\right)\left(k^2 - \xi m_W^2\right)}, \tag{1.28}$$

with

$$\Pi^{'\mu} = \left(m_q P_L - m_{q'} P_R\right)\left(\not{q}_2 + m_{q'}\right)\gamma^\mu\left(\not{q}_1 + m_{q'}\right) \times \left(m_q P_R - m_{q'} P_L\right), \tag{1.29}$$

where $P_{L,R}$ is the chirality projector, q' stands for the internal quark and $V_{qq'}$ is the CKM matrix element.

Again after four-momentum integration, the gauge parameter drops out and the following gauge independent contribution to the quark CMDM is obtained:

$$a_q^W\left(q^2\right) = \sum_{q'} \frac{G_F m_q^2 \left|V_{qq'}\right|^2}{4\sqrt{2}\pi^2} \mathscr{F}_{qq'}^W\left(q^2\right), \tag{1.30}$$

with the dominant term arising from the diagonal CKM matrix element ($V_{qq} \approx 1$). There is no agreement with the result of [25] as those authors consider that the external and internal quark masses are degenerate.

Higgs boson exchange

The remaining SM contribution to the quark CMDM arises from the diagram with Higgs boson exchange, which is gauge independent. The corresponding contribution to the $\bar{q}qg$ vertex function is given by

$$\Gamma_h^\mu = \frac{ig^2 m_q^2}{4m_W^2} \int \frac{d^D k}{(2\pi)^D} \frac{\left(\not{q}_2 + m_q\right)\gamma^\mu\left(\not{q}_1 + m_q\right)}{\left(q_2^2 - m_q^2\right)\left(q_1^2 - m_q^2\right)\left(k^2 - m_h^2\right)}. \tag{1.31}$$

The algebra is straightforward and we obtain after four-momentum integration:

$$a_q^h\left(q^2\right) = -\frac{G_F m_q^2}{4\sqrt{2}\pi^2} \mathscr{F}_q^h\left(q^2\right), \tag{1.32}$$

which for $q^2 = 0$ agrees with the results presented in [25].

1.2 Numerical evaluation and discussion

We now turn to the numerical evaluation of the one-loop contribution to the CMDM of quarks. We first present a numerical estimate of the quark CMDM in the SM, which is aimed to make a comparison with previous results, which can be useful to settle any ambiguity.

1.2.1 Off-shell CMDM of quarks in the SM

We first analyze the behavior of the parameter $\hat{\mu}_= a_q/2$ in the SM, which is the one studied by the experimental collaborations [21]. Although the top quark CMDM is the one mainly studied in the literature, for the sake of completeness we include in our analysis an estimate for all the SM

quarks. Since the results for the QCD contribution have not sense in perturbative calculations at $q^2 = 0$, as pointed out above, we study the case $q^2 \neq 0$. Anomalous top quark couplings have been studied at the LHC through $\bar{t}t$ production [38, 39, 40, 28], moreover, its effects to the $\bar{t}t$ cross section have been analyzed in [41, 42]. The transition CMDM could contribute at the leading order through the diagrams of Fig. 1.4, where the top quark CMDM contributions are marked by a dot and we include the $gg\bar{t}t$ interaction arising from Lagrangian (1.1). Since the outgoing top quarks are on-shell, the gluon four-momentum in the s-channel diagrams obeys $\|q\| \geq 2m_t$, whereas in the t and u channels there are no such kinematical constraint.

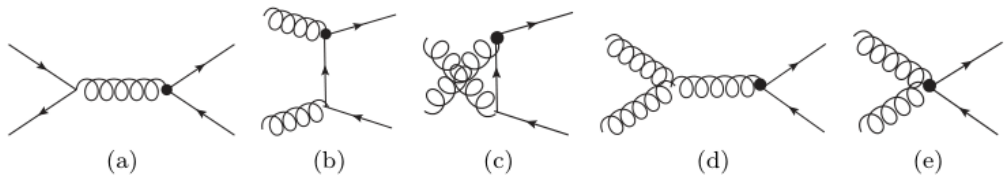

Figure 1.4: Feynman diagrams for $\bar{t}t$ production via the Lagrangian of Fig. 1.1. The dots correspond to the contributions of the top quark CMDM to the $\bar{t}t$ production

.

We have implemented the strong coupling constant $\alpha_s\left(q^2\right)$ as the three loop approximate solution of the renormalization group equation of QCD [43, 44]. We consider gluon four-momentum transfer in the 30-1000 GeV region, where $\alpha_s \sim 0.1$, since for $\|q\|$ less than around 1 GeV the theory becomes strongly interacting [45]. In addition, at next-to-leading order QCD calculations, EW corrections are neglected, so only the pure QCD contribution to the CMDM of quarks would be relevant.

For the numerical analysis we use the results in terms of Passarino-Veltman scalar functions, which were evaluated via the LoopTools [46] and Collier [47] packages, though we cross-check with the results obtained by numerical integration of the Feynman parameter results, which however shows more numerical instability.

Light quarks CMDM

We show in Fig. 1.5 the behavior of the real Re $\left[\widehat{\mu}_q\right]$ and imaginary Im $\left[\widehat{\mu}_q\right]$ parts of the CMDM of the light SM quarks as functions of the gluon transfer momentum $\|q\|$. We observe that in both cases the largest estimates correspond to the b quark CMDM, whereas the smallest estimates are obtained for the u and d quarks. This stems from the fact that the CMDM is proportional to the quark mass for $q^2 \neq 0$. We also note that the real and imaginary parts of $\hat{\mu}_q$ are about the same magnitude for all the light quarks. Numerical predictions for the CMDM of light quarks are shown in Table 1.1 for some selected values of $\|q\|$.

We now turn to analyze the behavior of the partial contributions to $\hat{\mu}_q$ for a light quark. Thus, by way of illustration, we show in Fig. 1.6 the real and imaginary parts of the partial contributions to the c quark CMDM. All other light quark's contributions exhibit a similar behavior, though there are slight changes for the b quark as explained below. We first note that the dominant contributions arise from the triple gluon vertex (the so-called QCD_2 contribution), though at high energies the QCD_1, γ, Z and W contributions are of similar size. In particular, the imaginary parts of the EW gauge bosons contributions are slightly larger than the one of the QCD_1 contribution for $\|q\| \gtrsim 600$ GeV, whereas the real parts of both QCD contributions

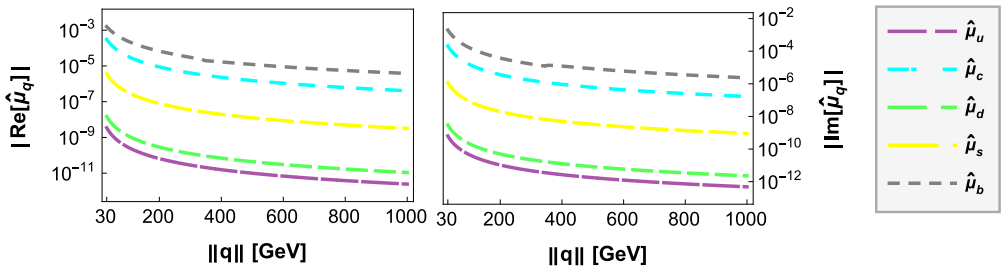

Figure 1.5: Real (left plot) and imaginary (right plot) parts of the light quarks CMDM $\widehat{\mu}_q$ as function of the transfer momentum of the gluon.

dominate in all the studied energy interval. On the other hand, the Higgs boson contributions are the smallest ones: for the u and d quarks, such contributions are negligibly small, of the order of $10^{-20} - 10^{-21}$. Note that for $\|q\| > 30$ GeV all the partial contributions to $\hat{\mu}_q$ develop an imaginary part as $q^2 > 4m^2$, with m the mass of the virtual particles attached to the external gluon, except for the W contribution to $\hat{\mu}_b$, which is purely real for $q^2 < 4m_t^2$ as long as one neglects the contributions of the loops with internal u and c quarks.

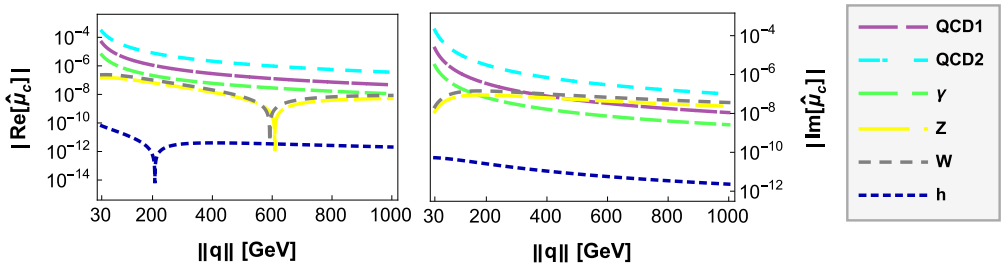

Figure 1.6: Real (left plot) and imaginary (right plot) parts of the SM one-loop partial contributions to $\hat{\mu}_c$ as functions of the transfer momentum of the gluon $\|q\|$.

Top quark CMDM

We now turn to analyze the behavior of the CMDM of the top quark. We first show in Fig. 1.7 $\hat{\mu}_t$ as a function of $\|q\|$ as well as its partial QCD and EW contributions. We observe that both the real and imaginary parts are dominated by the QCD contributions, though the real part of the EW contribution is of comparable size around the threshold $\|q\| = 2m_t$, where all the contributions show a peak due to a flip of sign. Both the QCD and EW contributions decrease as $\|q\|$ increases: above the $2m_t$ threshold the real part of the EW contribution becomes negligible, whereas its imaginary part is about one order of magnitude below the imaginary part of the QCD contribution for $\|q\| \sim 1000$ GeV. However, at very large $\|q\|$ (much larger than 1000 GeV) the imaginary part of the EW contribution becomes dominant since the imaginary part of the QCD contribution decreases quickly at very high energies.

We now show in Fig. 1.8 the real and imaginary parts of all the partial contributions to $\hat{\mu}_t$ as functions of $\|q\|$. As far as the real parts are concerned, we observe that at low and high energies the QCD_2 contribution dominates, but around $\|q\| = 2m_t$ the Z and h contributions become the dominant ones, which explains the behavior of the EW contribution shown in Fig.

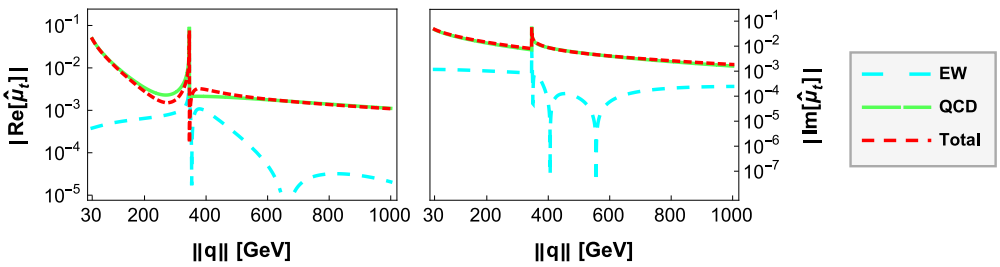

Figure 1.7: Real (left plot) and imaginary (right plot) parts of the EW, QCD and total contributions to the top quark CMDM $\widehat{\mu}_t$ as function of the transfer momentum norm of the gluon $\|q\|$.

1.7 at $\|q\| \simeq 2m_t$. Nevertheless such contributions are of opposite sign and they tend to cancel each other out. On the other hand, as for the imaginary contributions, below the threshold $\|q\| = 2m_t$ all but the QCD_2 and W contributions vanish and above this threshold the Z and h contributions develop imaginary parts of the same order of magnitude than that of the three-gluon contribution (QCD_2), which remains slightly larger as $\|q\|$ increases. We can conclude that the QCD contributions is always dominant, nevertheless the imaginary part of the EW contribution become comparable to the QCD one at high energies. After the threshold $\|q\| = 2m_t$ the top quark CMDM exhibits a peak due to a flip of sign. Such a behavior is not observed however in the CEDM of light quarks as we are studying energies far from the threshold region.

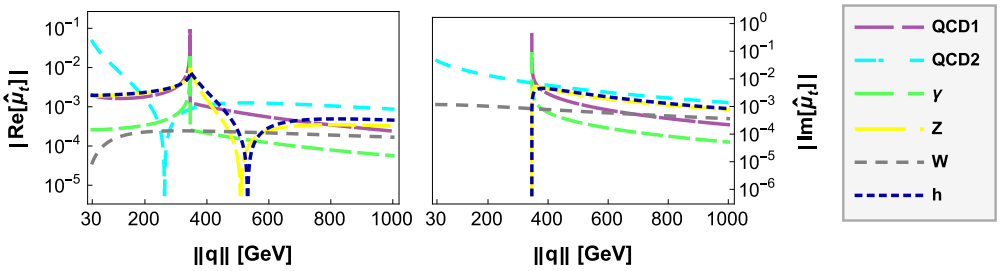

Figure 1.8: Real (left plot) and imaginary (right plot) parts of the SM one-loop partial contributions to the top quark CMDM $\widehat{\mu}_t$ as functions of the transfer momentum of the gluon $\|q\|$.

Finally, we show in Table 1.1 the numerical estimates of $\hat{\mu}_q$ for all the SM quarks at a few selected values of the gluon transfer momentum $\|q\|$. As expected, the largest estimate corresponds the top quark CMDM, though the bottom and charm quarks CMDM could also be non-negligible in some energy regions. The CMDM of all quarks is in general complex, with real and imaginary parts of comparable size, though the real parts are always slightly larger. We have compared our numerical results with those reported in [26] for the top quark CMDM at $q^2 = \pm m_Z^2$ and find a good agreement. In this case the imaginary part of $\hat{\mu}(q^2)$ arises from the QCD_2 and W exchange contributions, whereas the remaining contributions are purely real as q^2 is below the kinematic threshold where an imaginary part is developed.

Table 1.1: Estimates for the SM contribution to the CMDM $\hat{\mu}_q$ of the SM quarks for select values of the gluon transfer momentum $\|q\|$.

Quark	$\|q\| = 30$ GeV	$\|q\| = m_Z$	$\|q\| = 500$ GeV
d	$1.47 \times 10^{-8} - i2.96 \times 10^{-9}$	$1.44 \times 10^{-9} - i2.55 \times 10^{-10}$	$4.33 \times 10^{-11} - i8.21 \times 10^{-12}$
u	$3.47 \times 10^{-9} - i6.33 \times 10^{-10}$	$3.35 \times 10^{-10} - i5.47 \times 10^{-11}$	$9.94 \times 10^{-12} - i1.75 \times 10^{-12}$
s	$3.63 \times 10^{-6} - i1.17 \times 10^{-6}$	$3.8 \times 10^{-7} - i1.01 \times 10^{-7}$	$1.23 \times 10^{-8} - i3.25 \times 10^{-9}$
c	$3.08 \times 10^{-4} - i2.10 \times 10^{-4}$	$3.96 \times 10^{-5} - i1.87 \times 10^{-5}$	$1.51 \times 10^{-6} - i6.07 \times 10^{-7}$
b	$1.55 \times 10^{-3} - i1.95 \times 10^{-3}$	$2.72 \times 10^{-4} - i1.96 \times 10^{-4}$	$1.24 \times 10^{-5} - i6.56 \times 10^{-6}$
t	$-4.81 \times 10^{-2} - i4.69 \times 10^{-2}$	$-1.33 \times 10^{-2} - i2.66 \times 10^{-2}$	$2.24 \times 10^{-3} - i5.43 \times 10^{-3}$

Quark	$\|q\| = 800$ GeV
d	$1.67 \times 10^{-11} - i3.42 \times 10^{-12}$
u	$3.84 \times 10^{-12} - i7.32 \times 10^{-13}$
s	$4.88 \times 10^{-9} - i1.37 \times 10^{-9}$
c	$6.21 \times 10^{-7} - i2.53 \times 10^{-7}$
b	$5.3 \times 10^{-6} - i2.73 \times 10^{-6}$
t	$1.36 \times 10^{-3} - i2.6 \times 10^{-3}$

1.3 Remarks

In this chapter we have presented a new evaluation of the SM prediction of the CMDM $\hat{\mu}_q$ of quarks at the one-loop level, which is aimed to address some inconsistencies appearing in previous calculations. We considered the most general case with non-zero transfer momentum of the gluon q^2 and the calculation was performed within both a renormalizable linear R_ξ gauge and the BFM for arbitrary gauge parameters. It was found that the off-shell CMDM is gauge independent, which assures us that it is an observable quantity. For completeness the loop integrals are presented in terms of Feynman parameter integrals, Passarino-Veltman scalar functions and closed form functions, which are useful to make a cross-check of the numerical results. It is found that the QCD contribution arising from the Feynman diagram with a three-gluon vertex has an infrared divergence and it thus not defined at $q^2 = 0$, which is due to the fact that the static CMDM has not perturbative sense, as it has also been pointed out by the authors of Refs. [25, 26]. We then perform a numerical analysis and examine the behavior of the CMDM of all the SM quarks in the region 30 GeV$< \|q\| <$ 1000 GeV, where the QCD coupling constant $\alpha(q^2)$ is of the order of 10^{-1}. In this energy region the CMDMs are complex in general, with the imaginary parts being about the same order of magnitude than the real parts. Furthermore, the QCD contributions dominate over the EW contributions, which suggests that two-loop contributions can be relevant. On the other hand, the imaginary part of the EW contribution is only comparable to the QCD contribution at very high energies. Since the CMDM is proportional to the quark mass, the largest contributions correspond to the top quark CMDM, which is of the order of $10^{-2} - 10^{-3}$, with the imaginary part of the EW contributions of the same size than the QCD contributions around the threshold $q^2 = 4m_t^2$.

Chapter 2

Bounds on the absorptive parts of the CMDM and CEDM dipole moments of the top quark from LHC data

Quite recently, the study of the chromomagnetic dipole moment (CMDM) $\hat{\mu}_t$ of the top quark has arisen interest both theoretically and experimentally. In the theoretical side, a new evaluation of the lowest order contributions to $\hat{\mu}_t$ within the framework of the standard model (SM) was presented very recently [48] in order to settle some ambiguities of previous evaluations. Also, several non SM contributions have been calculated up to the one-loop level in the framework of extension theories such as two Higgs doublet models (THDM) [15], fourth-generation THDMs [13], 331 models [49], etc. As far as the SM prediction is concerned, in contrast to what was claimed before [14], it is now clear that the CMDM is infrared divergent, with the divergence arising from the non-abelian term of the gluon field tensor [48]. Therefore, the study of the static CMDM has no sense in perturbative QCD. It was also pointed out [48] that the off-shell CMDM is finite and gauge independent in the SM, which are necessary conditions for an observable quantity. On the other hand, the top quark chromoelectric dipole moment (CEDM) $\hat{d}_t$, which is induced up to the three-loop level in the SM [22] and could give a clear signal of CP violation, has also been a topic of interest in the literature as it can arise at the one-loop level in several beyond the SM (BSM) theories [13, 49], thereby opening the possibility of an enhanced value. In general, both the off-shell CMDM and CEMD can have non-zero imaginary parts, which however remain almost unexplored.

In the experimental side, the leading order corrections to the cross section of top quark pair production induced by the top quark CMDM and CEDM have been studied in [50, 42, 41, 51, 52, 53, 54, 40, 55, 56, 57], and the next to leading order corrections have also been calculated more recently [58, 59, 60]. The CMS collaboration has imposed the following current bounds on the top quark CMDM and CEDM: $-0.014 < \hat{\mu}_t < 0.004$ and $-0.020 < \hat{d}_t < 0.012$ [28], which where obtained via two opposite sign leptons (e^+e^-, $e^\pm\mu^\mp$, $\mu^+\mu^-$) in the final state. Furthermore, the CMS collaboration also set the limits $\hat{\mu}_t = -0.024^{+0.013}_{-0.009}(\text{stat})^{+0.016}_{-0.011}(\text{syst})$ and $|\hat{d}_t| < 0.03$ [61], which were obtained by the analysis of lepton+jets events in the final state. These bounds were extracted from experimental data by assuming that the top quark CMDM and CEDM are real quantities. Nevertheless, it is clear that even if we consider the experimental errors, the bounds

on $\hat{\mu}_t$ seem to be incompatible. Therefore, a further analysis is in order.

The anomalous $\bar{t}tg$ interaction can be induced through Lagrangian (1.1) and it also describes the interaction between an off-shell gluon and two on-shell quarks [29]. Since the CMDM and CEDM of the top quark are complex in general, they can be written as

$$\hat{\mu}_t = \mathrm{Re}\big[\hat{\mu}_t\big] + i\mathrm{Im}\big[\hat{\mu}_t\big], \tag{2.1}$$

$$\hat{d}_t = \mathrm{Re}\big[\hat{d}_t\big] + i\mathrm{Im}\big[\hat{d}_t\big]. \tag{2.2}$$

As far as the SM predictions are concerned, the real and imaginary parts of the off-shell top quark CMDM are of the order of $10^{-2} - 10^{-3}$ [48], whereas the predictions for the off-shell CEDM are not available yet. Nevertheless, in BSM theories both real and imaginary parts of the off-shell top quark CEDM are of the order of 10^{-19} [49]. The effects of the absorptive parts of the CMDM and CEDM at LHC processes were first studied in [40] but to our knowledge there is no update on such analysis, which we believe is in order given the current experimental bounds on these observables.

In this chapter we obtain bounds on the absorptive parts of the CMDM and CEDM of the top quark using the data for top quark pair production at the LHC run 2. Our work is organized as follows. In Sec. 2.1 we discuss the framework for the study of the CMDM and CEDM absorptive parts. Section 2.2 is devoted to present a novel calculation of the parton cross-sections of $t\bar{t}$ production for complex CMDM and CEDM, which to our knowledge has not been reported before. In Sec. 2.3 a numerical simulation is presented for top quark pair production at the LHC via MadGraph5, where the effective Lagrangian of Eq. (1.1) was implemented with the help of the FeynRules package. The results for the $t\bar{t}$ cross section as a function of the real and imaginary parts of $\hat{\mu}_t$ and $\hat{d}_t$ are then used to obtain bounds on their absorptive parts. The possibility that kinematic distributions could be helpful to disentangle the top quark CMDM and CEDM absorptive parts is examined in Section 2.4. Finally, in Sec. 2.5 we present our conclusions.

2.1 Remarks on the absorptive parts of the CMDM in the SM

In the SM, the CMDM of quarks arises at the one-loop level through the Feynman diagrams of Figs. 1.2 (QCD contribution) and 1.3 (electroweak contribution). The off-shell CMDM $\hat{\mu}_q(q^2)$ can develop an absorptive (imaginary) part when the gluon transfer four-momentum $\hat{q} = \sqrt{q^2}$ crosses the threshold such that the virtual particles attached to the gluon are allowed to be pair produced, namely $\hat{q} \geq 2m$, with m the mass of such particles. This is true for all energy values of the external gluon in the case of the Feynman diagram (b) of Fig. 1.2, whereas the threshold is $\hat{q} \geq 2m_q$ for the Feynman diagrams (a) of Fig. 1.2 as well as diagrams (a) and (c) of Fig. 1.3, whereas an absorptive part is developed for $\hat{q} \geq 2m_{q'}$ in the Feynman diagram (b) of Fig. 1.3. The absorptive contributions to the CMDM can also arise from higher order Feynman diagrams and can been extracted by the Cutkosky rules [62], which yield the same results obtained via the usual techniques for Feynman diagram calculation [63].

Therefore, for the top quark CMDM, the contribution from diagram (b) of Fig. 1.3 develops an absorptive part at $\hat{q} = 2m_b$, whereas that from diagram (b) of Fig. 1.2 is complex for any $\hat{q}$ value. The remaining contributions become complex at $\hat{q} = 2m_t$. Evidently, the corresponding contributions to the top quark CEDM would also become complex at the same energy thresholds. It is thus interesting to obtain a bound on the absorptive part of the top quark CMDM consistent

with the CMS limits. With this aim we have performed a numerical evaluation of the analytical expressions of Ref. [48] to find the energy interval of the transfer momentum of the gluon such that the real part of the top quark CMDM predicted by the SM matches with the CMS results [28, 61]. We obtain that the value $\mathrm{Re}\big[\hat{\mu}_t\big] = -0.024$ reported in Ref [61] corresponds to the 57 GeV$\leqslant \hat{q} \leqslant$ 59 GeV interval, with the corresponding absorptive part in the same interval being $\mathrm{Im}\big[\hat{\mu}_t\big] \approx -0.034$. On the other hand, if we consider the limits $-0.014 < \mathrm{Re}\big[\hat{\mu}_t\big] < 0.004$ reported in Ref. [28] we find that these values are consistent with energies above $\hat{q} = 85$ GeV, where the absorptive part can be one order of magnitud larger than in the previous case: for values around $\hat{q} = 85$ GeV we obtain $\mathrm{Im}\big[\hat{\mu}_t\big] \approx -0.028$, but at higher energies the corresponding value is of the order of 10^{-3} and remains almost constant as the energy increases.

2.2 Contributions of CMDM and CEDM to $\bar{t}t$ production

Top pair production can receive contributions from the anomalous $\bar{t}tg$ coupling [42, 41] of Eq. (1.1) but also from the $\bar{t}tgg$ vertex arising from the non-abelian part of the gluon field strength tensor. The corresponding Feynman rules follow straightforwardly and are shown in Fig. 2.1.

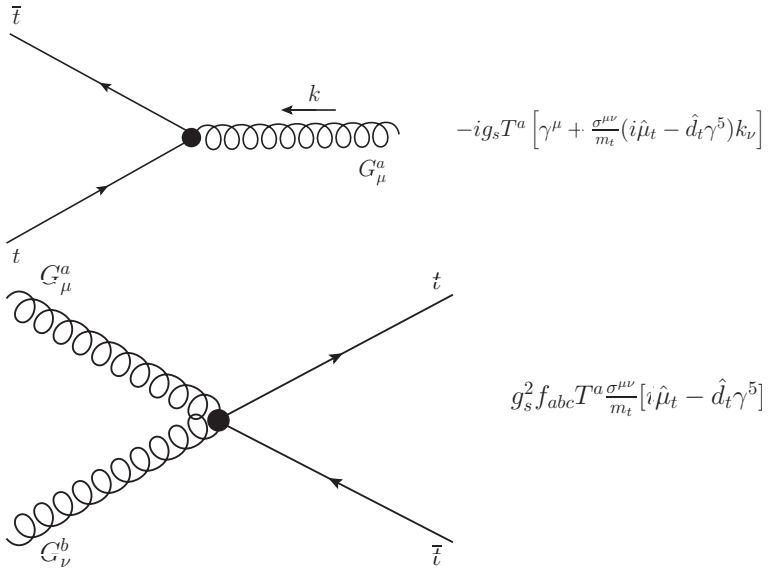

Figure 2.1: Feynman rules for the anomalous $\bar{t}tg$ and $\bar{t}tgg$ couplings arising from Lagrangian (1.1).

The most recent analyses on top quark production assume that both CMDM and CEDM are purely real [28, 61]. In this work we are interested in the study of the contributions of the absorptive parts of these dipole moments. Therefore we consider that both $\hat{\mu}_t$ and $\hat{d}_t$ are complex and calculate the following parton cross-sections:

$$\begin{aligned}\hat{\sigma}_{q\bar{q}} &\equiv \sigma(\bar{q}q \to \bar{t}t),\\ \hat{\sigma}_{gg} &\equiv \sigma(gg \to \bar{t}t),\end{aligned} \tag{2.3}$$

which apart from the SM contribution receive a new one from the Feynman diagrams of Fig. 2.2, where the large dot represents the anomalous CMDM and CEDM contributions.

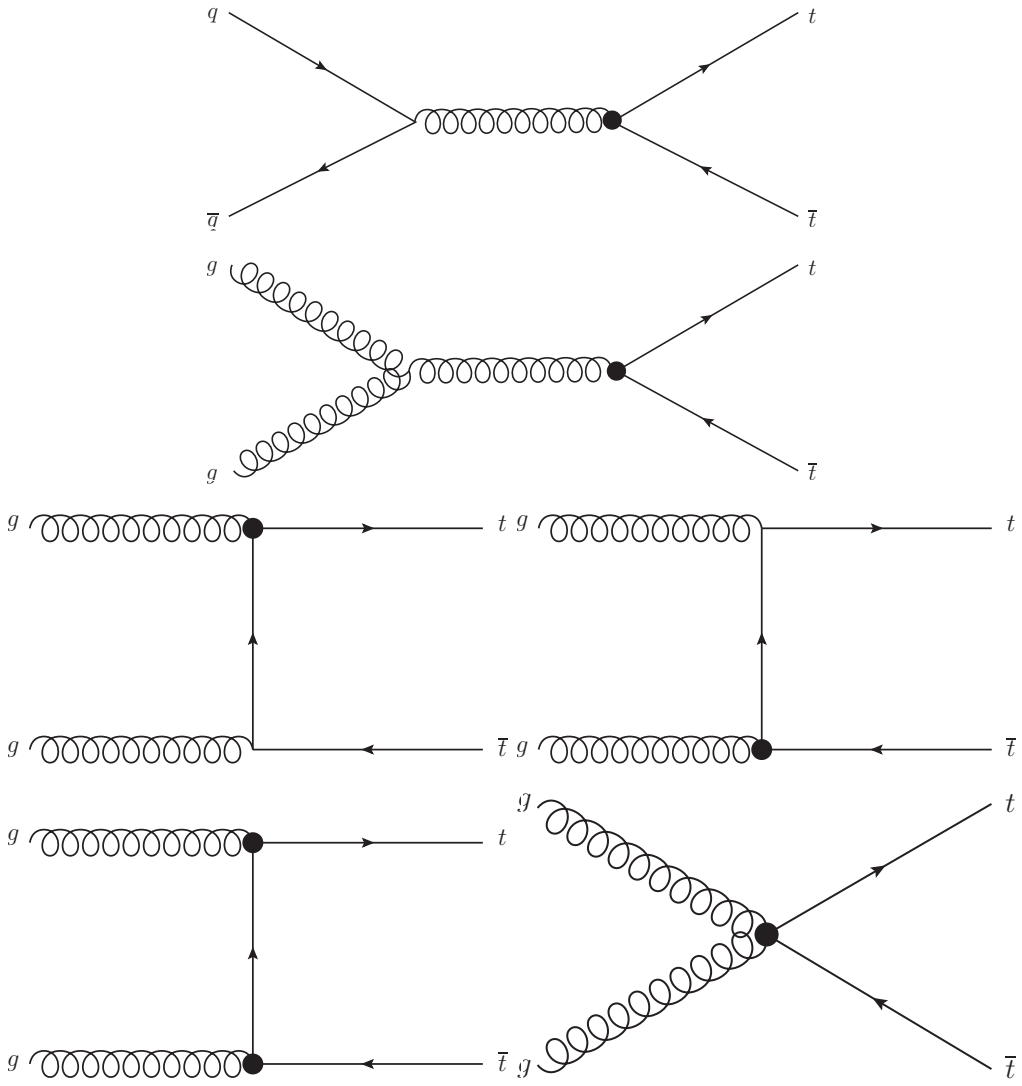

Figure 2.2: Feynman diagrams for the contribution to the parton cross-sections $\hat{\sigma}_{q\bar{q}}$ and $\hat{\sigma}_{gg}$ at the leading order. Crossed diagrams are not shown. The large dot represents the anomalous couplings induced by the CMDM and CEDM. The SM tree-level contribution is obtained after replacing the anomalous $\bar{t}tg$ coupling by the SM one.

After some algebra we obtain the respective differential cross sections for general complex CMDM and CEDM:

$$\frac{d\hat{\sigma}_{q\bar{q}}}{d\hat{t}} = \frac{\pi\alpha_s^2}{\hat{s}^2}\frac{8}{9}\left[\frac{1}{2} - v + z + 2\mathrm{Re}\big[\hat{\mu}_t\big] + \Big(\mathrm{Re}\big[\hat{\mu}_t\big]^2 + \mathrm{Im}\big[\hat{\mu}_t\big]^2 - \mathrm{Re}\big[\hat{d}_t\big]^2 - \mathrm{Im}\big[\hat{d}_t\big]^2\Big) + \Big(\mathrm{Re}\big[\hat{\mu}_t\big]^2 + \mathrm{Im}\big[\hat{\mu}_t\big]^2 + \mathrm{Re}\big[\hat{d}_t\big]^2 + \mathrm{Im}\big[\hat{d}_t\big]^2\Big)\frac{v}{z}\right], \tag{2.4}$$

and

$$\begin{aligned}\frac{d\hat{\sigma}_{gg}}{d\hat{t}} =&\frac{\pi\alpha_s^2}{\hat{s}^2}\frac{1}{12}\Bigg[\Big(\frac{4}{v}-9\Big)\Big(\frac{1}{2}-v-2z(1-\frac{z}{v})+2\ \mathrm{Re}\big[\hat{\mu}_t\big]\Big)+\frac{1}{8vz}\Big[v\Big(55\ \mathrm{Re}\big[\hat{d}_t\big]^2+\mathrm{Re}\big[\hat{\mu}_t\big]^2(55-144z)\Big)\\
&+z\Big(4\ \mathrm{Re}\big[\hat{d}_t\big]^2+70\ \mathrm{Re}\big[\hat{\mu}_t\big]^2\Big)+\frac{1}{vz}\Big[-16v^3\Big(4\Big(\mathrm{Re}\big[\hat{\mu}_t\big]^2\mathrm{Im}\big[\hat{d}_t\big]^2-4\ \mathrm{Re}\big[\hat{\mu}_t\big]\ \mathrm{Im}\big[\hat{\mu}_t\big]\ \mathrm{Re}\big[\hat{d}_t\big]\ \mathrm{Im}\big[\hat{d}_t\big]\\
&+\mathrm{Im}\big[\hat{\mu}_t\big]^2\ \mathrm{Re}\big[\hat{d}_t\big]^2\Big)+9z\Big(\mathrm{Im}\big[\hat{\mu}_t\big]^2+\mathrm{Im}\big[\hat{d}_t\big]^2\Big)\Big)+v^2z\Big(-512\ \mathrm{Re}\big[\hat{\mu}_t\big]\ \mathrm{Im}\big[\hat{\mu}_t\big]\ \mathrm{Re}\big[\hat{d}_t\big]\ \mathrm{Im}\big[\hat{d}_t\big]\\
&+\mathrm{Im}\big[\hat{d}_t\big]^2\Big(16\ \mathrm{Re}\big[\hat{\mu}_t\big]\Big(15\ \mathrm{Re}\big[\hat{\mu}_t\big]+7\Big)+288z+63\Big)+3\ \mathrm{Im}\big[\hat{\mu}_t\big]^2\Big(80\ \mathrm{Re}\big[\hat{d}_t\big]^2+48z+21\Big)\Big)\\
&-2vz^2\Big(92\ \mathrm{Im}\big[\hat{\mu}_t\big]\ \mathrm{Re}\big[\hat{d}_t\big]\ \mathrm{Im}\big[\hat{d}_t\big]+\Big(1-8\ \mathrm{Re}\big[\hat{d}_t\big]^2\Big)\mathrm{Im}\big[\hat{\mu}_t\big]^2+2\ \mathrm{Im}\big[\hat{d}_t\big]^2\Big(-\mathrm{Re}\big[\hat{\mu}_t\big]\Big(4\ \mathrm{Re}\big[\hat{\mu}_t\big]+41\Big)\\
&+72z+17\Big)\Big)+128\ \mathrm{Im}\big[\hat{d}_t\big]^2z^3\Big]+\mathrm{Re}\big[\hat{\mu}_t\big]\Big(\mathrm{Re}\big[\hat{\mu}_t\big]^2+\mathrm{Im}\big[\hat{\mu}_t\big]^2+\mathrm{Re}\big[\hat{d}_t\big]^2\Big)\Big(\frac{14}{z}-\frac{5}{2v}\Big)\\
&+\Big(\Big(\mathrm{Re}\big[\hat{\mu}_t\big]^2+\mathrm{Im}\big[\hat{\mu}_t\big]^2\Big)^2+2\Big(\mathrm{Re}\big[\hat{\mu}_t\big]^2\ \mathrm{Re}\big[\hat{d}_t\big]^2+\mathrm{Im}\big[\hat{\mu}_t\big]^2\ \mathrm{Im}\big[\hat{d}_t\big]^2\Big)+\Big(\mathrm{Re}\big[\hat{d}_t\big]^2+\mathrm{Im}\big[\hat{d}_t\big]^2\Big)^2\Big)\\
&\times\Big(-\frac{1}{z}+\frac{1}{v}+\frac{4v}{z^2}\Big)\Bigg],\end{aligned}\tag{2.5}$$

where $\hat{s}$, $\hat{t}$ and $\hat{u}$ are the usual parton Mandelstam variables and we introduced the definitions

$$z=\frac{m_t^2}{\hat{s}},\tag{2.6}$$

$$v=\frac{1}{\hat{s}^2}(\hat{t}-m_t^2)(\hat{u}-m_t^2).\tag{2.7}$$

In the $t\bar{t}$ center of mass frame, the parameter t, is related to the angle θ between the outgoing top quark and the momenta of the incoming parton as

$$m_t^2-t=\frac{s}{2}(1-\beta\cos\theta),\tag{2.8}$$

with $\beta=\sqrt{1-4z}$.

For $\hat{\mu}_t=\hat{d}_t=0$ the above cross sections reduce to the known SM results [64] as expected. We also have verified that in the scenario with purely real CMDM and CEDM, Eq. (2.4) reproduces the result reported in Ref. [42, 41]. Nevertheless, in the same scenario we do not find agreement with our result for Eq. (2.5) and the one previously reported [42, 41], which apparently is incomplete as there is no agreement in the coefficients of $\hat{\mu}_t^2$ and $\hat{d}_t^2$.

2.3 Bounds on absorptive parts of the CMDM and CEDM of the top quark

We now turn to constrain the absorptive parts $\mathrm{Im}\big[\hat{\mu}_t\big]$ and $\mathrm{Im}\big[\hat{d}_t\big]$ via the LHC data on top quark pair production [28, 65, 61]. We follow a similar approach to that discussed in [54]. We use Monte Carlo simulation to obtain the theoretical predictions for the leading order contribution to the $\sigma(pp\to t\bar{t})$ cross section. In order to compute the corresponding contributions from the top quark CMDM and CEDM, we use MadGraph5 [66], where the anomalous interactions of Eq. (1.1) were implemented with the help of FeynRules [67].

We will consider the most recent LHC results for top quark pair production at a center-of-mass energy $\sqrt{s}$ =13 TeV. Therefore we use the ATLAS cross section in the lepton plus jets channel [65]

$$\sigma_{\rm Exp} = (830 \pm 39) \quad \text{pb}, \tag{2.9}$$

whereas for the theoretical SM prediction we use [68]

$$\sigma_{\rm Theo} = (831.8 \pm 43) \quad \text{pb}, \tag{2.10}$$

which does not include contributions from the CMDM and CEDM of the top quark. In both cases the errors have been added in quadrature. The ratio between the measured and predicted cross sections is thus

$$\mathscr{R} = \frac{\sigma_{\rm Exp}}{\sigma_{\rm Theo}} = 0.99 \pm 0.069. \tag{2.11}$$

Following Ref. [54], we will interpret the error of Eq. (2.11) as a window to BSM effects in top quark pair production and use it to set constraints on the absorptive parts of $\hat{\mu}_t$ and $\hat{d}_t$. We first set $\hat{\mu}_t = \hat{d}_t = 0$ and obtain the SM cross section $\sigma_{\rm SM}$, afterwards we generate the new physics contribution $\sigma_{\rm NP}$ for non-zero $\text{Re}\big[\hat{\mu}_t\big]$, whereas all the remaining parameters are set to zero. This procedure is repeated for each one of the $\text{Im}\big[\hat{\mu}_t\big]$, $\text{Re}\big[\hat{d}_t\big]$ and $\text{Im}\big[\hat{d}_t\big]$ parameters. All our event samples for the $pp \to \bar{t}t$ cross section are generated at $\sqrt{s}$ =14 TeV. We show in Fig. 2.3 the ratio $\sigma_{\rm NP}/\sigma_{\rm SM}$ as a function of the real and absorptive parts of the CMDM (left plot) and CEDM (right plot), where the MadGraph5 estimated error is included.

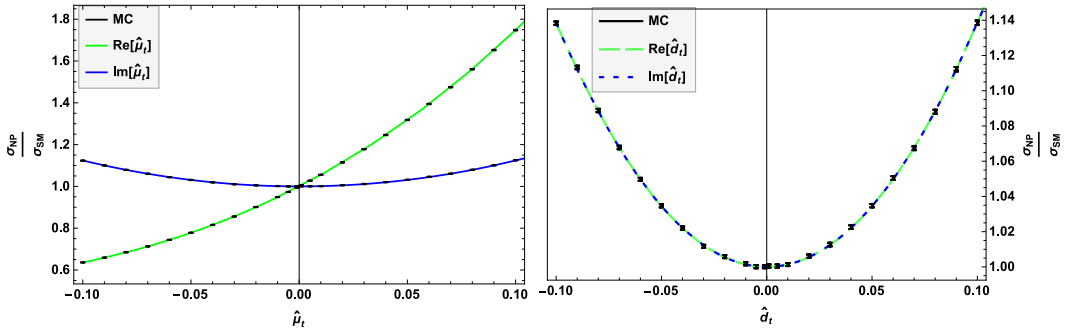

Figure 2.3: Ratio $\mathscr{R} = \sigma_{\rm NP}(pp \to \bar{t}t)/\sigma_{\rm SM}(pp \to \bar{t}t)$ as a function of the real (green lines) and imaginary parts (blue lines) of the CMDM (left plot) and CEDM (right plot) of the top quark at $\sqrt{s} = 14$ TeV. The bars represent the MadGraph5 estimated errors. The solid lines are the best fit curves.

To fit the data of Fig. 2.3, we have not considered the interference terms of the real and absorptive parts of $\hat{\mu}_t$ and $\hat{d}_t$. Such an approach has been used in the past to study the implications of the top quark CMDM and CEDM in $t\bar{t}$ production [54, 57, 58]. Thus, from Eqs. (2.4) and (2.5) we observe that the ratio $\mathscr{R}$ is a polynomial of fourth order in the real and imaginary parts of $\hat{\mu}_t$ and $\hat{d}_t$, although only the even powers of $\text{Im}\big[\hat{\mu}_t\big]$, $\text{Re}\big[\hat{d}_t\big]$ and $\text{Im}\big[\hat{d}_t\big]$ are present. The expression obtained from the fit of Fig. 2.3 reads

$$\begin{aligned}\mathscr{R} \simeq\ & 1 + 5.33\ \text{Re}\big[\hat{\mu}_t\big] + 19.14\ \text{Re}\big[\hat{\mu}_t\big]^2 + 21.98\ \text{Re}\big[\hat{\mu}_t\big]^3 + 5.78\ \text{Re}\big[\hat{\mu}_t\big]^4 \\ & + 12.35\ \text{Im}\big[\hat{\mu}_t\big]^2 + 4.38\ \text{Im}\big[\hat{\mu}_t\big]^4 + 13.79\ \text{Re}\big[\hat{d}_t\big]^2 + 5.58\ \text{Re}\big[\hat{d}_t\big]^4 \\ & + 13.78\ \text{Im}\big[\hat{d}_t\big]^2 + 6.15\ \text{Im}\big[\hat{d}_t\big]^4.\end{aligned} \tag{2.12}$$

We observe that the contributions of $\mathrm{Im}\big[\hat{\mu}_t\big]$, $\mathrm{Re}\big[\hat{d}_t\big]$ and $\mathrm{Im}\big[\hat{d}_t\big]$ are rather similar, with the lowest order coefficients being of similar size, which is actually in accordance with Eq. (2.5). We also note that the top quark dipole contribution is dominated by $\mathrm{Re}\big[\hat{\mu}_t\big]$, which enters linearly into $\mathscr{R}$, whereas the remaining dipole contributions enter quadratically and are thus more suppressed. The values predicted for the off-shell top quark CMDM are of the order of $10^{-2} - 10^{-3}$ in the SM [48], whereas the typical values predicted for the CEDM in some BSM theories are of the order of $10^{-19} - 10^{-20}$ [49]. Therefore the effects of their real and absorptive parts on top quark pair production seems to be too small to be observable at the cross section level.

As already mentioned, constraints on the the top quark CMDM and CEDM have been obtained from the LHC data under the assumption that they are purely real. Hence, to study the effects of the corresponding absorptive parts we will proceed as follows. We fix the real parts of the top quark CMDM and CEDM using the CMS limits [28, 61] and we then constrain the absorptive parts $\mathrm{Im}\big[\hat{\mu}_t\big]$ and $\mathrm{Im}\big[\hat{d}_t\big]$ via Eqs. (2.12) and (2.11), where the error will be attributed to the anomalous $\bar{t}tg$ contributions. In other words, we fix $\mathrm{Re}\big[\hat{\mu}_t\big]$ and $\mathrm{Re}\big[\hat{d}_t\big]$ to their current constraints and find the allowed area of $\mathrm{Im}\big[\hat{\mu}_t\big]$ and $\mathrm{Im}\big[\hat{d}_t\big]$ values.

Since the bounds of Ref. [61] are in principle partially excluded by those of Ref. [28], we consider both bounds in our analysis. We thus assume the following three scenarios:

- Scenario I: we use the lower bounds reported in [28] and set $\mathrm{Re}\big[\hat{\mu}_t\big] = -0.014$ and $\mathrm{Re}\big[\hat{d}_t\big] = -0.02$.
- Scenario II: we use the upper bounds of [28] and set $\mathrm{Re}\big[\hat{\mu}_t\big] = 0.004$ and $\mathrm{Re}\big[\hat{d}_t\big] = 0.012$.
- Scenario III: we set the real part of $\hat{\mu}_t$ to the value given in [61] and use the upper bound for the real part of $\hat{d}_t$: $\mathrm{Re}\big[\hat{\mu}_t\big] = -0.024$ and $\mathrm{Re}\big[\hat{d}_t\big] = 0.03$.

Notice that we do not consider the scenario where $\mathrm{Re}\big[\hat{d}_t\big]$ is fixed to its lower (negative) bound [61] as it yields similar bounds to those obtained in scenario III, which stems from the fact that $\mathscr{R}$ is an even function of $\mathrm{Re}\big[\hat{d}_t\big]$. We also do not consider other scenarios as they yield bounds of similar order of magnitude.

The allowed areas in the $\mathrm{Im}\big[\hat{\mu}_t\big] - \mathrm{Im}\big[\hat{d}_t\big]$ plane at the 95% C.L. are shown in Fig. 2.4 for the three scenarios discussed above. We observe that the allowed areas are concentric ellipses. Hence the following bounds are obtained: $|\mathrm{Im}\big[\hat{\mu}_t\big]| \lesssim 0.127$ and $|\mathrm{Im}\big[\hat{d}_t\big]| \lesssim 0.12$ in scenario I (blue solid lines); $|\mathrm{Im}\big[\hat{\mu}_t\big]| \lesssim 0.139$ and $|\mathrm{Im}\big[\hat{d}_t\big]| \lesssim 0.133$ in scenario III (green dashed lines); as well as $|\mathrm{Im}\big[\hat{\mu}_t\big]| \lesssim 0.094$ and $|\mathrm{Im}\big[\hat{d}_t\big]| \lesssim 0.09$ the allowed area in scenario II(orange dashed line). The latter scenario yields actually the intersection area of the three scenarios, which means that the corresponding bounds are consistent with both CMS limits. Note that the bounds are very similar for the absorptive parts of the $\hat{\mu}_t$ and $\hat{d}_t$, both of them being of the order of $10^{-1} - 10^{-2}$ at the 95% C.L.

It is worth comparing our bounds with the theory predictions of the SM and some BSM theories. In particular, for a transfer momentum in the interval 30 GeV $\leqslant s \leqslant$ 1000 GeV, the SM prediction for the absorptive part of $\hat{\mu}_t(q^2)$ can be as large as 10^{-2} [48], which is close to our bounds. On the other hand, several BSM theories predict values for the absorptive part of $\hat{d}_t(q^2)$ of the order of 10^{-19}, which is far away from our bound.

We have also made the same analysis but including the interference terms of Eq. (2.5). Nonetheless, the obtained fit is still consistent with Eq. (2.12) and the bounds are similar to those of Fig. 2.4. Thus, the interference terms can indeed be neglected as their contribution is not relevant.

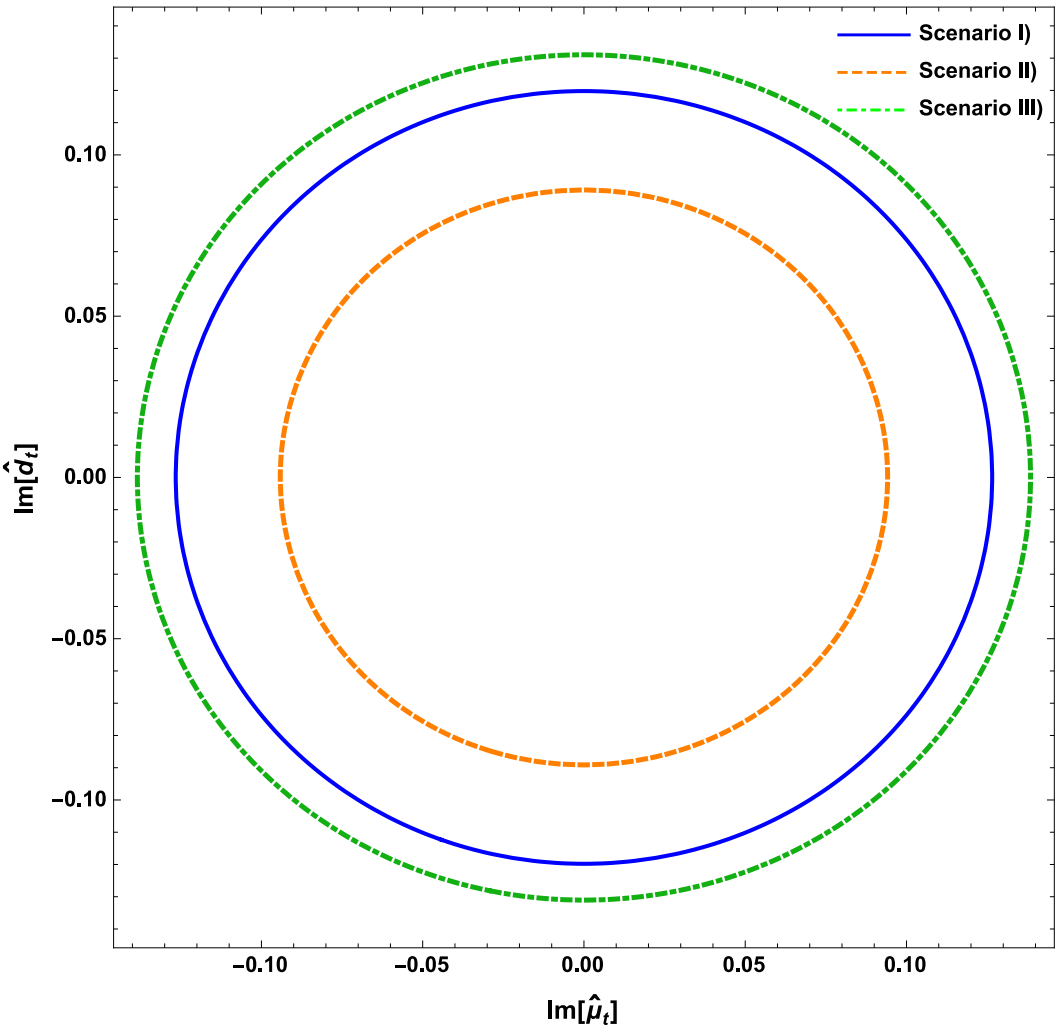

Figure 2.4: Allowed area at the 95% C.L. for the imaginary parts of the CMDM and CEDM of the top quark in the three scenarios discussed in the text for the corresponding real parts.

2.4 Kinematic distributions

The effects of $\mathrm{Re}\big[\hat{\mu}_t\big]$ and $\mathrm{Re}\big[\hat{d}_t\big]$ on the differential cross section of top quark pair production have been analyzed in the past as some kinematic distributions can be sensitive to these parameters [50, 41, 59, 56]. Nevertheless, to our knowledge the effects of the absorptive parts $\mathrm{Im}\big[\hat{\mu}_t\big]$ and $\mathrm{Im}\big[\hat{d}_t\big]$ have only been explored in Ref. [40] through the longitudinal t and $\bar{t}$ polarizations. Therefore, we will examine the possibility that the differential cross sections for top quark pair production could be sensitive to the absorptive parts of the top quark CMDM and CEDM. In order to study such effects, we compare the kinematic distributions in the case where the CMDM and CEDM are purely real with that in which both dipole moments develop an absorptive part. We use the CMS constrains on the real parts of the top quark dipole form factors, hence we set to $\mathrm{Re}\big[\hat{\mu}_t\big] = -0.014$ and $\mathrm{Re}\big[\hat{d}_t\big] = 0.01$. We then consider three cases for the values of $\mathrm{Im}\big[\hat{\mu}_t\big]$ and $\mathrm{Im}\big[\hat{d}_t\big]$:

i) $\mathrm{Im}\big[\hat{\mu}_t\big] = \mathrm{Im}\big[\hat{d}_t\big] = 0.01$.

ii) $\mathrm{Im}\big[\hat{\mu}_t\big] = \mathrm{Im}\big[\hat{d}_t\big] = 0.05$.

iii) $\mathrm{Im}\big[\hat{\mu}_t\big] = 0.01$ and $\mathrm{Im}\big[\hat{d}_t\big] = -0.01$.

The reason why we are considering values of the order of 10^{-2} is that they are consistent with the SM prediction for the CMDM and the constraints of Sec. 2.3. Furthermore, while cases i and ii allow us to explore the possibility that the kinematic distributions can be sensitive to small changes in the absorptive terms, scenario iii allows us to test the effect of a flip of sign.

For the graphical analysis we use MADANALYSIS 5 [69]. In Figs. 2.5(a) and 2.5(b) we show the kinematic distributions of the $t\bar{t}$ invariant mass and the top quark transverse momentum in the cases discussed above. It is observed that there is no considerable distinction between the kinematic distributions obtained in the general case with complex top quark dipole form factors and those obtained in the scenario in which they are purely real. This was also observed when studying the contributions of the real part of the top quark dipole moments as compared to the SM leading order contribution [52, 56]. A similar situation occurs for the kinematic distribution of the rapidity η, which is shown in Fig. 2.5(c).

We have also examined the sensitivity of the forward-backward (FB) asymmetry to the CMDM and CEDM in top quark pair production at the LHC, which could be possible at the leading order in some models [70, 52], whereas in the SM there is only a significant deviation up to next-to-leading order [70]. Unfortunately, Eqs. (2.4) and (2.5) cannot be expreseed as a linear combination of $\cos\theta$ via Eq. (2.8). Thus, a deviation to the FB asymmetry at the leading order is not possible [71]. However, other asymmetries could be sensitive indeed to the CMDM and CEDM of the top quark, as shown in Ref. [40, 54]. Thus, all the kinematic distributions studied here show no significant deviation from the SM leading order contribution to top quark pair production arising from the real and absorptive parts of the top quark dipole form factors.

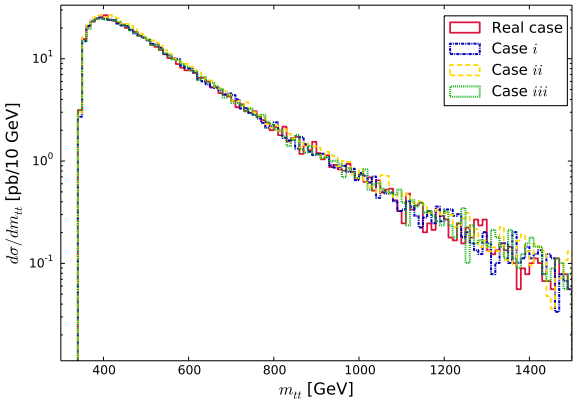

(a)

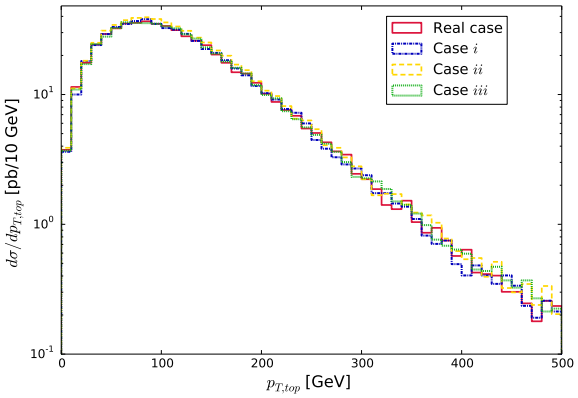

(b)

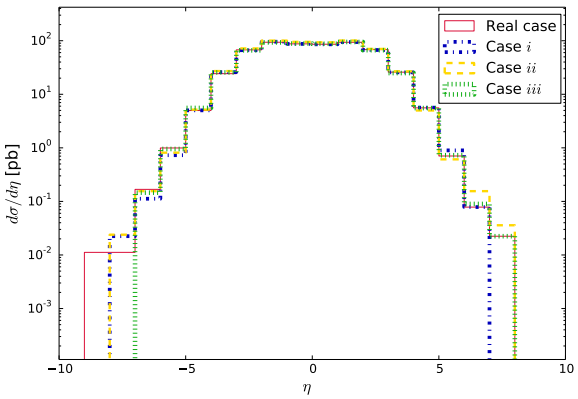

(c)

Figure 2.5: Invariant mass (a), top quark transverse momentum (b) and rapidity (c) kinematic distributions for top quark pair production at the LHC at $\sqrt{s} = 14$ TeV in the three scenarios discussed in the text for the absorptive parts of $\hat{\mu}_t$ and $\hat{d}_t$.

2.5 Remarks

The off-shell CMDM and CEDM of quarks have become a topic of interest recently [48]. However, the study of their absorptive (imaginary) parts remains almost unexplored. In this work we have obtained bounds on the absorptive parts of the off-shell top quark CMDM and CEDM via the experimental data of top quark pair production at the LHC, which to our knowledge are the first limits of this kind. We present explicit expressions for the corresponding differential parton cross-sections considering complex CMDM and CEDM, which have also been calculated for the first time. We point out that there is a disagreement between our result for the $gg \to t\bar{t}$ differential cross section and the expression previously reported in the scenario where only the real part of the top quark dipole form factors are considered [42, 41]. Our bounds for the absorptive parts were obtained using the most recent data for the top quark CMDM and CEDM obtained by the CMS collaboration [28, 61]. It was found that the upper bound on the absorptive parts of both dipole moments are of the order of $10^{-1} - 10^{-2}$. In particular, values of the order of 10^{-2} are consistent with all the CMS results. We also note that our bound is consistent with the SM prediction for the absorptive part of $\hat{\mu}_t$, which is of the order of $10^{-2} - 10^{-3}$ [48]. On the other hand, in some BSM theories the absorptive part of the CEDM could be of the order of 10^{-19} [49], which seems far from detection in the near future.

We also explored the possibility that several kinematic distributions for top quark pair production at the LHC can be sensitive to the absorptive parts of the CMDM and CEDM, but we find that there are no significant deviation from the scenario where the CMDM and CEDM are purely real. In fact, even in the case of real CMDM and CEDM, there is no significant deviation from the leading order SM contribution as discussed previously [52, 56].

Chapter 3

CMDM and CEDM dipole moments of the top quark in the reduced 331 model

In this chapter we are interested in the contributions to the top quark CMDM and CEDM in the reduced 331 model [72]. The study of elementary particle models based on the $SU(3)_L \times U(1)_N$ gauge symmetry dates back to the 1970s, when it was still not clear that Weinberg's $SU(2)_L \times U(1)_Y$ model was the right theory of electroweak interactions [73]. After the discovery of the Z and W gauge bosons, since the electroweak gauge group is embedded into $SU(3)_L \times U(1)_N$, the so called 331 models [74, 75] became serious candidates to extend the SM and explain some issues for which it has no answer, such as the flavor problem and a possible explanation for the large splitting between the mass of the top quark and those of the remaining fermions. Several realizations of the 331 model have been proposed in the literature, which predict new fermions, gauge bosons and scalar bosons, so their phenomenologies have been considerably studied [76, 77, 78, 79, 80, 81, 82, 83].

The minimal 331 model [74, 75] requires a very large scalar sector, which introduces three scalar triplets to give masses to the new heavy gauge bosons and one scalar sextet to endow the leptons with small masses. The complexity of this model has lead to the appearance of alternative 331 models aimed to economize the scalar sector. In particular, the reduced 331 model (RM331) [72] only requires two scalar triplets, thereby being considerably simpler than the minimal version [84, 85]. In the RM331, the physical scalar states obtained after the symmetry breaking are two neutral scalar bosons only, with the lightest one being identified with the SM Higgs boson [86], and a doubly charged one. Unlike other 331 models, no singly charged scalar boson arises in the RM331 [87, 88, 89]. In the gauge sector, there are one new neutral gauge boson Z', a new pair of singly charged gauge bosons $V^{\pm}$, and a pair of doubly charged gauge bosons $U^{\pm\pm}$. Like other 331 models, the RM331 also predicts three new exotic quarks. The original RM331 is strongly disfavored by experimental data [90], though it would still be allowed as long as left-handed quarks are introduced via a particular $SU(3)_L \times U(1)_N$ representation [91, 92], which in fact would give rise to flavor changing neutral current (FCNC) effects.

The contributions to the electron and muon anomalous MDM have been already studied in the RM331 [77] within another 331 realization [93]. As for the CMDM of quarks, there is only a previous calculation in the context of an old version of the 331 model [14], though such a calculation is limited to the on-shell case. However, since the on-shell CMDM is infrarred

divergent in the SM [48], a calculation of the off-shell CMDM is mandatory. To our knowledge there is no calculation of the off-shell CMDM of quarks, let alone their off-shell CEDM, in 331 models. Furthermore, in the model studied in [14], the new contributions only arise in the gauge sector, whereas in the RM331 there are additional contributions from the neutral scalar bosons, which are absent in other 331 models.

In this chapter we present a study on the contributions of the RM331 to the off-shell CMDM and CEDM of the top quark. It is organized as follows. In Section II we present a brief description of the RM331, with the Feynman rules necessary for our calculation being presented in Appendix A.2. The analytical calculation of the new contributions to the dipole form factors of the $\bar{t}tg$ vertex are presented in Sec. III; our results in terms of Feynman parameter integrals and Passarino-Veltman scalar functions are presented in Appendix A.4. Section IV is devoted to a review of the current constraints on the parameter space of the model and the numerical analysis of the off-shell CMDM and CEDM of the top quark. Finally, in Sec. V the conclusions and outlook are presented.

3.1 Brief outline of the RM331

We will describe briefly the main features of each sector of the RM331, focusing only on those details relevant to our calculation.

3.1.1 Scalar and gauge boson eigenstates

As far as the scalar sector is concerned, the scalar potential is given by

$$V(\chi,\rho)=\mu_1^2\rho^\dagger\rho+\mu_2^2\chi^\dagger\chi+\lambda_1\left(\rho^\dagger\rho\right)^2+\lambda_2\left(\chi^\dagger\chi\right)^2+\lambda_3\left(\rho^\dagger\rho\right)\left(\chi^\dagger\chi\right)+\lambda_4\left(\rho^\dagger\chi\right)\left(\chi^\dagger\rho\right), \quad (3.1)$$

where the scalar triplets transform as $\rho=\left(\rho^+,\rho^0,\rho^{++}\right)^T\sim(1,3,1)$ and $\chi=\left(\chi^-,\chi^{--},\chi^0\right)^T\sim(1,3,-1)$. To induce the spontaneous symmetry breaking (SSB), the neutral scalar bosons ρ^0 and χ^0 develop non-zero vacuum expectation values (VEVs) under the shifting of the fields as

$$\rho^0,\chi^0\to\frac{1}{\sqrt{2}}\left(v_{\rho,\chi}+R_{\rho,\chi}+iI_{\rho,\chi}\right), \quad (3.2)$$

which leads to the following constraints

$$\mu_1^2+\lambda_1v_\rho^2+\frac{\lambda_3v_\chi^2}{2}=0,$$
$$\mu_2^2+\lambda_2v_\chi^2+\frac{\lambda_3v_\rho^2}{2}=0.$$

The $SU(3)_C\times SU(3)_L\times U(1)_N$ breaks down into the SM gauge group following the pattern

$$SU(3)_L\times U(1)_N\xrightarrow{\langle\chi^0\rangle}SU(2)_L\times U(1)_Y\xrightarrow{\langle\rho^0\rangle}U(1)_{\rm EM}, \quad (3.3)$$

where v_ρ can be identified with the SM Higgs VEV v. The left-over of SSB are two neutral scalar bosons and a pair of doubly charged ones $h^{\pm\pm}$ as explained below.

The mass matrix of the neutral scalar bosons in the $\left(R_\chi, R_\rho\right)$ basis is

$$\mathbf{m}_0^2 = \frac{\upsilon_\chi^2}{2}\begin{pmatrix} 2\lambda_2 & \lambda_3 t \\ \lambda_3 t & 2\lambda_1 t^2 \end{pmatrix},$$

where $t = \upsilon_\rho/\upsilon_\chi$. After diagonalization, the mass eigenstates in the limit $\upsilon_\chi \gg \upsilon_\rho$ are

$$h_1 = c_\beta R_\rho - s_\beta R_\chi, \quad h_2 = c_\beta R_\chi + s_\beta R_\rho, \tag{3.4}$$

with masses

$$m_{h_1}^2 = \left(\lambda_1 - \frac{\lambda_3^2}{4\lambda_2}\right)\upsilon_\rho^2, \tag{3.5}$$

$$m_{h_2}^2 = \lambda_2\upsilon_\chi^2 + \frac{\lambda_3^2}{4\lambda_2}\upsilon_\rho, \tag{3.6}$$

where λ_1, $\lambda_2 > 0$ and $c_\beta \equiv \cos\beta \approx 1 - \lambda_3^2\upsilon_\rho^2/(8\lambda_2^2\upsilon_\chi^2)$. The SM Higgs boson h can be recovered in the $s_\beta \to 0$ limit, thus h_1 must be identified with the Higgs boson discovered at the LHC. Since $m_h \simeq 125$ GeV, from Eq. (3.5) we obtain the relation $\lambda_1 - \lambda_3^2/(4\lambda_2) \approx 0.26$ [94]. In the case λ_2, $\lambda_2 < 1$, and $\lambda_3 < \lambda_2$ we obtain $m_{h_1}^2 = \lambda_1\upsilon_\rho^2$, which recovers the SM case and thus $\lambda_1 \approx 0.26$.

In the gauge sector there are two new singly charged gauge bosons $V^\pm$, two doubly charged gauge bosons $U^{\pm\pm}$ and a neutral gauge bosons Z'. They acquire their masses as follows. The would-be Goldstone bosons $\chi^\pm$ are eaten by the singled charged gauge bosons, whereas a linear combination of the doubly charged would-be Goldstone bosons $\rho^{\pm\pm}$ and $\chi^{\pm\pm}$ are absorbed by the doubly charged gauge boson $U^{\pm\pm}$. Also, the orthogonal combination of $\rho^{\pm\pm}$ and $\chi^{\pm\pm}$ gives rise to a physical doubly charged scalar boson pair $h^{\pm\pm}$. Finally, the would-be Goldstone boson I_χ becomes the longitudinal components of the Z' gauge boson. Thus, the masses of the new gauge bosons at leading order at υ_χ are [95]

$$m_{Z'}^2 = \frac{g^2 c_W^2}{3(1-4s_W^2)}\upsilon_\chi^2, \tag{3.7}$$

$$m_{V^\pm}^2 = \frac{g^2}{4}\upsilon_\chi^2, \tag{3.8}$$

$$m_{U^{\pm\pm}}^2 = \frac{g^2}{4}\left(\upsilon_\rho^2 + \upsilon_\chi^2\right). \tag{3.9}$$

As far as the SM gauge bosons are concerned, the would-be Goldstone bosons $\rho^\pm$ and I_ρ endow with masses the Z and $W^\pm$ gauge bosons, respectively.

3.1.2 Gauge and scalar boson couplings to the top quark

The number of new fermions necessary to fill out the $SU(3)_L \times U(1)_N$ multiplets as well as their quantum numbers depend on the particular 331 model version. There are no new leptons in the

RM331, but a new quark is required for each quark triplet. They transform as

$$Q_{iL} = \begin{pmatrix} d_i \\ -u_i \\ J_i \end{pmatrix}_L \sim (3, 3^*, -1/3), \quad i = 1, 2, \quad Q_{3L} = \begin{pmatrix} u_3 \\ d_3 \\ J_3 \end{pmatrix}_L \sim (3, 3, +2/3),$$

with the numbers between parentheses representing the field transformations under the $SU(3)_C \times SU(3)_L \times U(1)_N$ gauge group, whereas J_1, J_2 and J_3 are the new exotic quarks with electric charges $Q_{J_{1,2}} = -4/3e$ and $Q_{J_3} = 5/3e$. Under this representation the theory is anomaly free [91].

Charged currents

In the quark sector, the charged currents relevant for our calculation are given by the following Lagrangian

$$\mathscr{L}_q^{CC} = \frac{g}{\sqrt{2}} \overline{u}_L V_{\rm CKM}^q \gamma^\mu d_L W_\mu^+ + \frac{g}{\sqrt{2}} \overline{J}_{3_L} \gamma^\mu \left(V_L^u\right)_{3a} u_{a_L} V_\mu^+ + \frac{g}{\sqrt{2}} \overline{u}_{l_L} \left(V_L^{u\dagger}\right)_{li} \gamma^\mu J_{i_L} U_\mu^{++} + \text{H.c.},$$

where the family index a runs over 1, 2 and 3, whereas i and l run over 1 and 2. Also $V_{\rm CKM}^q = V_L^{u\dagger} V_L^d$ stands for the Cabibbo-Kobayashi-Maskawa matrix, with the mixing matrices V_L^u (V_L^d) transforming the left-handed up (down) quarks flavor eigenstates into their mass eigenstates. It is assumed that the new quarks are given in their diagonal basis. Note that the doubly charged gauge boson $U^{\pm\pm}$ does not couples to the top quark.

FCNC currents

Since the Z' gauge boson couplings to the quarks are non-universal, flavor changing neutral currents (FCNCs) are induced at the tree level. The corresponding Lagrangian for the up quark sector reads

$$\mathscr{L}_{Z'}^{FCNC} = \frac{g}{2c_W \sqrt{3(1-4s_W^2)}} \left(\sum_{a=1}^{3} \left(\overline{u}'_{aL} \gamma^\mu (1 - 2s_W^2) u'_{aL} \right) + \overline{u}'_{3L} \gamma^\mu (2s_W^2) u'_{3L} \right) Z'_\mu, \tag{3.10}$$

where the up quarks u' are in the flavor basis. It is evident that the above Lagrangian induces FCNC at the tree level after the rotation to the mass eigenstate basis.

On the other hand, the interactions between up quarks and the neutral scalar bosons arise from the lagrangian

$$\mathscr{L}_S = \sum_{i,j=1}^{3} \overline{u}'_{iL} \Gamma^u_{1\,ij} u'_{Rj} h_1 + \overline{u}'_{iL} \Gamma^u_{2\,ij} u'_{jR} h_2 + \text{H.c.}, \tag{3.11}$$

where u' is an up quark triplet $u'^T = (u', c', t')$ and

$$\mathbf{\Gamma}_1^u = \frac{c_\beta}{v_\rho} \mathbf{m}^u - \frac{s_\beta}{v_\chi} \begin{pmatrix} 0 & 0 & 0 \\ 0 & 0 & 0 \\ m_{31}^u & m_{32}^u & m_{33}^u \end{pmatrix},$$

$$\mathbf{\Gamma}_2^u = \frac{s_\beta}{v_\rho}\mathbf{m}^u + \frac{c_\beta}{v_\chi}\begin{pmatrix} 0 & 0 & 0 \\ 0 & 0 & 0 \\ m_{31}^u & m_{32}^u & m_{33}^u \end{pmatrix},$$

with $\mathbf{m}^u$ being the quark mass matrix in the flavor basis [91]. After rotating to the mass eigenstate basis, only the terms proportional to $\mathbf{m}^u$ are diagonalized, whereas the remaining term gives rise to FCNC couplings, which can be written as

$$\mathscr{L}_S^{FCNC} = \sum_{i,j=1}^{3}\left(-s_\beta \overline{u}_{iL}{\eta^u}_{ij}u_{jR}h_1 + c_\beta \overline{u}_{iL}{\eta^u}_{ij}u_{jR}h_2\right) + \text{H.c.}, \tag{3.12}$$

where

$$\boldsymbol{\eta}^u = \mathbf{V}_L^u \begin{pmatrix} 0 & 0 & 0 \\ 0 & 0 & 0 \\ \frac{m_{31}^u}{v_\chi} & \frac{m_{32}^u}{v_\chi} & \frac{m_{33}^u}{v_\chi} \end{pmatrix} (\mathbf{V}_R^u)^\dagger .$$

Through the parametrization given in [96] for the $\mathbf{V}_{L,R}^{u,d}$ mixing matrices it is possible to obtain numerical values for the entries of the $\boldsymbol{\eta}^{u,d}$ matrix. Under this framework $m_{31}^u = 0$, $m_{32}^u = 0$, and $m_{33}^u = m_t$.

3.2 CMDM and CEDM of the top quark in the RM331

Apart from the pure SM contributions, at the one-loop level there are new contributions to the CMDM of the top quark arising in both the gauge and scalar sectors of the RM331. The corresponding Feynman diagrams are depicted in Fig. 4.2. In the gauge sector the new contributions arise from the neutral Z' gauge boson, which are induced by both diagonal and non-diagonal couplings. There are also a new contribution from the singly-charged gauge boson $V^\pm$, which is accompanied by the new exotic quark J_3. As already noted, the doubly-charged gauge boson $U^{\pm\pm}$ does not couples to the top quark, thus there is no contribution from this gauge boson to the top quark CMDM and CEDM. As for the scalar sector, there are new contributions from the neutral scalar bosons h_1 and h_2, which in fact are the novel contributions from the RM331 as they are absent in other 331 model versions. The SM-like Higgs boson h_1 yields new contributions arising from its FCNC couplings, which are induced at the tree-level, but also from its diagonal coupling, which has a small deviation from its SM value. As for the new Higgs boson h_2, it also contributes via both diagonal and non-diagonal couplings. We would like to point out that such scalar contributions are absent in the 331 model studied in Ref. [14], where the on-shell CMDM of the top quark was calculated. Even more, as long as complex FCNC couplings are considered, there are non-vanishing contributions to the CEDM. This class of contributions has also not been studied before in the context of 331 models.

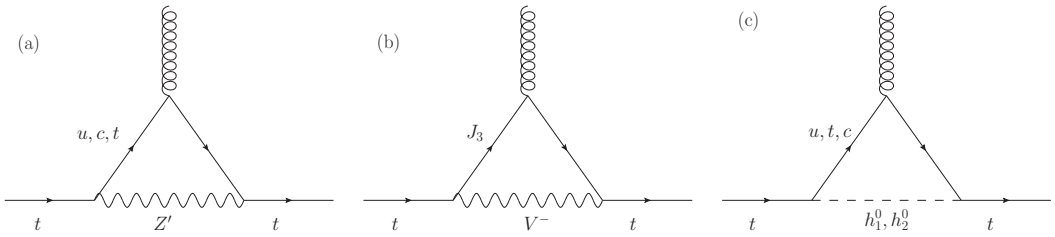

Figure 3.1: New one-loop contributions of the RM331 to the CMDM and CEDM of the top quark in the unitary gauge. In the conventional linear R_ξ gauge there are additional Feynman diagrams where the gauge bosons are replaced by their associated Goldstone bosons.

We are interested in the off-shell CMDM and CEDM of the top quark. Since off-shell Green functions are not associated with an S-matrix element, they can be plagued by pathologies such as being gauge non-invariant, gauge dependent, ultraviolet divergent, etc. Along these lines, the pinch technique (PT) was meant to provide a systematic approach to construct well-behaved Green functions [32], out of which valid observable quantities can be extracted. It was later found that there is an equivalence at least at the one-loop level between the results found via the PT and those obtained through the background field method (BFM) via the Feynman gauge [33]. This provides a straightforward computational method to obtain gauge independent Green functions. It is thus necessary to verify whether the RM331 contributions to the CMDM and CEDM of quarks are gauge independent for $q^2 \neq 0$. Nevertheless, we note that from the Feynman diagrams of Fig. 4.2, the gauge parameter ξ only enters into the amplitudes of the Feynman diagrams (a) and (b) via the propagators of the gauge bosons and their associated would-be Goldstone bosons. Those kind of diagrams have an amplitude that shares the same structure to those mediated by the electroweak gauge bosons Z and W in the SM, which are known to yield a gauge independent contribution to the CMDM for an off-shell gluon when the contribution of their associated would-be Goldstone bosons are added up. See for instance Ref. [48], where we calculate the electroweak contribution to the CMDM of quarks in the conventional linear R_ξ gauge and verify that the gauge parameter ξ drops out. Furthermore, the dipole form factors cannot receive contributions from self-energy diagrams, which are required to cancel gauge dependent terms appearing in the monopolar terms via the PT approach. Thus both the CMDM and CEDM must be gauge independent for an off-shell gluon and thus valid observable quantities.

Below we present the analytical results of our calculation in a model-independent way, out of which the results for the RM331 and other SM extensions would follow easily. The corresponding coupling constants for the RM331 are presented in Appendix A.2. For the loop integration we used the Passarino-Veltman reduction method and for completeness our calculation was also performed by Feynman parametrization via the unitary gauge, which provides alternative expressions to cross-check the numerical results. The Dirac algebra and the Passarino-Veltman reduction were done in Mathematica with the help of Feyncalc [35] and Package-X [36].

3.2.1 New gauge boson contributions

We first consider the generic contribution of a new gauge boson V with the following interaction to the quarks

$$\mathscr{L}^{Vqq'} = \frac{g}{c_W}\overline{q}\left(g_V^{Vqq'} - g_A^{Vqq'}\gamma^5\right)\gamma_\mu q' V^\mu + \text{H.c.}, \tag{3.13}$$

where the coupling constants $g_{V,A}^{Vqq'}$ are taken in general as complex quantities. By hermicity they should obey $g_{V,A}^{Vqq'} = g_{V,A}^{Vq'q*}$.

The above interaction gives rise to a new contribution to the quark CMDM and CEDM via a Feynman diagram similar to that of Fig. 4.2(a). The corresponding contribution to the quark CMDM can be written as

$$\hat{\mu}_q^V(q^2) = \frac{G_F m_W^2}{2\sqrt{2}\pi^2 r_V^2 c_W^2} \sum_{q'} \left| g_V^{Vqq'} \right|^2 \mathscr{V}_{qq'}^V(q^2) + \left(\begin{array}{c} g_V^{Vqq'} \to g_A^{Vqq'} \\ m_q' \to -m_q' \end{array} \right), \tag{3.14}$$

where we introduced the auxiliary variable $r_a = m_a/m_q$ and the $\mathscr{V}_{qq'}^V(q^2)$ function is presented in Appendix A.4 in terms of Feynman parameter integrals and Passarino-Veltman scalar functions. The second term of the right-hand side stands for the first term with the indicated replacements. As for the contribution to the quark CEDM, it can arise as long as there are flavor changing complex couplings and is given by

$$\hat{d}_q^V(q^2) = \frac{G_F m_W^2}{\sqrt{2}\pi^2 r_V^2 c_W^2} \sum_{q'} \mathrm{Im}\left(g_V^{Vqq'} g_A^{Vqq'*} \right) \widetilde{\mathscr{D}}_{qq'}^V(q^2), \tag{3.15}$$

where again the $\mathscr{D}_{qq'}^V(q^2)$ function is presented in Appendix A.4.

From Eqs. (3.14) y (3.15) we can obtain straightforwardly the contributions to the quark CMDM and CEDM of the neutral gauge boson Z' and the singly charged gauge boson $V^{\pm}$ after replacing the coupling constants and the gauge boson masses.

3.2.2 New scalar boson contributions

Following the same approach as above, we now present the generic contribution to the quark CMDM and CEDM arising from FCNC mediated by a new scalar boson S, which arise from the Feynman diagram of Fig 4.2(c). We consider an interaction of the form

$$\mathscr{L}^{Sqq'} = -\frac{g}{2}\overline{q}\left(G_S^{Sqq'} + G_P^{Sqq'}\gamma^5 \right) q' S + \text{H.c.} \tag{3.16}$$

The above scalar interaction leads to the following contribution to the quark CMDM

$$\hat{\mu}_q^S(q^2) = -\frac{G_F m_W^2}{8\sqrt{2}\pi^2} \sum_{q'} \left| G_P^{Sqq'} \right|^2 \mathscr{P}_{qq'}^S(q^2) + \left(\begin{array}{c} G_P^{Sqq'} \to G_S^{Sqq'} \\ m_q' \to -m_q' \end{array} \right), \tag{3.17}$$

whereas the corresponding contribution to the quark CEDM is given by

$$\hat{d}_q^S(q^2) = \frac{G_F m_W^2}{4\sqrt{2}\pi^2} \sum_{q'} \mathrm{Im}\left(G_S^{Sqq'} G_P^{Sqq'*} \right) \widetilde{\mathscr{D}}_{qq'}^S(q^2), \tag{3.18}$$

where the $\mathscr{P}_{qq'}^S(q^2)$ and $\widetilde{\mathscr{D}}_{qq'}^S(q^2)$ functions are presented in Appendix A.4.

From the above expression we can obtain the contribution of the new scalar Higgs boson of the RM331 as well as the contribution of the SM Higgs boson, which in the RM331 has tree-level FCNC couplings.

3.3 Numerical analysis and discussion

We now turn to the numerical analysis. The coupling constants that enter into the Feynman rules and are necessary to evaluate the CMDM and CEDM of the top quark [c.f. Eqs. (3.13) through (3.18)] are presented in Tables A.1 and A.2 of Appendix A.2. We note that these couplings depend on several free parameters, such as the mass parameter m_{33}^u, the VEV υ_χ, the parameters of the scalar potential λ_2 and λ_3, as well as the entries of the matrices $\mathbf{V}_L^u$, $\mathbf{K}_L$ and $\boldsymbol{\eta}^u$. To obtain an estimate of the contributions of the RM331 to the CMDM and CEDM of the top quark we need to discuss the most up-to-date constrains on these parameters from current experimental data.

3.3.1 Constraints on the parameter space

Heavy particle masses

As already mentioned, the mass parameter m_{33}^u can be identified with the top quark mass [91], whereas the VEV υ_χ determines the masses of the heavy gauge bosons and the heavy quark J_3. As for the mass of the new scalar boson m_{h_2}, it is determined by the parameters λ_2 and λ_3, along with the VEV υ_χ, which also determine the mixing angle s_β.

We will first discuss the current indirect constraints on the heavy neutral gauge boson masses. From the muon $g-2$ discrepancy, the following constraint was obtained $\upsilon_\chi \geq 2$ TeV [92], from which bounds on the heavy gauge boson masses follow. Nevertheless, there are also indirect constrains obtained through the experimental data on $B^0-\overline{B}^0$ oscillations. The RM331 contribution to Δm_B arises from FCNC couplings mediated by the Z' gauge boson and the h_1 and h_2 scalar bosons [91, 95], then using the parametrization of [96], the experimental limit on Δm_B leads to the following bounds $m_{Z'} \gtrsim 3.3$ TeV, $m_{V^\pm} \gtrsim 0.33$ TeV and $m_{h_2} \gtrsim 0.34$ TeV [91]. Similar limits have been imposed using de mass difference of the $K^0-\overline{K}^0$ and $D-\overline{D}^0$ systems [95]. On the other hand, the current experimental bounds on the masses of new neutral and charged heavy gauge bosons from collider searches are model dependent [94]. At the LHC, the ATLAS and CMS Collaborations have searched for an extra charged gauge boson W' at $\sqrt{s}=13$ TeV via the decay modes $W' \to \ell\nu_\ell$ [97, 98] and $W' \to qq'$. The most stringent bounds are obtained for a W' gauge boson with SM couplings (sequential SM). The respective lower bounds on $m_{W'}$ are 6.0 TeV (5.1 TeV) for the $W' \to e\nu_e$ ($W' \to \mu\nu_\mu$) decay channel, whereas for the decay $W' \to qq'$ the corresponding bound is less stringent, of the order of 4 TeV [99, 100]. As far as an extra neutral gauge boson Z' is concerned, the search at the LHC at $\sqrt{s}=13$ TeV via its decays into a lepton pair has been useful to impose the lower limit $m_{Z'} \geq 4.5,5$ TeV for a Z' gauge boson model arising in the sequential SM and in an E_6-motivated Gran Unification model [101, 102]. Along these lines, it has been pointed out recently that the LHC might be able to constrain the mass of the heavy Z' boson up to the 5 TeV level in several 331 models [103, 104, 105]. Although these bounds are model dependent and relies on several assumptions, if we consider the conservative value of 5 TeV for the gauge boson masses we obtain a lower constraint on υ_χ of the order of 10 TeV. Thus, we will use this value in our analysis to be consistent with experimental constraints and limits from FCNC couplings.

As far as direct constraints on the mass of exotic quarks are concerned, the ATLAS and CMS Collaborations have used the $\sqrt{s}=13$ TeV data to search for vector-like quarks with electric charge of 5/3 via its decay into a top quark and a W gauge boson, with the final state consisting of a single charged lepton (muon or electron), missing transverse momentum, and several jets. A mass exclusion limit up to 1.6 TeV is obtained depending on the properties of the vector-like

quark [106, 107, 108]. We will thus use $m_{J_3} = 2$ TeV to be consistent with the experimental bound.

Mixing angle s_β and parameters $\lambda_{2,3}$

According to Eq. (3.5) the mass of the SM-like Higgs boson receives new corrections through the λ_2 and λ_3 parameters. As discussed above, the SM case is recovered when $\lambda_1 \approx 0.26$ and $\lambda_3 < \lambda_2 < 1$, thus the new corrections to m_{h_1} must lie within the experimental error of the SM Higgs boson mass $m_h = 125.10 \pm 0.14$ GeV [94]. This allows one to constrain the λ_2 and λ_3 parameters, which in turn translates into constraints on s_β and m_{h_2} once the v_χ value is fixed. Again we take a conservative approach and only consider the experimental uncertainty in the Higgs boson mass, whereas theoretical uncertainties from higher order corrections are not taken into account. We observe in Fig. 3.2 the allowed regions in the planes λ_2 vs λ_3 and s_β vs m_{h_2} consistent with the experimental error of the Higgs boson mass at 95% C.L. We note that for a given λ_2, λ_3 must be about one order of magnitude below. In our calculation we use $\lambda_2 = 0.9$ and $\lambda_3 = 0.06$, though there is no great sensitivity of the top quark CMDM and CEDM to mild changes in the values of these parameters. In addition, we find that values ranging from 0.002 to 0.013 are allowed for s_β provided that $v_\chi \geq 10$ TeV and $m_{h_2} \gtrapprox 300$ GeV, which is consistent with recent searches for new neutral scalar bosons at the LHC [94].

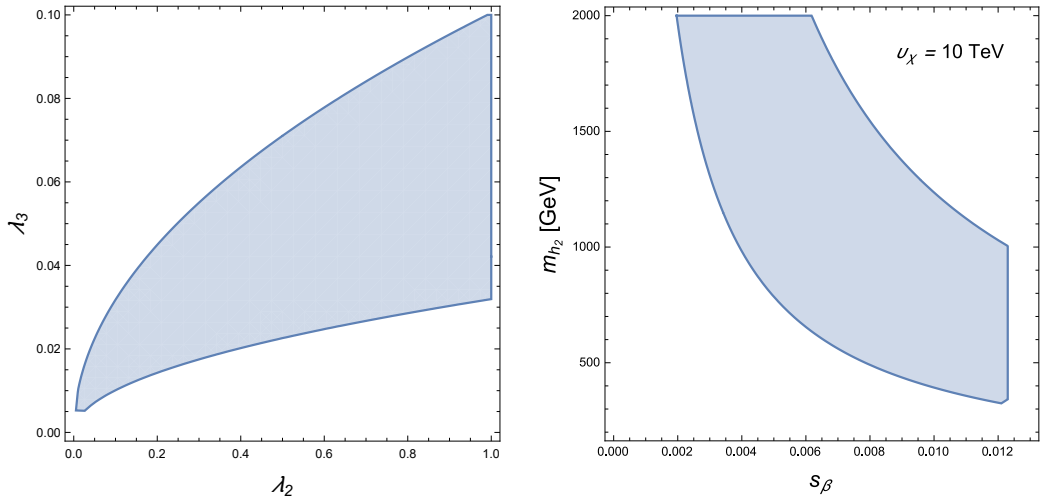

Figure 3.2: Allowed areas in the planes λ_3 vs λ_2 and s_β vs m_{h_2} in agreement with the experimental error of the Higgs boson mass $m_h = 125.10 \pm 0.14$ GeV [94] at 95% C.L. We consider $\lambda_1 \approx 0.26$ and $\lambda_3 < \lambda_2 < 1$, which yield the SM limit.

Mixing matrices

As for the mixing matrices, we can obtain the absolute values for the entries of the matrices $\mathbf{V}_L^u$, $\mathbf{K}_L$ and $\boldsymbol{\eta}^u$. The entries of the last matrix are given in terms of v_χ, s_β and the m_{ij}^q matrix elements and their values are obtained following the parametrization used in [96]. In general $\mathbf{K}_L$ and $\boldsymbol{\eta}^u$ are in terms of the entries of $\mathbf{V}_L^u$ and $\mathbf{V}_R^u$, the complex matrices that diagonalize the mass matrices of up quarks. These matrices can be assumed to be triangular, then using the experimental data on quark masses and the mixing angles it is possible to obtain values of their entries [109]. It is also assumed that the only non-negligible mixing is that arising between the

third and second fermion families. Furthermore, since the CP violation phases are expected to be very small, we take a conservative approach and assume complex phases of the order of 10^{-3}.

We present in Table 3.1 a summary of the numerical values we will use in our numerical evaluation.

Table 3.1: Values of the parameters used in our evaluation of the CMDM and CEDM of the top quark in the RM331. For the entries of the matrices $\mathbf{V}_L^u$, $\mathbf{K}_L$ and $\boldsymbol{\eta}^u$ we use the values obtained in [91] using the parametrization of [96], where the mass parameter m_{33}^u is identified with the top quark mass. We use λ_2 and λ_3 values allowed by the experimental error in the Higgs boson mass and also assume that the only non-negligible mixing is that arising between the third and second fermion families.

Parameter	Value
$\lvert(K_L)_{tc}\rvert$	6.4×10^{-4}
$\lvert V_{33}^u\rvert$	1
$\lvert\eta_{tc}^u\rvert$	6.4×10^{-4}
$\lvert\eta_{ct}^u\rvert$	4.62×10^{-6}
m_{33}^u	m_t
υ_χ	10 TeV
s_β	10^{-2}
m_{h_2}	300 GeV
$\phi_{\eta_{tc}^u}$, $\phi_{\eta_{ct}^u}$	10^{-3}

3.3.2 Top quark CMDM

As already mentioned, in the RM331 there are new contributions to the off-shell top quark CMDM $\mu_t(q^2)$ arising from the heavy gauge bosons Z' and $V^\pm$ as well as the neutral scalar bosons h_1 and h_2. Below we will use the notation A_{BC} for the contribution of particle A due to the ABC coupling. Thus, for instance Z'_{tc} will denote the contribution of the loop with the Z' gauge boson due to the $Z'tc$ coupling. Since we would like to assess the magnitude of the new physics contributions to $\hat{\mu}_t(q^2)$, we will extract from our calculation the pure SM contributions. Thus, apart from the contribution due to the tree-level FCNCs of the SM-like Higgs boson h_1, we only consider the contribution arising from the small deviation of the diagonal coupling h_1tt from the SM htt coupling. This contribution will be denoted by δh_{1tt}.

We will examine the behavior of the CMDM of the top quark as a function of $\|q\| \equiv \sqrt{|q^2|}$, where q is the gluon four-momentum. In the left plot of Fig. 3.3 we show the real part of the partial contributions to $\hat{\mu}_t(q^2)$ as a function of $\|q\|$ for the parameter values of Table 3.1, whereas the real and imaginary parts of the total contribution are shown in the right plot. In general there is little dependence of Re $\left[\hat{\mu}_t(q^2)\right]$ on $\|q\|$, except for the δh_{1tt}, h_{2tt} and h_{2tc} contributions, which have a change sign. We also note that the $V_{tJ_3}^\pm$ contribution is the largest one, whereas the remaining contributions are negligible, with the h_{1tc} contribution being the smallest one. Thus the curve for the real part of the total contribution seems to overlap with that of the $V_{tJ_3}^\pm$ contribution, though the former shows a small peak at $\|q\| \simeq 2m_t$. This can be explained by the peak appearing in the δh_{1tt} contribution, which can be as large as the $V^\pm{}_{tJ_3}$ contribution for $\|q\| \simeq 2m_t$. We conclude that $\hat{\mu}_t(q^2)$ can have a real part of the order of 10^{-5}.

As far as the imaginary parts of the partial contributions to $\hat{\mu}_t(q^2)$, they are several orders

of magnitude smaller than the corresponding real parts. As observed in the right plot of Fig. 3.3, the imaginary part of the total contribution is negligible for $\|q\| \leqslant 2m_t$, but increases up to about 10^{-6} around $\|q\| = 400$ GeV, where it starts to decrease up to one order of magnitude as $\|q\|$ increases up to 1 TeV.

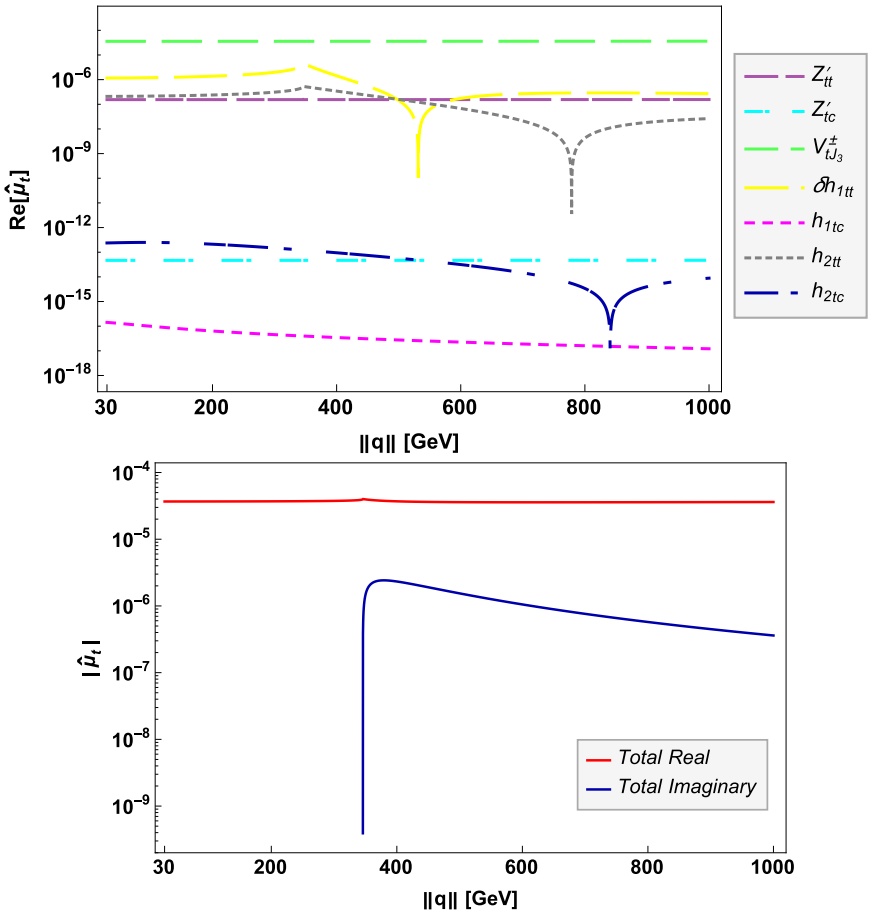

Figure 3.3: Real part of the partial contributions of the RM331 to the top quark CMDM (left plot) as a function of $\|q\| \equiv \sqrt{|q^2|}$ for the parameter values of Table 3.1. The real and imaginary parts of the total contribution are shown in the right plot.

Analogue plots to those of Fig. 3.3, but now for the behavior of $\hat{\mu}_t(q^2)$ as a function of v_χ for $\|q\| = 500$ GeV and the parameter values of Table 3.1, are shown in Fig. 3.4. In this case we observe that the real parts of the partial contributions to $\hat{\mu}_t(q^2)$ show a variation of about one order of magnitude when v_χ increases from 10 TeV to 20 TeV. As already noted, the $V^{\pm}_{tJ_3}$ contribution yields the bulk of the total contribution to $\hat{\mu}_t$, whose imaginary part is slightly larger than its real part. Therefore both real and imaginary contributions of the RM331 to the top quark CMDM can be as large as 10^{-5}.

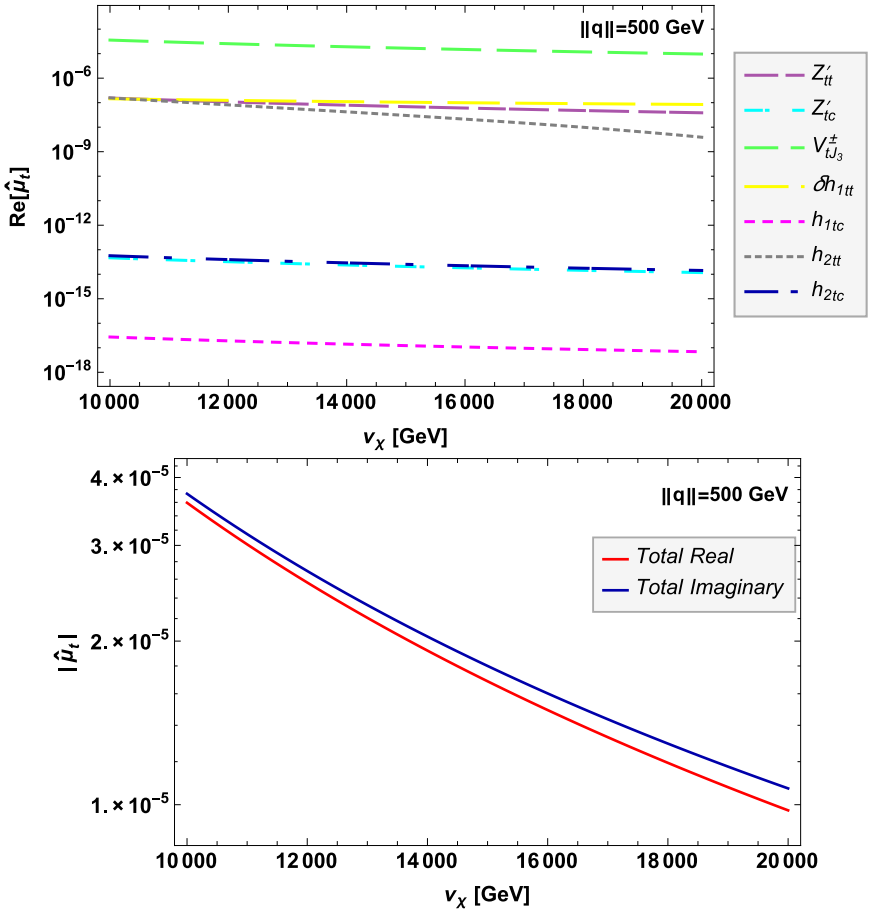

Figure 3.4: The shames as in Fig. 3.3 but for the contributions of the RM331 to the top quark CMDM as functions of v_χ for $\|q\|$=500 GeV. For the remaining parameters we use the values of Table 3.1.

In summary, for $v_\chi \geqslant 10$ TeV the real part of the the RM331 new contribution to $\hat{\mu}_t(q^2)$ would be three orders of magnitude smaller than the real part of the SM electroweak contribution [48], whereas its imaginary part can be as large than its real part. In general there is no appreciable variation in the magnitude of $\hat{\mu}_t$ for mild changes in the parameters of Table 3.1. Although $\hat{\mu}_t(q^2)$ can be of similar size than the SM electroweak prediction for $v_\chi \leq 10$ TeV, such values are disfavored by the current constrains on the heavy gauge bosons masses. Finally, we note that the RM331 can give a contribution larger than the ones predicted by other extension models where a new neutral Z gauge boson is predicted [26]. The real and imaginary parts of the top quark CMDM are of order $10^{-6} - 10^{-7}$ and $10^{-10} - 10^{-11}$ respectively in such models.

3.3.3 Top quark CEDM

A potential new source of CP violation can arise in the RM331 through the FCNC couplings mediated by the neutral scalar bosons, which are proportional to the entries of the non-symmetric complex mixing matrix $\boldsymbol{\eta}^u$ [91], thereby allowing the presence of a non-zero CEDM, which is absent in other 331 models. Thus, it is a novel prediction of the RM331.

There are only two partial contributions to the top quark CEDM in the RM331, thus we only analyze the behavior of the total contribution. We show in Fig. 3.5 the contour lines of the real part (left plot) and the imaginary part (right plot) of $d_t(q^2)$ in the υ_χ vs $\|q\|$ plane for the parameter values of Table 3.1. We have found that the new scalar boson h_2 yields the dominant contribution to $d_t(q^2)$, whose real (imaginary) part can be as large as 10^{-19} (10^{-20}), whereas the contribution from the h_1 scalar boson is three or more orders of magnitude below. We also observe that the real part of $d_t(q^2)$ decreases as υ_χ and $\|q\|$ increase, while the imaginary part remains almost constant. For $\|q\| \geqslant 600$ GeV, the RM331 contribution to the CEDM of the top quark is expected to be below the 10^{-20} level, which seems to be much smaller than the values predicted in other extension models [26], where the real and imaginary parts are of order $10^{-7} - 10^{-8}$ and $10^{-12} - 10^{-13}$ respectively. In the range 2 TeV$\leqslant \upsilon_\chi \lesssim 10$ TeV our results for $d_t(q^2)$ are enhanced by one order of magnitude, but as already noted, this interval is disfavored by current constraints.

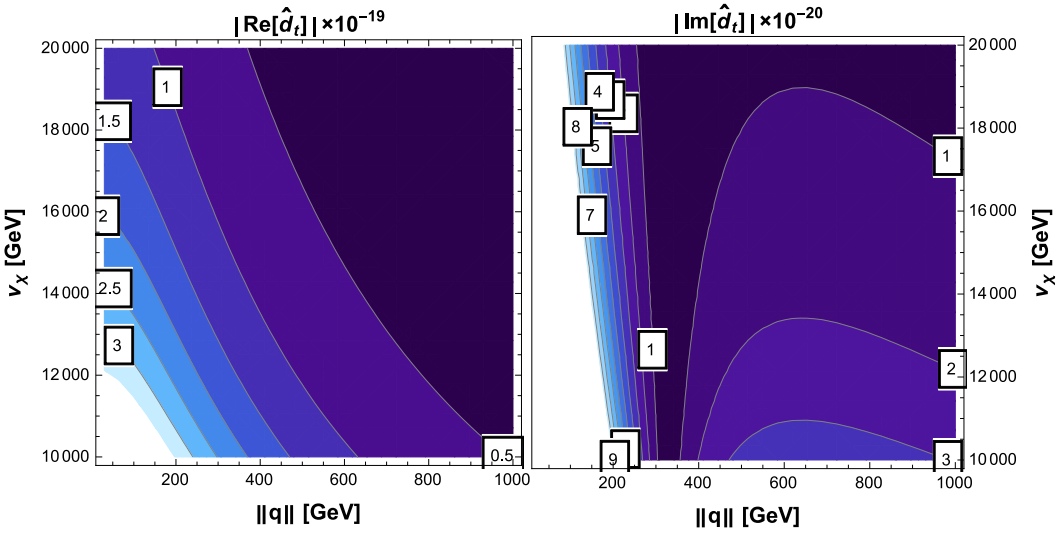

Figure 3.5: Real part (left plot) and imaginary part (right plot) of the total contribution to the CEDM of the top quark in the RM331 in the plane υ_χ vs $\|q\|$. We use the parameter values of Table 3.1.

For comparison, a compilation of the predictions of several extension models of the top quark CMDM and CEDM for $q^2 = 0$ is presented in Table 3.2. We would like to stress that to our knowledge there is no previous estimate of the top quark CEDM in 331 models. We also note that though these values seem to be much larger than the results obtained for $q^2 \neq 0$ in the RM331, the dipole form factors are expected to decrease as q^2 increases. Such a behavior is indeed observed in the SM case [48], where the magnitude of $\hat{a}_t$ decreases as $\|q\|$ increases.

3.4 Remarks

We have presented a calculation of the one-loop contributions to the CMDM and CEDM, $\hat{\mu}_t(q^2)$ and $\hat{d}_t(q^2)$, of the top quark in the framework of the RM331, which is an economic version of the so-called 331 models with a scalar sector comprised by two scalar triplets only. We have

Table 3.2: Predictions of the CMDM and CEDM of the top quark in several extension models at $q^2 = 0$.

Model	$\hat{a}_t$	$\hat{d}_t$
SM	10^{-2} [48]	
THDMs	10^{-3}–10^{-1} [15]	10^{-5} [110, 15]
4GTHDM	10^{-2}–10^{-1} [13]	10^{-5}–10^{-4} [13]
331	10^{-5} [14]	
Technicolor	10^{-2} [14]	
Extra dimensions	10^{-3} [14]	
Little Higgs model	10^{-6} [17]	
MSSM	10^{-1} [18]	$10^{-5} - 10^{-4}$ [111]
Unparticle model	10^{-2} [19]	
Vector-like multiplets		10^{-4} [20]

considered the general case of an off-shell gluon as it has been pointed out before that the QCD contribution to $\hat{\mu}_t(q^2)$ is infrared divergent and the CMDM has no physical meaning for $q^2 = 0$. We argue that the results are gauge independent for $q^2 \neq 0$ and represent valid observable quantities since the structure of the gauge boson contributions are analogue to those arising in the SM. To our knowledge, no previous calculations of the off-shell CMDM and CEDM of the top quark have been presented before in the context of 331 models.

Apart from the usual SM contributions, in the RM331, the CMDM of the top quark receives new contributions from two new heavy gauge bosons Z' and $V^{\pm}$ as well as one new neutral scalar boson h_2, along with a new contribution from the neutral scalar boson h_1, which must be identified with the 125 GeV scalar boson detected at the LHC. This model also predicts tree-level FCNCs mediated by the Z' gauge boson and the two neutral scalar bosons h_1 and h_2, which at the one-loop level can also give rise to a non-vanishing CEDM provided that there is a CP-violating phase. The analytical results are presented in terms of both Feynman parameter integrals and Passarino-Veltman scalar functions, which are useful to cross-check the numerical results.

We present an analysis of the region of the parameter space of the model consistent with experimental data and evaluate the CMDM and CEDM of the top quark for parameter values still allowed. It is found that the new one-loop contributions of the RM331 to the real (imaginary) part of $\hat{\mu}_t(q^2)$ are of order of 10^{-5} (10^{-6}), which are larger than the predictions of other SM extensions [26], with the dominant contribution arising from the $V^{\pm}$ gauge boson, whereas the remaining contributions are considerably smaller. It is also found that there is little dependence of $\mu_t(q^2)$ on $\|q\|$ in the 30-1000 GeV interval for a mass m_V of the order of a few hundreds of GeV. As far as the CEDM of the top quark is concerned, it is mainly induced by the loop with h_2 exchange and can reach values of the order of 10^{-19} for realistic values of the CP-violating phases. Such a contribution is smaller than the ones predicted by other SM extensions [26].

Chapter 4

Contributions to ZZV^* $(V = \gamma, Z, Z')$ couplings from CP violating flavor changing couplings

Trilinear gauge boson couplings (TGBCs) have long been the subject of considerable interest both theoretically and experimentally. In the experimental area, constraints on the corresponding form factors were first obtained at the LEP [112, 113, 114] and the Tevatron [115, 116, 117] colliders, whereas the current bounds were extracted from the LHC data at 8 TeV [118, 119, 120] and 13 TeV [121, 122, 123] by the ATLAS and CMS collaborations. Among TGBCs are of special interest the ones involving only neutral gauge bosons, namely, the trilinear neutral gauge boson couplings (TNGBCs) ZZV^* and $Z\gamma V^*$ ($V = Z$,γ), which can only arise up to the one-loop level in renormalizable theories and have been widely studied within the standard model (SM) and beyond. The SM contributions to TNGBCs were studied in Refs. [124, 125], whereas new physics contributions have been studied within several extension models, such as the minimal supersymmetric standard model (MSSM)[124, 125, 126], the CP-violating two-Higgs doublet model (2HDM) [127, 128, 129], models with axial and vector fermion couplings [127], models with extended scalar sectors [130], and also via the effective Lagrangian approach [131]. In the theoretical side, the phenomenology of TNGBCs at particle colliders was widely studied long ago [132, 133, 134, 135, 136, 137, 126, 138] and also has been of interest lately [139, 140, 141, 142]. Even more, study of the potential effects of TNGBCs at future colliders has been the source of renewed interest very recently [143, 144, 145, 146, 147]. TNGBCs, which require one off-shell gauge boson at least to be non-vanishing due to Bose statistics, are induced through dimension-six and dimension-eight operators [124, 131, 148, 149] and can be parametrized in a model independent way by two CP-even and two CP-odd form factors. In the SM, only the CP-conserving form factors arise at the one-loop level of perturbation theory, whereas the CP-violating ones are absent at this order and require new sources of CP violation [124, 148]. In the SM, CP violation is generated via the Cabbibo-Kobayashi-Maskawa (CKM) mixing matrix, though the respective amount is not enough to explain the asymmetry between matter and anti-matter in the universe, *i.e.* the so-called baryogenesis problem. Therefore, new sources of CP violation are required, which is in fact one of the three Sakharov's conditions to explain the baryon asymmetry of the universe [150]. In this work we are interested in the study of possible CP-

violating effects in the TNGBCs via tree-level flavor changing neutral currents (FCNCs) mediated by the Z gauge boson [151], which are forbidden in the SM but can arise in several SM extensions [152, 153]. The possible effects of Z-mediated FCNC couplings on CP-conserving TNGBCs have already been studied [124], nevertheless, possible contributions to the CP-violating ones have not been reported yet to our knowledge. These new contributions are worth studying as they could shed some light in the path to a more comprehensive SM extension.

Possible evidences of new heavy gauge boson have been searched for at the LHC by the CMS collaboration [154], which has been useful to set bounds on the masses of new neutral and charged heavy vector bosons. Such particles are predicted by a plethora of SM extensions with extended gauge sector, for instance, little Higgs models [155, 156], 331 models [157], left-right symmetric models [158], etc. Some of these models allow tree-level FCNCs mediated by a new neutral gauge boson, denoted from now on by Z' [159], which means that CP-violating contributions to VZZ'^* couplings ($V = \gamma$, Z) are possible. To our knowledge TNGBCs with new neutral bosons have not received much attention in the literature up to now, though decays of the kind $Z' \to VZ$ ($V = \gamma$,Z) [160] and $Z' \to \gamma A_H$ [161] were already studied. Here A_H stands for a heavy photon.

In this chapter we present a study of the one-loop contributions to the most general TNGBCs ZZV^* ($V = \gamma$, Z, Z') arising from a generic model allowing tree-level FCNCs mediated by the SM Z gauge boson and a new heavy neutral gauge boson Z'. The rest of this presentation is as follows. In Sec. II we present a short review of the analytical structure of TNGBCs along with the theoretical framework of the FCNCs Z and Z' couplings via a model independent approach. Section III is devoted to the calculation of the one-loop contributions to the CP-conserving and CP-violating ZZV^* ($V = \gamma$, Z, Z') couplings, for which we use the Passarino-Veltman reduction scheme. In Sec. IV we present the numerical analysis and discussion, whereas the conclusions and outlook are presented in Sec. V.

4.1 Theoretical framework

4.1.1 Trilinear neutral gauge boson couplings ZZV ($V = \gamma$, Z, Z')

We now turn to discuss the Lorentz structure of TNGBCs, which are induced by dimension-six and dimension-eight operators. In this work we only focus on the contribution of dimension-six operators as it is expected to be the dominant one. In particular, the TNGBC ZZV^* ($V = \gamma$, Z) coupling can be parametrized by two form factors:

$$\Gamma^{\alpha\beta\mu}_{ZZV^*}(p_1,p_2,q) = \frac{i(q^2-m_V^2)}{m_Z^2}\Big[f_4^V\left(q^\alpha g^{\mu\beta}+q^\beta g^{\mu\alpha}\right) - f_5^V\,\epsilon^{\mu\alpha\beta\rho}\,(p_1-p_2)_\rho\Big], \tag{4.1}$$

where we have followed Ref. [124], with the notation for the gauge boson four-momenta being depicted in Fig. 4.1. From Eq. (4.1) it is evident that when the V^* gauge boson becomes on-shell ($q^2 = m_V^2$), $\Gamma^{\alpha\beta\mu}_{ZZV^*}(p_1,p_2,q)$ vanishes, which is due to Bose statistics and angular momentum conservation. The general form of this vertex for three off-shell gauge bosons can be found in [148, 131]. The form factor f_5^V is CP-conserving, whereas f_4^V is CP-violating. The former is the only one induced at the one-loop level in the SM via a fermion loop since $W^\pm$ boson loops give vanishing contributions [124]. It was found that f_5^V decreases quickly as q^2 becomes large [124]. The current bounds on the form factors f_4^V and f_5^V ($V = Z, \gamma$) were obtained by the CMS collaboration at $\sqrt{s} = 13$ TeV [123]:

$$-0.00066 < f_4^Z < 0.0006, \tag{4.2}$$
$$-0.00055 < f_5^Z < 0.00075, \tag{4.3}$$
$$-0.00078 < f_4^\gamma < 0.00071, \tag{4.4}$$
$$-0.00068 < f_5^\gamma < 0.00075. \tag{4.5}$$

These constrains are of the order of the SM prediction for the CP-conserving form factors [124]. Thus, corrections to the form factors f_5^V and f_4^V ($V = \gamma,\, Z$) from models of new physics might play an important role.

As far as TNGBCs with new gauge bosons are concerned, they remain almost unexplored. For our purpose, following Eq. (4.1), we will parametrize the ZZZ'^* coupling as follows

$$\Gamma^{\alpha\beta\mu}_{ZZZ'^*}(p_1,p_2,q) = \frac{iq^2}{m_{Z'}^2}\Big[f_4^{Z'}\left(q^\alpha g^{\mu\beta}+q^\beta g^{\mu\alpha}\right) - f_5^{Z'}\epsilon^{\mu\alpha\beta\rho}\left(p_1-p_2\right)_\rho\Big], \tag{4.6}$$

where we only consider the contributions of the dimension-six operators given in Ref. [148] and have replaced the electromagnetic $F_{\mu\nu}$ tensor by $Z'_{\mu\nu} = \partial_\mu Z'_\nu - \partial_\nu Z'_\mu$ in the operator basis that induce the $ZZ\gamma^*$ vertex. We also set the energy scale that corrects the operator dimension to the new physics scale $m_{Z'}$. Of course, the form factor $f_4^{Z'}$ ($f_5^{Z'}$) is CP violating (CP-conserving). We also note in Eq. (4.6) that this TNGBC does not vanish for an on-shell Z' gauge boson. In fact, the Z' gauge boson can decay into a Z gauge boson pair if kinematically allowed. We will see below that our calculation is consistent with the Lorentz structure presented in Eq. (4.6).

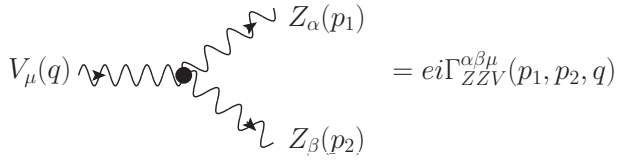

Figure 4.1: Nomenclature for the TNGBCs ZZV^* ($V = \gamma,\, Z,\, Z'$).

4.2 Derivation of the couplings

4.2.1 Vertex ZZZ^*

The six-dimension Lagrangian that induces the ZZZ^* can be written as

$$\mathscr{L}_{ZZZ^*} = \frac{e}{m_Z^2}\left[-f_4^Z(\partial_\mu Z^{\mu\beta})Z_\alpha(\partial^\alpha Z_\beta) + f_5^Z(\partial^\sigma Z_{\sigma\mu})\tilde{Z}^{\mu\beta}Z_\beta\right], \tag{4.7}$$

where

$$\tilde{Z}_{\mu\nu} = \frac{1}{2}\epsilon_{\mu\nu\sigma\rho}Z^{\sigma\rho}, \quad Z_{\mu\nu} = \partial_\mu Z^\nu - \partial_\nu Z^\mu, \tag{4.8}$$

then

$$\begin{aligned}\tilde{Z}_{\mu\nu} =&\frac{1}{2}\left(\epsilon_{\mu\nu\rho\tau}\partial^{\rho}Z^{\tau} - \epsilon_{\mu\nu\rho\tau}\partial^{\tau}Z^{\rho}\right) \\ =&\frac{1}{2}\left(\epsilon_{\mu\nu\rho\tau}\partial^{\rho}Z^{\tau} - \epsilon_{\mu\nu\tau\rho}\partial^{\rho}Z^{\tau}\right) \\ =&\frac{1}{2}\left(\epsilon_{\mu\nu\rho\tau}\partial^{\rho}Z^{\tau} + \epsilon_{\mu\nu\rho\tau}\partial^{\rho}Z^{\tau}\right) \\ =&\epsilon_{\mu\nu\rho\tau}\partial^{\rho}Z^{\tau}\end{aligned} \tag{4.9}$$

for on-shell particles the equations of motion are

$$\partial_{\mu}\partial^{\mu}A^{\nu} - m^2A^{\nu} = 0, \tag{4.10}$$

to go to the space of moments for an incoming particle (with four-moment κ) we use

$$\partial_{\nu} \to i\kappa^{\nu}, \tag{4.11}$$

whereas for an outgoing particle we have

$$\partial_{\nu} \to -i\kappa^{\nu}, \tag{4.12}$$

Thus, the equation of motion (for an incoming or outgoing particle) becomes

$$\kappa^2A^{\nu} - m^2A^{\nu} = 0. \tag{4.13}$$

We will use the kinematics shown in Fig. an we note that Eq. (4.7) can be written as

$$\begin{aligned}\mathscr{L}_{ZZZ^*} =&\frac{e}{m_Z^2}[-f_4^Z\left(\partial_{\mu}[\partial^{\mu}Z^{\beta} - \partial^{\beta}Z^{\mu}]\right)Z_{\alpha}\partial^{\alpha}(Z_{\beta}) + f_5^Z\partial^{\sigma}[\partial_{\sigma}Z_{\mu} - \partial_{\mu}Z_{\sigma}]\epsilon^{\mu\beta\rho\iota}\partial_{\rho}(Z_{\iota})Z_{\beta}] \\ =&\frac{e}{m_Z^2}[-f_4^Z(\partial_{\mu}\partial^{\mu}Z^{\beta} - \partial^{\beta}\partial_{\mu}Z^{\mu})Z_{\alpha}\partial^{\alpha}(Z_{\beta}) + f_5^Z\left(\partial^{\tau}\partial_{\tau}Z_{\mu} - \partial_{\mu}\partial^{\tau}Z_{\tau}\right)\epsilon^{\mu\beta\rho\iota}\partial_{\rho}(Z_{\iota})Z_{\beta}].\end{aligned} \tag{4.14}$$

Because of Bose statistics we must to consider all the possible combinations between the three moments and three Z fields. We assign to each field their corresponding moment as: $Z^{\mu}(p)$. Thus, in the space of moments Lagrangian (4.7) is

$$
\begin{aligned}
\mathscr{L}_{ZZZ^*} =& \frac{-ie}{m_Z^2}\big[- f_4^Z\big(m_Z^2 q^\alpha\big\{Z^\beta(p_1)Z_\alpha(p_2)Z^*_\beta(q) \\
&+ Z^\beta(p_2)Z_\alpha(p_1)Z^*_\beta(q)\big\} - m_Z^2\big\{p_2^\alpha Z^\beta(p_1)Z^*_\alpha(q)Z_\beta(p_2) \\
&+ p_1^\alpha Z^\beta(p_2)Z^*_\alpha(q)Z_\beta(p_1)\big\} - q^2\big\{p_1^\alpha Z^{\beta*}(q)Z_\alpha(p2)Z_\beta(p_1) \\
&+ p_2^\alpha Z^{\beta*}(q)Z_\alpha(p_1)Z_\beta(p_2)\big\} - p_1^\beta p_{1\mu}\big\{q^\alpha Z^\mu(p_1)Z_\alpha(p_2)Z^*_\beta(q) \\
&- p_2^\alpha Z^\mu(p_1)Z^*_\alpha(q)Z_\beta(p_2)\big\} - p_2^\beta p_{2\mu}\big\{q^\alpha Z^\mu(p_2)Z_\alpha(p_1)Z^*_\beta(q) \\
&- p_1^\alpha Z^\mu(p_2)Z^*_\alpha(q)Z_\beta(p_1)\big\} + q^\beta q_\mu\big\{p_1^\alpha Z^{\mu*}(q)Z_\alpha(p2)Z_\beta(p_1) \\
&+ p_2^\alpha Z^{\mu*}(q)Z_\alpha(p_1)Z_\beta(p_2)\big\}\big) \\
&+ f_5^Z\epsilon^{\mu\beta\rho\iota}\big(m_Z^2\big\{Z_\iota(p_2)Z^*_\beta(q)p_{2\rho}\big(- Z_\mu(p_1) + p_{1\mu}p_1^\tau Z_\tau(p_1)\big) \\
&+ Z^*_\iota(q)Z_\beta(p_2)q_\rho\big(Z_\mu(p_1) - p_{1\mu}p_1^\tau Z_\tau(p_1)\big) \\
&+ Z_\iota(p_1)Z^*_\beta(q)p_{1\rho}\big(- Z_\mu(p_2) + p_{2\mu}p_2^\tau Z_\tau(p_2)\big) \\
&+ Z^*_\iota(q)Z_\beta(p_1)q_\rho\big(Z_\mu(p_2) - p_{2\mu}p_2^\tau Z_\tau(p_2)\big)\big\} \\
&+ q^2\big\{p_{1\rho}Z_\iota(p_1)Z_\beta(p_2)\big(- Z^*_\mu(q) + q_\mu q^\tau Z^*_\tau(q)\big) \\
&+ p_{2\rho}Z_\iota(p_2)Z_\beta(p_1)\big(- Z^*_\mu(q) + q_\mu q^\tau Z^*_\tau(q)\big)\big\}\big)\big].
\end{aligned}
\tag{4.15}
$$

We want to write the fields in the following way: $Z_\alpha(p_1)Z_\beta(p_2)Z^*_\mu(q)$, therefore we must to change indexes and use $q = p_1 + p_2$. Thus, our Lagrangian is

$$
\begin{aligned}
\mathscr{L}_{ZZZ^*} =& \frac{-ie}{m_Z^2}Z_\alpha(p_1)Z_\beta(p_2)Z^*_\mu(q)\big[- f_4^Z\big(m_Z^2\big\{q^\beta g^{\mu\alpha} + q^\alpha g^{\mu\beta}\big\} \\
&- m_Z^2 q^\mu g^{\beta\alpha} - q^2\big\{p_1^\beta g^{\mu\alpha} + p_2^\alpha g^{\mu\alpha}\big\} - p_1^\mu p_1^\alpha q^\beta + p_1^\beta p_1^\alpha p_2^\mu \\
&- q^\alpha p_2^\mu p_2^\beta + q^\mu p_2^\alpha p_2^\beta + q^\mu q^\alpha p_1^\beta + q^\mu q^\beta p_2^\alpha\big) \\
&+ f_5^Z\big(\epsilon^{\mu\alpha\beta\rho}\big\{m_Z^2\big(- p_{2\rho} - q_\alpha + p_{1\rho} + q_\alpha\big) \\
&q^2\big(- p_{1\rho} + p_{2\rho}\big)\big\} + m_Z^2\epsilon^{\lambda\mu\rho\beta}\big(p_1^\alpha p_{1\lambda}p_{2\rho} + p_1^\alpha p_{1\lambda}q_\rho\big) \\
&+ m_Z^2\epsilon^{\lambda\mu\rho\alpha}\big(p_2^\beta p_{2\lambda}p_{1\rho} + p_2^\beta p_{2\lambda}p_{1\rho}\big) \\
&+ q^2\epsilon^{\lambda\beta\rho\alpha}\big(q^\mu q_\lambda p_{1\rho} - q^\mu q_\lambda p_{2\rho}\big)\big)\big],
\end{aligned}
\tag{4.16}
$$

we consider the transversality conditions

$$
p_1^\alpha = 0, \quad p_2^\beta = 0. \tag{4.17}
$$

In the decay $f\overline{f} \to VV$ the terms q^μ give rise to mass terms m_f, therefore we can neglect them as they will be very small at high energies. We do not consider the case of $m_f = m_t$, since the partons are not composed of top quarks

$$
\begin{aligned}
\mathscr{L}_{ZZZ^*} =& \frac{-ie}{m_Z^2}Z_\alpha(p_1)Z_\beta(p_2)Z^*_\mu(q)\big[f_4^Z\big(q^2 - m_Z^2\big)\big\{q^\beta g^{\mu\alpha} + q^\alpha g^{\mu\beta}\big\} \\
&- f_5^Z\epsilon^{\mu\alpha\beta\rho}\big(q^2 - m_Z^2\big)\big\{p_{1\rho} - p_{2\rho}\big\}\big],
\end{aligned}
\tag{4.18}
$$

if we follow the vertex definition given in Fig. 4.1 ant the convention where the Feynman rules

are obtained as $-i\mathscr{L}$, we get the vertex

$$\Gamma^{\alpha\beta\mu}_{ZZZ^*}(p_1,p_2,q) = \frac{i\left(q^2-m_Z^2\right)}{m_Z^2}\left[f_4^Z\left\{q^\beta g^{\mu\alpha}+q^\alpha g^{\mu\beta}\right\} - f_5^Z\,\epsilon^{\mu\alpha\beta\rho}\left\{p_{1\rho}-p_{2\rho}\right\}\right], \tag{4.19}$$

which actually is the vertex (4.1). The case $ZZ\gamma^*$ is less difficult to obtain as we only need to consider the combinations of two Z bosons.

4.2.2 FCNCs mediated by the Z and Z' gauge bosons

Beyond the SM, there are some extension theories that allow FCNC couplings mediated by the Z gauge boson [152, 153]. Such an interaction can be expressed by the following Lagrangian

$$\begin{aligned}\mathscr{L} = &-\frac{e}{2s_W c_W} Z^\mu \overline{F}_i \gamma_\mu \left(g^i_{VZ} - \gamma^5 g^i_{AZ}\right) F_i \\ &- \frac{e}{2s_W c_W} Z^\mu \overline{F}_i \gamma_\mu \left(g^{ij}_{VZ} - \gamma^5 g^{ij}_{AZ}\right) F_j,\end{aligned} \tag{4.20}$$

where $F_{i,j}$ are SM fermions in the mass eigenbasis. Here $g^i_{VZ,AZ}$ are the diagonal SM couplings, whereas the non-diagonal couplings $g^{ij}_{VZ,AZ}$ ($i \neq j$) will be taken as complex since we are interested in the CP-violating contribution. The latter must fulfil $g^{ij*}_{VZ,AZ} = g^{ji}_{VZ,AZ}$ because of their hermiticity. It is also customary to express the Lagrangian of Eq. (4.20) in terms of the left- and right-handed projectors P_L and P_R, with the chiral couplings denoted by $\epsilon^Z_{L_{ij},R_{ij}}$, which are given in terms of the vector and vector-axial couplings $g^{ij}_{VZ,AZ}$ as follows

$$g^{ij}_{VZ,AZ} = \frac{\epsilon^Z_{L_{ij}} \pm \epsilon^Z_{R_{ij}}}{2}. \tag{4.21}$$

Below we will use both the $g^{ij}_{VZ,AZ}$ and $\epsilon^Z_{L_{ij},R_{ij}}$ parametrizations. The former is useful for the purpose of comparison with previous works, whereas the latter is best suited for our numerical analysis.

Possible phenomenological implications of FCNC couplings mediated by the Z gauge boson have been studied within the SM [162, 163, 164, 165], fourth-generation models [166, 162, 163, 167, 168], See-Saw models [169], etc. Such FCNC couplings have been constrained via the $b \to s$ transition [152, 153], Kaon decays [170, 171], $B - \overline{B}$ mixing [166], and B^0 decays [172, 173]. More, recently constraints on FCNC top quark decays $t \to qZ$ were reported by the ATLAS Collaboration at $\sqrt{s} = 13$ TeV [174].

As for models with FCNC mediated by a new neutral gauge boson, which we generically have denoted by Z', they have been widely studied in the literature [175, 176]. In Table 4.1 we present a summary of some of the more popular models that predict a new Z' gauge boson.

To describe the FCNC Z' couplings we follow the formalism presented in [159, 175] and introduce an effective Lagrangian analogue to that of Eq. (4.20) in terms of the chiral couplings $\epsilon^{Z'}_{L_{ij},R_{ij}}$, where i and j now run over all the SM fermions $f_{SM} = \nu_i, \ell_i, u_i, d_i$. though there can

Table 4.1: Models in which there is a new neutral gauge boson with FCNC couplings [175].

New heavy neutral gauge boson	Model	Gauge group
Z_h	Sequential Z	$SU_L(2) \times U_Y(1) \times U'(1)$
Z_{LR}	Left-right symmetric	$SU_L(2) \times SU_R(2) \times U_Y(1)$
Z_χ	Gran Unification	$S0(10) \to SU(5) \times U(1)$
Z_ψ	Superstring-inspired	$E_6 \to SO(10) \times U(1)$
$Z_\eta \equiv \sqrt{3/8}Z_\chi - \sqrt{5/8}Z_\psi$	Superstring-inspired	$E_6 \to$ Rank-5 group

also be new hypothetical fermions. We thus write

$$\mathscr{L}_{Z'}^{FCNC} = -g_{Z'} \sum_{i=f_{SM}} Z'_\mu \bar{\mathbf{F}}_i \gamma^\mu \left(\boldsymbol{\epsilon}_{L_i}^{Z'} P_L + \boldsymbol{\epsilon}_{R_i}^{Z'} P_R \right) \mathbf{F}_i, \tag{4.22}$$

where $\mathbf{F}_i$ is a massive fermion triplet in the flavor basis, $\mathbf{F}_\ell^T = (e, \mu, \tau)$, $\mathbf{F}_d^T = (d, s, b)$, and $\mathbf{F}_d^T = (u, c, t)$, with $\boldsymbol{\epsilon}_{L_i}^{Z'}$ and $\boldsymbol{\epsilon}_{R_i}^{Z'}$ being 3×3 matrices containing the corresponding Z' couplings. We will focus on the quark up-type sector since we expect that the largest contribution to TNGBCs arise from the top quark, which will become evident in Sec. 4.3. As it was pointed out in Ref. [159], we assume that the Z' couplings to down-type quarks d, charged leptons ℓ and neutrinos ν are flavor-diagonal and family-universal, namely, $\boldsymbol{\epsilon}_{L_i,R_i}^{Z'} = Q_{L,R}^i \mathbf{I}_{3\times3}$ for $i = d, \ell, \nu$, where $\mathbf{I}_{3\times3}$ is the identity matrix and $Q_{L,R}^i$ are the respective chiral charges. As far as the couplings of the Z' gauge boson to up-type quarks are concerned, we assume that they are family non-universal and are given in the flavor basis as

$$\boldsymbol{\epsilon}_{L_u}^{Z'} = Q_L^u \begin{pmatrix} 1 & 0 & 0 \\ 0 & 1 & 0 \\ 0 & 0 & x \end{pmatrix}, \qquad \boldsymbol{\epsilon}_{R_u}^{Z'} = Q_R^u \mathbf{I}_{3\times3}. \tag{4.23}$$

Thus, non-universal couplings are only induced through left-handed up-type quarks, with x a parameter that characterizes the size of the FCNCs and will be taken as $x \lesssim \mathscr{O}(1)$. The chiral $U'(1)$ charges of the up-type quarks $Q_{L,R}^u$ differ in each model as shown in Table 4.2.

Table 4.2: Chiral charges for the models with a new heavy neutral gauge boson of Table 4.1. A detailed discussion about the determination of these couplings can be found in Ref. [159].

	Sequential Z	$Z_{L,R}$	Z_χ	Z_ψ	Z_η
Q_L^u	0.3456	-0.08493	$\frac{-1}{2\sqrt{10}}$	$\frac{1}{\sqrt{24}}$	$\frac{-2}{2\sqrt{15}}$
Q_R^u	-0.1544	0.5038	$\frac{1}{2\sqrt{10}}$	$\frac{-1}{\sqrt{24}}$	$\frac{2}{2\sqrt{15}}$
Q_L^d	-0.4228	-0.08493	$\frac{-1}{2\sqrt{10}}$	$\frac{1}{\sqrt{24}}$	$\frac{-2}{2\sqrt{15}}$
Q_R^d	0.0772	-0.6736	$\frac{-3}{2\sqrt{10}}$	$\frac{-1}{\sqrt{24}}$	$\frac{-1}{2\sqrt{15}}$
Q_L^e	-0.2684	0.2548	$\frac{3}{2\sqrt{10}}$	$\frac{1}{\sqrt{24}}$	$\frac{1}{2\sqrt{15}}$
Q_R^e	0.2316	-0.3339	$\frac{1}{2\sqrt{10}}$	$\frac{-1}{\sqrt{24}}$	$\frac{2}{2\sqrt{15}}$
Q_L^ν	0.5	0.2548	$\frac{3}{2\sqrt{10}}$	$\frac{1}{\sqrt{24}}$	$\frac{1}{2\sqrt{15}}$

After rotating to the mass eigenstates, we obtain the left- and right-handed up quark fields in the mass eigenbasis via the $\mathbf{V}_{L_u}$ and $\mathbf{V}_{R_u}$ matrices respectively. Thus the up-quark term of

the Lagrangian of Eq. (4.22) reads

$$\begin{aligned}\mathscr{L} = -g_{Z'} Z'_\mu \bar{\mathbf{F}}_u^M \gamma_\mu \Big(& \mathbf{V}_{L_u}^\dagger \boldsymbol{\epsilon}_{L_u}^{Z'} \mathbf{V}_{L_u} P_L \\ & + \mathbf{V}_{R_u}^\dagger \boldsymbol{\epsilon}_{R_u}^{Z'} \mathbf{V}_{R_u} P_R \Big) \mathbf{F}_u^M, \end{aligned} \tag{4.24}$$

where the superscript M denotes the mass eigenbasis. For simplicity we will drop this superscript below and assume that we are referring to the fermions in the mass eigenstate basis. In general $\mathbf{B}_L^u \equiv \mathbf{V}_{L_u}^\dagger \epsilon_{L_u}^{Z'} \mathbf{V}_{L_u}$ will be non-diagonal. Since no mixing in the down-quark sector is assumed we will have $\mathbf{V}_{CKM} = \mathbf{V}_{L_u}^\dagger \mathbf{V}_{L_d} = \mathbf{V}_{L_u}^\dagger$ [159]. Therefore, the flavor mixing will be determined by the CKM matrix:

$$\begin{aligned}\mathbf{B}_L^u &\equiv \mathbf{V}_{CKM} \boldsymbol{\epsilon}_{L_u}^{Z'} \mathbf{V}_{CKM}^\dagger \\ &\approx \begin{pmatrix} 1 & (x-1)V_{ub}V_{cb}^* & (x-1)V_{ub}V_{tb}^* \\ (x-1)V_{cb}V_{ub}^* & 1 & (x-1)V_{cb}V_{tb}^* \\ (x-1)V_{tb}V_{ub}^* & (x-1)V_{tb}V_{cb}^* & x \end{pmatrix}, \end{aligned} \tag{4.25}$$

where we have used the unitarity conditions of $\mathbf{V}_{CKM}$. As for the right-handed couplings $\mathbf{B}_R^u \equiv \mathbf{V}_{R_u}^\dagger \epsilon_{R_u}^{Z'} \mathbf{V}_{R_u}$, it is easy to see that they are flavor-diagonal.

The gauge coupling $g_{Z'}$ is the same as that of the SM for the Z gauge boson in the sequential Z model, namely, $g_{Z'} = e/(2s_W c_W)$, whereas in the remaining models of Table 4.1, it is given by

$$g_{Z'} = \sqrt{\frac{5}{3}} \frac{e}{c_W} \lambda_g^{1/2}, \tag{4.26}$$

where $\lambda_g \sim \mathscr{O}(1)$. Below we will assume that $\lambda_g = 1$. Constraints on FCNCs arise from $D^0 - \overline{D^0}$ mixing [159, 177], single top-quark production at the LHC [178] and a simple ansatz analysis [179]. Implications of FCNC of a new neutral gauge boson Z' have been studied in leptonic decays of the Higgs boson and the weak bosons [180], tZ' production at the LHC [181], Z' decays [182], B_s and B_d decays [183], etc.

4.3 Analytical results

We now turn to present the calculation of the contribution to the TNGBCs ZZV^* ($V = Z,\gamma, Z'$) arising from complex FCNC couplings mediated by the SM Z gauge boson and a new neutral heavy gauge boson Z' as shown in Eqs. (4.20) and (4.24), respectively. This would allow non-vanishing CP-violating form factors. For our calculation we will assume conserved vector currents and consider Bose symmetry [124]. This last condition will allows us to obtain all the Feynman diagrams contributing to the TNGBCs. We will see, however, that we only need to calculate the three generic Feynman diagrams depicted in Fig. 4.2 since the amplitudes of the additional diagrams follow easily. For the calculation of the loop amplitudes we use the Passarino-Veltman reduction scheme with the help of the FeynCalc package [35].

4.3.1 $ZZ\gamma^*$ coupling

In this case there are 4 contributing Feynman diagrams, but due to gauge invariance we only need to calculate the amplitude of diagram 4.2(a) $\mathscr{M}_2^{\alpha\beta\mu}$ since the amplitudes of the remaining

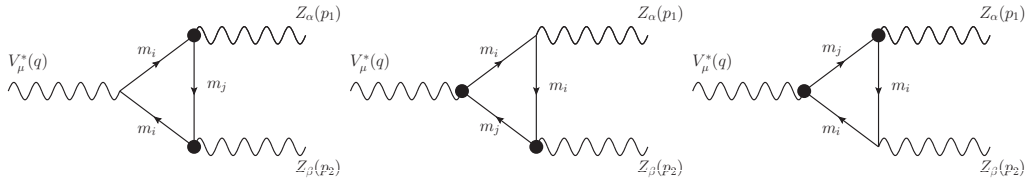

Figure 4.2: Generic Feynman diagrams required for the contribution of FCNC couplings to TNGBCs ZZV^* and $Z\gamma V^*$ ($V = Z,\gamma, Z'$).

diagrams are easily obtained as follows. There is an additional diagram that is obtained after the exchange $f_i \leftrightarrow f_j$ so its amplitude follows from $\mathscr{M}_2^{\alpha\beta\mu}$ after exchanging the fermion masses $\mathscr{M}_2^{\alpha\beta\mu}(f_i \leftrightarrow f_j)$. We also need to add a pair of diagrams where the Z gauge bosons are exchanged, which means that their total amplitude can be obtained from that of the two already described diagrams after the exchange $p_{1\mu} \leftrightarrow p_{2\nu}$ is done. We note that it is not possible to induce CP violation in the $ZZ\gamma^*$ coupling, which indeed was verified in our explicit calculation. Therefore there are only contributions to the form factor f_5^γ, which can be written as

$$f_5^\gamma = -\sum_i \sum_{j\neq i} \frac{N_i Q_i e^2 m_Z^2 \mathrm{Re}\left(g_{AZ}^{ij*} g_{VZ}^{ij}\right)}{8\pi^2 s_W^2 c_W^2 \left(q^2 - 4m_Z^2\right)^2 q^2} R_{ij}, \tag{4.27}$$

where m_i, N_i and Q_i are the mass, color number and electric charge of the fermion f_i. Note that $Q_j = Q_i$ since we are considering neutral currents. The analytical expression for R_{ij} is somewhat cumbersome and is presented in A.4 in terms of Passarino-Veltman scalar functions. We have verified that Eq. (4.27) reduces to that reported in Ref. [124] for real FCNC couplings of the Z gauge boson.

Asymptotic behavior

It is straightforward to obtain the high-energy limit $q^2 \gg m_i^2, m_j^2, m_Z^2$

$$f_5^\gamma \approx -\sum_i \sum_{j\neq i} \frac{e^2 Q_i N_i m_Z^2 \mathrm{Re}\left(g_{AZ}^{ij*} g_{VZ}^{ij}\right)}{4\pi^2 q^2 c_W^2 s_W^2}, \tag{4.28}$$

which agrees up to terms of the order q^{-2} with the one reported in [124] for the CP-conserving case ($m_i = m_j$), though we must consider a factor of $1/2$ as we are counting twice the number of Feynman diagrams (our results include the contribution of the diagrams with the exchange $f_i \leftrightarrow f_j$). It is evident that $f_5^\gamma \to 0$ in the high-energy limit as required by unitarity.

In the scenario where an ultra heavy fermion runs into the loop $m_i^2 \gg q^2, m_Z^2, m_j^2$ must be worked out more carefully as the expansion of the two- and three-point scalar Passarino-Veltman functions around small m_j diverge. This scenario could arise in 331 model [72] or little Higgs models [156], for instance, where new heavy quarks and neutrinos are predicted.

4.3.2 ZZZ^* coupling

The calculation of this coupling is more intricate than the previous one since there are 36 contributing Feynman diagrams, though we only need to calculate the three generic Feynman diagrams of Fig. 4.2, which by Bose symmetry must be complemented with the diagrams obtained by performing six permutations of four-momenta and Lorentz indices as well as the exchange of the fermions running into the loops. In this case there are both CP-violating and CP-conserving form factors. The former is due to the fact that the virtual boson is assumed to have complex FCNC couplings. As for the CP-conserving form factor f_5^Z, it can be written as

$$\begin{aligned} f_5^Z = &-\sum_i \sum_{j\neq i} \frac{e^2 N_i m_Z^2}{16\pi^2 c_W^3 s_W^3 \left(q^2 - 4m_Z^2\right)} \\ &\times \Big\{ g_{AZ}^i \left(\left| g_{AZ}^{ij} \right|^2 + \left| g_{VZ}^{ij} \right|^2 \right) \left(R_{1ij} + R_{2ij} \right) \qquad (4.29) \\ &+ 2 g_{VZ}^i \mathrm{Re}\left(g_{AZ}^{ij*} g_{VZ}^{ij} \right) \left(R_{1ij} - R_{2ij} \right) \\ &+ g_{AZ}^i \left[\left| g_{AZ}^{ij} \right|^2 - \left| g_{VZ}^{ij} \right|^2 \right] R_{3ij} + (i \leftrightarrow j) \Big\}, \qquad (4.30) \end{aligned}$$

where the R_{kij} ($k = 1, 2, 3$) functions are presented in A.4 in terms of Passarino-Veltman scalar functions. This results is in agreement with that reported in Ref. [124] for real FCNC couplings of the Z gauge boson.

As for the CP-violating form factor f_4^Z, it reads

$$\begin{aligned} f_4^Z = &-\sum_i \sum_{j\neq i} \frac{N_i e^2 m_i m_j m_Z^2}{24\pi^2 c_W^3 s_W^3 \left(q^2 - m_Z^2\right)\left(q^2 - 4m_Z^2\right) q^2} \\ &\times \mathrm{Im}\left(g_{AZ}^{ij*} g_{VZ}^{ij} \right) g_{AZ}^i S_{ij}, \qquad (4.31) \end{aligned}$$

where S_{ij} is presented in A.4. It is easy to see that f_4^Z vanishes for real couplings, which is also true if we consider the same fermion running into the loop ($i = j$). Thus, a non-vanishing f_4^Z requires complex FCNC couplings. Furthermore, we can also see that we need different complex phases for g_{VZ}^{ij} and g_{AZ}^{ij} to obtain a non-vanishing CP-violating form factor. Since f_4^Z is proportional to $m_i m_j$ we expect that the main contribution comes from FCNC couplings associated with the top quark. We would like to stress that the result of Eq. (4.31) has never been reported in the literature.

Asymptotic behavior

As we did it with the $ZZ\gamma^*$ vertex, we study the high-energy limit $q^2 \gg m_i^2, m_j^2, m_Z^2$

$$f_5^Z \approx -\sum_i \sum_{j\neq i} \frac{e^2 N_i m_Z^2}{8\pi^2 q^2 c_W^3 s_W^3} \Big(g_{AZ}^i \left(\left| g_{AZ}^{ij} \right|^2 + \left| g_{VZ}^{ij} \right|^2 \right) + 2 g_{VZ}^i \mathrm{Re}\left(g_{AZ}^{ij*} g_{VZ}^{ij} \right) \Big). \tag{4.32}$$

Our result for f_5^Z also reproduces the one reported in Ref. [124] for the CP-conserving case ($m_i = m_j$), though this time we must consider a factor of 1/6 as we are considering twice the three kinds of Feynman diagrams of Fig. 4.2 by the exchange $m_i \leftrightarrow m_j$. In ths case we also observe that $f_5 \to 0$ in the high-energy limit, which is consistent with unitarity. The same is true for the CP-violating form factor f_4^Z, which behaves in the high-energy limit as $f_4^Z \sim 1/q^4$, since $S_{ij} \sim q^2$ in this limit.

In the case $m_i^2 \gg q^2$, m_Z^2, m_j^2, both form factors diverge similar as in the case of the $ZZ\gamma^*$ vertex.

4.3.3 ZZZ'^* coupling

For the sake of completeness we now consider a Z' gauge boson with complex FCNCs couplings and calculate the corresponding contributions to the TNGBC ZZZ'^*. We first present the diagonal case, where there is no flavor violation. Since $m_i = m_j$, there is only one independent diagram in Fig. 4.2 and we only need to add one extra diagram obtained after the exchange $p_{1\mu} \leftrightarrow p_{2\nu}$. After some algebra, the CP-conserving form factor $f_5^{Z'}$ reads

$$f_5^{Z'} = -\sum_i \frac{e N_i m_{Z'}^2}{16\pi^2 c_W^2 s_W^2 q^2 \left(q^2 - 4m_Z^2\right)^2} \times \Big\{ g_{AZ'}^i \Big[(g_{VZ}^i)^2 \; L_{1i} + (g_{AZ}^i)^2 \; L_{2i} \Big] + g_{VZ'}^i \; g_{VZ}^i \; g_{AZ}^i \; L_{3i} \Big\}, \tag{4.33}$$

where the L_{ji} ($j = 1, 2, 3$) functions are presented in A.4. The CP-violating form factor $f_4^{Z'}$ is not induced at the one-loop level in this scenario.

As far as the non-diagonal case with complex FCNCs couplings, it requires more effort. Apart from the three generic Feynman diagram of Fig. 4.2, we must add those diagrams obtained after the exchanges $p_{1\mu} \leftrightarrow p_{2\nu}$ and $f_1 \leftrightarrow f_2$, so there are 12 contributing Feynman diagrams in total. However, we only need to calculate the amplitudes of the three generic diagrams. In this scenario both $f_5^{Z'}$ and $f_4^{Z'}$ form factors are non-vanishing. The CP-conserving form factor can be written as

$$
\begin{aligned}
f_5^{Z'} = & -\sum_i \sum_{j\neq i} \frac{eN_i m_{Z'}^2}{16\pi^2 c_W^2 s_W^2 q^2 \left(q^2 - 4m_Z^2\right)^2} \\
& \times \Big\{ 2g_{AZ}^i \Big[\mathrm{Re}\left(g_{VZ}^{ij} g_{VZ'}^{ij*}\right) U_{1ij} \\
& + \mathrm{Re}\left(g_{AZ'}^{ij} g_{AZ}^{ij*}\right) U_{2ij} \Big] + 2g_{VZ'}^i \mathrm{Re}\left(g_{VZ}^{ij} g_{AZ}^{ij*}\right) U_{3ij} \\
& + 2g_{VZ}^i \Big[\mathrm{Re}\left(g_{VZ}^{ij} g_{AZ'}^{ij*}\right) U_{4ij} + \mathrm{Re}\left(g_{VZ'}^{ij} g_{AZ}^{ij*}\right) U_{5ij} \Big] \\
& + g_{AZ'}^i \Big[\left|g_{AZ}^{ij}\right|^2 U_{6ij} + \left|g_{VZ}^{ij}\right|^2 U_{7ij} \Big] \Big\},
\end{aligned} \tag{4.34}
$$

whereas the CP-violating one reads

$$
\begin{aligned}
f_4^{Z'} = & \sum_i \sum_{j\neq i} \frac{eN_i m_{Z'}^2}{12\pi^2 c_W^2 s_W^2 q^6 \left(q^2 - 4m_Z^2\right)} \\
& \times \Big\{ g_{VZ}^i \Big[\mathrm{Im}\left(g_{VZ'}^{ij} g_{VZ}^{ij*}\right) T_{1ij} + \mathrm{Im}\left(g_{AZ'}^{ij} g_{AZ}^{ij*}\right) T_{2ij} \Big] \\
& + g_{AZ'}^i \mathrm{Im}\left(g_{VZ}^{ij} g_{AZ}^{ij*}\right) T_{3ij} \\
& + g_{AZ}^i \Big[\mathrm{Im}\left(g_{AZ'}^{ij} g_{VZ}^{ij*}\right) T_{4ij} + \mathrm{Im}\left(g_{VZ'}^{ij} g_{AZ}^{ij*}\right) T_{5ij} \Big] \Big\},
\end{aligned} \tag{4.35}
$$

where the U_{kij} ($k = 1 \ldots 7$) and T_{kij} ($k = 1 \ldots 5$) functions are presented in A.4. We note that $f_5^{Z'}$ ($f_4^{Z'}$) depends only on the real (imaginary) part of the combinations of products of the vector and axial couplings. We also note that it is not necessary that both Z and Z' gauge bosons have simultaneously complex FCNC couplings to induce the CP-violating form factor.

Asymptotic behavior

In the diagonal case the form factor $f_5^{Z'}$ can be written in the high-energy limit $q^2 \gg m_i^2$, m_j^2, m_Z^2 as

$$
\begin{aligned}
f_5^{Z'} \simeq & -\sum_i \frac{e^2 m_{Z'}^2 N_i}{32\pi^2 c_W^3 s_W^3 q^2} \Big\{ g_{AZ'}^i \left((g_{AZ}^i)^2 + (g_{VZ}^i)^2 \right) \\
& + 2g_{AZ}^i \; g_{VZ}^i \; g_{VZ'}^i \Big\},
\end{aligned} \tag{4.36}
$$

whereas in the non-diagonal case we obtain

$$\begin{aligned} f_5^{Z'} \simeq & -\sum_i \sum_{j\neq i} \frac{e^2 m_{Z'}^2 N_i}{16\pi^2 c_W^3 s_W^3 q^2} \\ & \times \Big\{ g_{AZ'}^i \left(\left| g_{AZ}^{ij} \right|^2 + \left| g_{VZ}^{ij} \right|^2 \right) \\ & + 2\Big[g_{AZ}^i \Big(\mathrm{Re}\left(g_{AZ'}^{ij} g_{AZ}^{ij*} \right) + \mathrm{Re}\left(g_{VZ}^{ij} g_{VZ'}^{ij*} \right) \Big) \\ & + g_{VZ}^i \Big(\mathrm{Re}\left(g_{VZ'}^{ij} g_{AZ}^{ij*} \right) + \mathrm{Re}\left(g_{VZ}^{ij} g_{AZ'}^{ij*} \right) \Big) \\ & + g_{VZ'}^i \mathrm{Re}\left(g_{VZ}^{ij} g_{AZ}^{ij*} \right) \Big] \Big\}. \end{aligned} \tag{4.37}$$

We note that in both scenarios $f_5^{Z'} \sim m_{Z'}^2/q^2$, thereby decreasing quickly when $q^2 \geqslant m_{Z'}^2$. However this effect is attenuated for $q^2 \lesssim m_{Z'}^2$ due to the mass of the heavy Z' boson. We also note that Eq. (4.37) reduces to Eq. (4.36) except by a factor of 6, which is due to the fact that the CP-violating form factor receives the contribution of twelve Feynman diagrams in the diagonal scenario instead of two as in the diagonal case.

On the other hand, the CP-violating form factor $f_4^{Z'}$ is of the order of $m_{Z'}^2/q^4$ in the high energy limit and decreases quickly as q^2 increases. The functions T_{kij} behave in this limit as $T_{kij} \sim q^4$, therefore the form factor $f_4^{Z'}$ as functions of q^2 has the form $f_4^{Z'} \sim 1/q^4$, which is similar to the vertex ZZZ^* in the high energy limit.

Furthermore, when $m_i^2 \gg q^2, m_Z^2, m_j^2$ both form factors also show the same behavior observed in the case of the vertices $ZZ\gamma^*$ and ZZZ^*.

4.4 Constraints on FCNC Z couplings

We would like to assess the magnitude of the new contributions to the f_4^V and f_5^V ($V = \gamma, Z, Z'$) form factors. It is thus necessary to obtain constraints on the FCNC Z couplings to obtain an estimate of the numerical values of such form factors. Since we expect that the main contributions arise from the FCNC couplings of the top quark, we use the current bounds on the branching ratios of the FCNC decays $t \to qZ$, where $q = c$, u [174] to constrain the $g_{VZ,AZ}^{tq}$ couplings.

4.4.1 Constraints on the FCNC Z couplings from $t \to qZ$ decay

A comprehensive compilation of the branching ratios of top FCNC decays within the SM and several extension models can be found in [165]. In the case of tree-level FCNC Z couplings, the decay width $t \to qZ$ can be written in terms of the vector and axial couplings for negligible m_q as follows

$$\begin{aligned} \Gamma_{t\to Zq} = & \frac{e^2 m_t^3}{64\pi c_W^2 m_Z^2 s_W^2} \left(\left| g_{AZ}^{tq} \right|^2 + \left| g_{VZ}^{tq} \right|^2 \right) \\ & \times \left(1 - \frac{m_Z^2}{m_t^2} \right)^2 \left(1 + 2\frac{m_Z^2}{m_t^2} \right). \end{aligned} \tag{4.38}$$

The current upper limits obtained by ATLAS collaboration at $\sqrt{s} = 13$ TeV are: $\mathscr{B}(t \to uZ) < 1.7 \times 10^{-4}$ and $\mathscr{B}(t \to cZ) < 2.4 \times 10^{-4}$ with 95% C.L. [174]. Previous results at $\sqrt{s} = 7$ TeV are also available [184]. The SM contribution to the $t \to cZ$ branching ratio is negligible: $\mathscr{B}(t \to cZ) \simeq 10^{-14}$ [165]. We thus obtain for the contribution of the FCNC couplings of the Z gauge boson:

$$\mathscr{B}(t \to qZ) = 0.915699 \left(\left| g_{AZ}^{tq} \right|^2 + \left| g_{VZ}^{tq} \right|^2 \right), \tag{4.39}$$

which allows us to obtain the following limits

$$\left| g_{AZ}^{tu} \right|^2 + \left| g_{VZ}^{tu} \right|^2 < 1.8 \times 10^{-4}, \tag{4.40}$$

and

$$\left| g_{AZ}^{tc} \right|^2 + \left| g_{VZ}^{tc} \right|^2 < 2.6 \times 10^{-4}. \tag{4.41}$$

Eqs. (4.40) and (4.41) can also be written in terms of the chiral couplings of Eq. (4.21).

We show in Fig. 4.3 the allowed areas on the $\left| g_{AZ}^{tq} \right|$ vs $\left| g_{VZ}^{tq} \right|$ and $|\epsilon_{R_{tq}}^{Z}|$ vs $|\epsilon_{L_{tq}}^{Z}|$ planes. The blue-solid (green-dashed) line corresponds to the $Z\bar{t}c$ ($Z\bar{t}u$) couplings. We observe that the FCNC couplings of the Z gauge boson can be as large as 10^{-1}. In fact, if we assume $\left| g_{AZ}^{tq} \right| \simeq \left| g_{VZ}^{tq} \right|$, we obtain

$$\left| g_{VZ}^{tu} \right| < 0.0096, \qquad \left| g_{VZ}^{tc} \right| < 0.011, \tag{4.42}$$

which in terms of the chiral coupling read

$$|\epsilon_{R_{tu}}^{Z}| < 0.013, \qquad |\epsilon_{R_{tc}}^{Z}| < 0.016. \tag{4.43}$$

Thus, our bounds are of the order of $10^{-2} - 10^{-3}$, which are similar to the constraints on FCNC couplings of down quarks obtained from B and Kaon meson decays. For instance the constraint on the $\left| g_{VZ}^{bd} \right|$ coupling is at the $10^{-2} - 10^{-3}$ level [152, 153, 173, 166, 170], whereas the $\left| g_{VZ}^{bs} \right|$ coupling is constrained to be below 10^{-1} [152]. In some extension models these couplings can be of the order of $10^{-4} - 10^{-7}$ [171, 172].

4.4.2 Constraints on the lepton flavor violating Z couplings from $Z \to \ell_i \ell_j$

Following the above approach, we now obtain constraints on the lepton flavor violating (LFV) couplings of the Z gauge boson from the experimental limits on the $Z \to \ell^{\pm}\ell^{\mp}$ decays, which have been obtained by the ATLAS and CMS collaborations: $\mathscr{B}(Z \to e\tau) < 5.8 \times 10^{-5}$, $\mathscr{B}(Z \to \mu\tau) < 2.4 \times 10^{-5}$ at $\sqrt{s} = 14$ TeV [185] and $\mathscr{B}(Z \to e\mu) < 7.3 \times 10^{-7} - 7.5 \times 10^{-7}$ at $\sqrt{s} = 8$ TeV [186, 187]. The decay width $Z \to \ell_i \ell_j$ is given by

$$\Gamma_{Z \to \ell_i \ell_j} = \frac{e^2 m_Z}{24\pi c_W^2 s_W^2} \left(\left| g_{AZ}^{\ell_i \ell_j} \right|^2 + \left| g_{VZ}^{\ell_i \ell_j} \right|^2 \right), \tag{4.44}$$

and the corresponding branching ratio is

$$\mathscr{B}\left(Z \to \ell_i \ell_j\right) = 0.250277 \left(\left| g_{AZ}^{\ell_i \ell_j} \right|^2 + \left| g_{VZ}^{\ell_i \ell_j} \right|^2 \right). \tag{4.45}$$

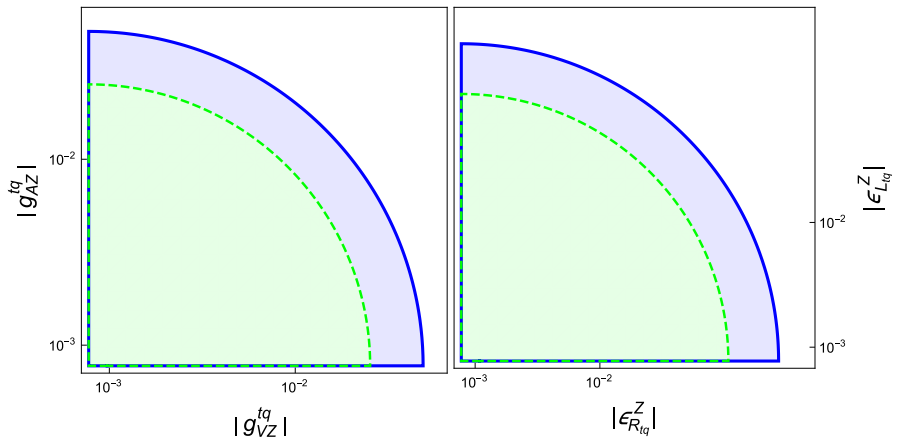

Figure 4.3: Allowed area with 95% C.L. in the $\left|g^{tq}_{AZ}\right|$ vs $\left|g^{tq}_{VZ}\right|$ (left) and $|\epsilon^{Z}_{R_{tq}}|$ vs $|\epsilon^{Z}_{L_{tq}}|$ (right) planes from the experimental bounds on $t \to Zq$ decays, for the $Z\bar{t}c$ and (solid-line boundaries) and $Z\bar{t}u$ (dashed-line boundaries) couplings.

If we assume that $\left|g^{\ell_i\ell_j}_{AZ}\right| \simeq \left|g^{\ell_i\ell_j}_{VZ}\right|$, we obtain with 95 % C.L.

$$|g^{\tau\mu}_{VZ}| < 0.0069, \qquad |g^{\tau e}_{VZ}| < 0.01, \qquad |g^{\mu e}_{VZ}| < 0.0012. \tag{4.46}$$

We note that the constraints on $|g^{\tau e}_{VZ}|$ and $|g^{\mu e}_{VZ}|$ are less competitive to those obtained through the $\mu \to eee$ and $\tau^- \to e^-\mu^+\mu^-$ decays [168], which yield $|g^{\tau e}_{VZ}| < 1.28 \times 10^{-3}$ and $|g^{\mu e}_{VZ}| < 3.05 \times 10^{-6}$. As for the bound on $|g^{\tau\mu}_{VZ}|$, it is of the same order than the one obtained from the $\tau^- \to \mu^-\mu^+\mu^-$ decay, namely, $|g^{\tau\mu}_{VZ}| < 1.295 \times 10^{-3}$ [168]. In our analysis below we consider the most stringent bounds, thus we will use the values reported in Ref. [168].

As far as the LFV Z couplings to neutrinos are concerned, there are no experimental data to obtain reliable constraints, so to obtain a rough estimate of these contributions we can assume couplings of the same order of magnitude than those used for the charged leptons. Nevertheless, the f_4^V and f_5^V form factors are mainly dominated by the contribution of the heaviest quarks, whereas the lepton contributions are negligibly.

Finally, in Table 4.3 we summarize the constraints on the FCNC Z gauge boson couplings that we will use in our numerical analysis, in terms of the corresponding chiral couplings.

Table 4.3: Bounds on the FCNC couplings of the Z gauge boson, with 95 % C.L., from the current experimental limits on FCNC Z decays. The second row stands for the limit when either $\epsilon^{Z}_{R_{ij}}$ or $\epsilon^{Z}_{L_{ij}}$ is taken as vanishing and the other one non-vanishing.

	$\bar{t}c$	$\bar{t}u$	$\bar{c}u$	$\bar{d}_i d_j$	$\bar{\ell}_i \ell_j$	$\bar{\nu}_i \nu_j$
$\left\|\epsilon^{Z}_{L_{ij}}\right\| \simeq \left\|\epsilon^{Z}_{R_{ij}}\right\|$	0.016	0.013	10^{-2}	10^{-2}	10^{-3}	10^{-3}
$\left\|\epsilon^{Z}_{L_{ij},R_{ij}}\right\|$	0.032	0.026	10^{-2}	10^{-2}	10^{-3}	10^{-3}

4.5 Numerical Analysis

We now turn to present the numerical evaluation of the TNGBCs. For the numerical analysis we evaluate the Passarino-Veltman scalar functions via the LoopTools [46] package and independently by the Collier [47] package, which give a good agreement. We first analyze the case of the ZZV^* ($V=\gamma,Z$) couplings. As a matter of convenience, we write the complex chiral FCNC Z couplings as

$$\epsilon^Z_{L_{ij},R_{ij}}=\bar{\epsilon}^Z_{L_{ij},R_{ij}}+i\tilde{\epsilon}^Z_{L_{ij},R_{ij}}, \tag{4.47}$$

where the bar (tilde) denotes the real (imaginary) part of each coupling. The CP-violating phase can then be written as

$$\arctan\left(\phi_{L_{ij},R_{ij}}\right)=\frac{\tilde{\epsilon}^Z_{L_{ij},R_{ij}}}{\bar{\epsilon}^Z_{L_{ij},R_{ij}}}. \tag{4.48}$$

We thus can write the real and imaginary terms that enter into the f_4^V and f_5^V ($V=\gamma,Z,Z'$) form factors [Eqs. (4.27)-(4.31)] as follows

$$\left|g^{ij}_{VZ,AZ}\right|^2=\frac{1}{4}\left(\left(\bar{\epsilon}^Z_{L_{ij}}\pm\bar{\epsilon}^Z_{R_{ij}}\right)^2+\left(\tilde{\epsilon}^Z_{L_{ij}}\pm\tilde{\epsilon}^Z_{R_{ij}}\right)^2\right), \tag{4.49}$$

$$\begin{aligned}2\mathrm{Re}\left(g^{ij*}_{AZ}g^{ij}_{VZ}\right)=\frac{1}{2}\Big(&\left(\bar{\epsilon}^Z_{L_{ij}}\right)^2-\left(\bar{\epsilon}^Z_{R_{ij}}\right)^2+\left(\tilde{\epsilon}^Z_{L_{ij}}\right)^2\\&-\left(\tilde{\epsilon}^Z_{R_{ij}}\right)^2\Big),\end{aligned} \tag{4.50}$$

$$2\mathrm{Im}\left(g^{ij*}_{AZ}g^{ij}_{VZ}\right)=\left(\bar{\epsilon}^Z_{L_{ij}}\tilde{\epsilon}^Z_{R_{ij}}-\bar{\epsilon}^Z_{R_{ij}}\tilde{\epsilon}^Z_{L_{ij}}\right). \tag{4.51}$$

Below we will analyze the behavior of the $f^V_{4,5}$ form factors as functions of the $\bar{\epsilon}^Z_{L_{ij},R_{ij}}$ and $\tilde{\epsilon}^Z_{L_{ij},R_{ij}}$ parameters as well as the transfer momentum q^2 of the V gauge boson.

4.5.1 $ZZ\gamma^*$ coupling

It is convenient to assume small phases of the FCNC Z couplings, namely, we consider that the imaginary parts of the left-handed couplings are smaller than ten percent of their real parts:

$$\phi_{L_{ij}}\simeq\frac{\tilde{\epsilon}^Z_{L_{ij}}}{\bar{\epsilon}^Z_{L_{ij}}}\leq O\left(10^{-1}\right), \tag{4.52}$$

whereas for the right-handed couplings we assume by simplicity that $\phi_{R_{ij}}=0$ ($\tilde{\epsilon}^Z_{R_{ij}}=0$). As far as the size of the chiral couplings $\tilde{\epsilon}^Z_{L_{ij},R_{ij}}$ we consider the bounds shown in Table 4.3 to obtain an estimate of f_5^γ, which is the only non-vanishing $ZZ\gamma^*$ form factor.

We show the behavior of the FCNC contributions to f_5^γ as a function of the photon transfer momentum q^2 in Fig. 4.4, where we only plot the non-negligible imaginary and real parts arising from each fermion loop as well as their total sum. We find that the only non-negligible

contributions arise from the up and down quarks, though the former are the only ones yielding a non-negligible imaginary part, which thus coincides with the total imaginary contribution. We have considered the parameter values of Table 4.3, but the curves shown in Fig. 4.4 exhibit a similar behavior for other parameter values: there is a shift upwards (downwards) when the chiral couplings values increase (decrease) as f_5^γ is proportional to $\mathrm{Re}\left(g_{AZ}^{ij*} g_{VZ}^{ij}\right)$. We then conclude that the contributions to f_5^γ arising from FCNCs Z couplings are expected to be considerably smaller than the SM contribution, which is of the order of 10^{-2}.

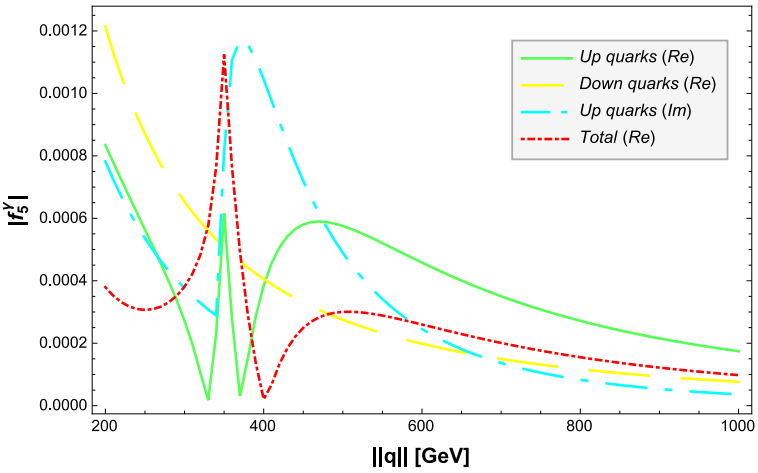

Figure 4.4: Behavior of the FCNC contributions to the f_5^γ form factor as a function of the momentum of the photon for $\phi_{L_{ij}} = 0.1$, $\phi_{R_{ij}} = 0$, $|\epsilon_{R_{ij}}^Z| = 0.9|\epsilon_{L_{ij}}^Z|$ and the $|\epsilon_{L_{ij}}^Z|$ values shown in Table 4.3. Only the non-negligible contributions are shown: up quarks (tc, tu and cu) and down quarks (bs, bd and sd). The total imaginary contribution coincides with the respective up quark contribution since the down quark contribution (not shown in the plot) is negligible.

4.5.2 ZZZ^* coupling

In this case both f_4^Z and f_5^Z are non-vanishing. For our analysis we find it convenient to consider two scenarios:

- Scenario I (Left- and right-handed couplings of similar size): $|\bar{\epsilon}_{R_{ij}}^Z| = 0.9|\bar{\epsilon}_{L_{ij}}^Z|$, $\phi_{L_{ij}} = 0.1$, and $\phi_{R_{ij}} = 0$.
- Scenario II (Dominating left-handed couplings): $|\bar{\epsilon}_{R_{ij}}^Z| \simeq 10^{-1} \times |\bar{\epsilon}_{L_{ij}}^Z|$, $\phi_{L_{ij}} = 0.1$, and $\phi_{R_{ij}} = 0$.

We do not consider the scenario with dominating right-handed couplings since there is no substantial change in the magnitude of the ZZZ^* form factors as that observed in Scenario II. We show in Fig. 4.5 the behavior of the FCNC contributions to f_5^Z as a function of the virtual Z transfer momentum q^2 in the two scenarios described above. Again we only show the real and imaginary parts arising from the up and down quarks along with the total contribution, though the imaginary part of the down quark contribution is negligible and is not shown in the plots. We observe that the largest values of f_5^Z are of the order of 10^{-6}, which are reached for smaller q^2 but decrease by one order of magnitude as q^2 becomes large. Again, the contribution to f_5^Z from FCNC Z couplings is smaller than the SM contribution.

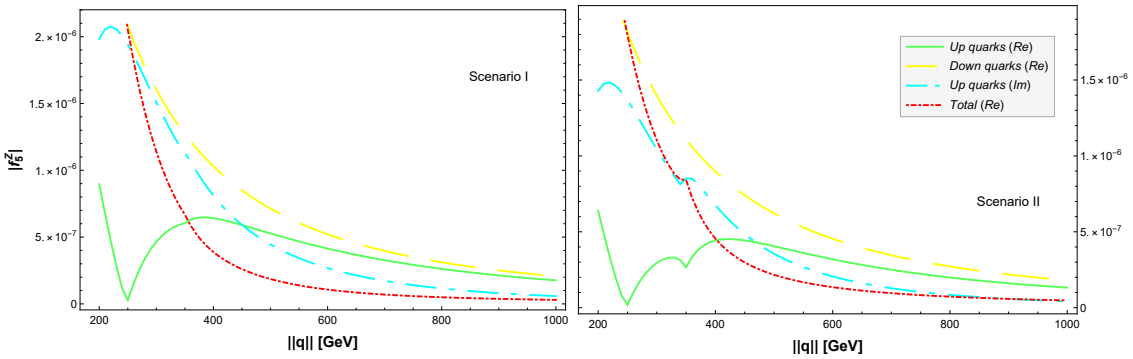

Figure 4.5: Behavior of the FCNC contributions to the f_5^Z form factor as a function of the momentum of the virtual Z gauge boson in the two scenarios discussed in the text. Only the non-negligible contributions are shown: up quarks (tc, tu and cu) and down quarks (bs, bd and sd). The total imaginary contributions coincide with the respective up quark contributions since the down quark contribution (not shown in the plot) is negligible.

We now analyze the f_4^Z form factor, which is absent in the SM up to the one-loop level, which means that any sizeable excess can be attributed to new physics effects. We find that the only non-negligible contributions to f_4^Z arise from the loops induced by the Ztc coupling, with the remaining up and down quark contributions being several orders of magnitude smaller. We thus show in the left plot of Fig. 4.6 the Ztc contribution to the f_4^Z form factor as a function of the virtual Z four-momentum, whereas in the right plot we show the Zbs and Zbd contributions. We have extracted the factor $\text{Im}\left(g_{AZ}^{qq'*} g_{VZ}^{qq'}\right)$, so for the Ztc contribution f_4^Z is of the order of

$$|f_4^Z| \simeq |\text{Im}\left(g_{AZ}^{tc*} g_{VZ}^{tc}\right)| \times 10^{-5}, \tag{4.53}$$

for relatively small $||q|| \sim 200$ GeV, but there is a decrease of up to two orders of magnitude as $||q||$ becomes of the order of a few TeVs. All the remaining contributions are considerably suppressed.

4.5.3 ZZZ'^* coupling

We now turn to the analysis of the CP-conserving $f_5^{Z'}$ and the CP-violating $f_4^{Z'}$ form factors for an off-shell Z' boson. For the FCNCs couplings mediated by the Z gauge boson we consider the same scenarios analyzed in the case of the ZZZ^* vertex. We thus use the constraints presented in Table 4.3, which were obtained from the data on $Z\overline{f}_i f_j$ decays. Furthermore, for the Z' couplings we use the interaction of Eq. (4.22), with the values of Table 4.2 for the chiral charges, along with $x = 0.1$ and $\phi_{L'ij} = 0.001$. Here x stands for the parameter characterizing the size of Z' FCNC couplings and $\phi_{L'ij}$ is the CP-violating phase of the Z' couplings to left-handed up quarks. Since all the models summarized in Table 4.2 give rise to similar results, we will only present the numerical results for the Z_η model.

We first analyze the behavior of the CP-conserving form factor $f_5^{Z'}$ in the scenario with no FCNCs (diagonal case). We show in Fig. 4.7 the behavior of $f_5^{Z'}$ as a function of the heavy Z' gauge boson transfer momentum q^2 (left plot) and the $m_{Z'}$ mass (right plot). We observe that the dominant contributions arise from the light quarks and leptons, whereas the

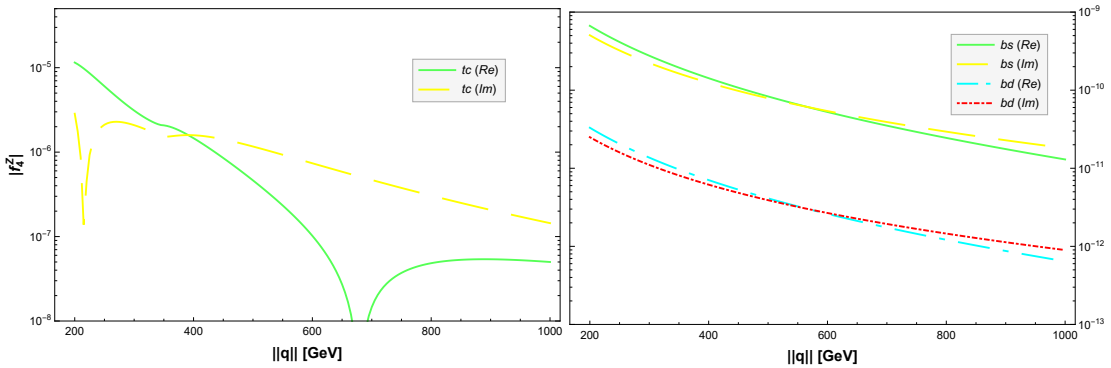

Figure 4.6: Behavior of the f_4^Z form factor as a function of the momentum $|q|$ of the virtual Z gauge boson. We have extracted a factor of Im $\left(g_{AZ}^{tc*} g_{VZ}^{qq'}\right)$ from the respective contribution. All other contributions not shown in the plots are well below the 10^{-10} level.

top quark contribution is the smaller one as its coupling with the Z' gauge boson is proportional to the x parameter, which is taken of the order of 10^{-1}. This behavior is also observed in the CP-conserving ZZZ^* form factor in the diagonal case [124]. We also note that $f_5^{Z'}$ decreases for increasing transfer momentum $|q|$, but it increases for large values of $m_{Z'}$. Since $f_5^{Z'}$ is proportional to $m_{Z'}$ [see Eq. (4.33)], a similar behavior is expected in the non-diagonal case. In Fig. 4.8 we present the contour lines of the total real (left plot) and imaginary (right plot) parts of $f_5^{Z'}$ in the $|q|$ vs $m_{Z'}$ plane. It is observed that at high energy, both real and imaginary parts of $f_5^{Z'}$ are considerably small, of the order of 10^{-2} and 10^{-3}, respectively, which is true even if the mass of the heavy boson is very large. For $m_{Z'} \gg 3000$ GeV and intermediate values of $|q|$, the value of the real part of $f_5^{Z'}$ can be of the order of $O(1)$, whereas the imaginary part is of the order of 10^{-2}.

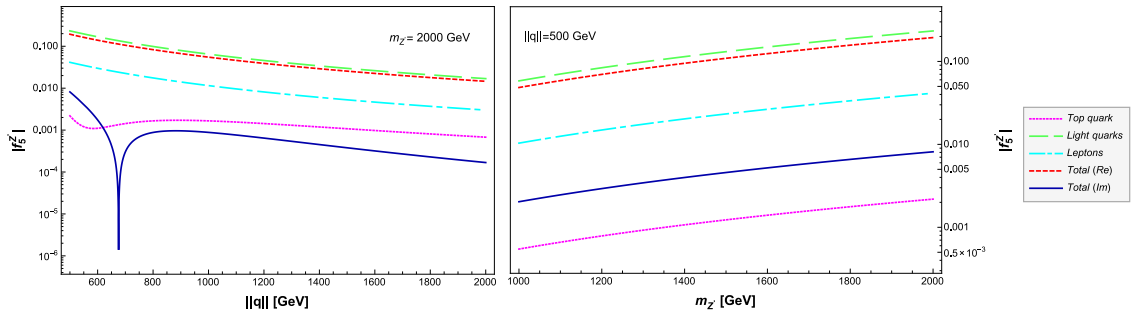

Figure 4.7: Behavior of the $f_5^{Z'}$ form factor as a function of the transfer momentum $|q|$ (left plot) and the $m_{Z'}$ mass (right plot) in the diagonal case .

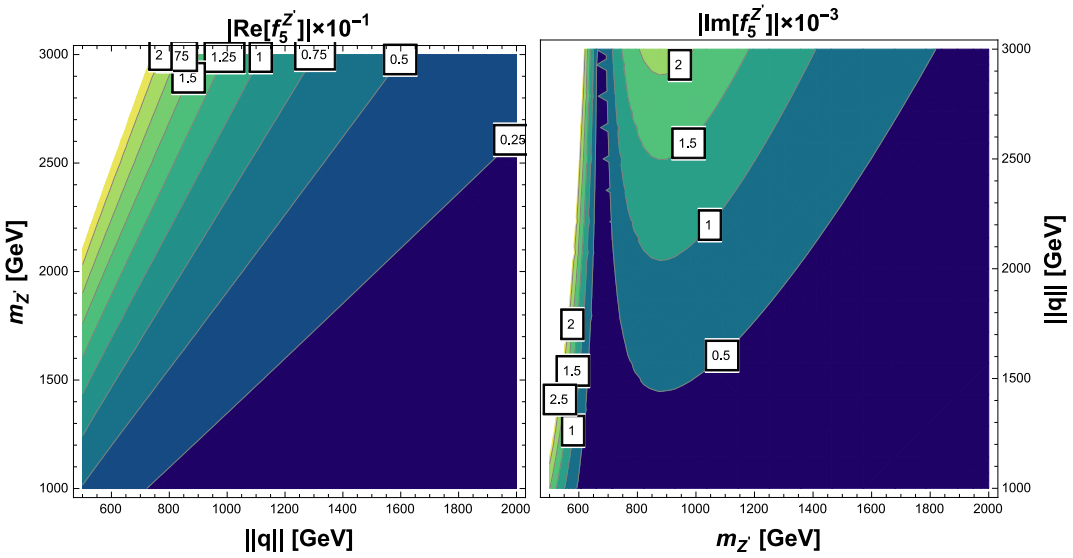

Figure 4.8: Contour lines of the $f_5^{Z'}$ form factor in the $|q|$ vs $m_{Z'}$ plane in the diagonal case.

We now show in Fig. 4.9 the form factor $f_5^{Z'}$ as function of the transfer momentum $|q|$ of the Z' gauge boson in the non-diagonal case. For the FCNCs couplings of the Z gauge boson, we consider both scenario I (left plot) and scenario II (right plot), which were also considered in the analysis of the ZZZ^* vertex. As we are assuming only flavor violation in the up quark sector for the FCNCs mediated by the Z' boson, we only plot this class of contributions. As in the analysis of the ZZZ^* form factor, we only show the non-negligible contributions, which are those where the top quark runs into the loops. We observe that in both scenarios the real parts of the $Z'tc$ and $Z'tu$ contributions are of similar size, although the largest contribution is distinct in each case. We also find that in scenario I the real parts of the $Z'tc$ and $Z'tu$ contributions are of the same sign, but they are of opposite sign in scenario II. Thus, they tend to cancel each other out. As for the imaginary parts of the partial contributions, they exhibit a similar behavior in both scenarios, nevertheless there is a peak in the 600 GeV$< |q| <$ 900 GeV region, which is present in a distinct contribution in each scenario. We also show in Fig 4.10 the contour lines in the $|q|$ vs $m_{Z'}$ plane of the real (left plot) and imaginary (right plot) parts of $f_5^{Z'}$ in scenario II, where it is manifest the cancellation effect between the real parts of the $Z'tc$ and $Z'tu$ contributions for $|q|$ around 900 GeV. In this scenario the form factor $f_5^{Z'}$ can be of the order of 10^{-6}, though for intermediate $|q|$ and large $m_{Z'}$ it can reach values one order of magnitude larger. As for scenario I, the real and imaginary parts of $f_5^{Z'}$ are of the order 10^{-4} in general, but they could be larger for small energies and an ultra heavy Z'.

It is also possible to induce the CP-violating form factor $f_4^{Z'}$ via FCNC Z and Z' couplings. We find that the only non-negligible contributions arise from the $Z'tc$ and $Z'tu$ couplings, though the dominant contribution to both real and imaginary parts of $f_4^{Z'}$ is the $Z'tc$ one, which is one order of magnitude larger than the $Z'tu$ contribution. We present in Fig. 4.11 the form factor $f_4^{Z'}$ as a function of $|q|$. We observe that the real and imaginary parts behave in a rather similar way. As was the case for the ZZZ^* CP-violating form factor, there is no considerable distinction between the results for scenario I and scenario II of the FCNC Z couplings, thus we only consider scenario I in our analysis. We also show in Fig. 4.12 the contour lines of the real part of $f_4^{Z'}$ in the $|q|$ vs $m_{Z'}$ plane. The behavior of the imaginary part is similar as already stated. We

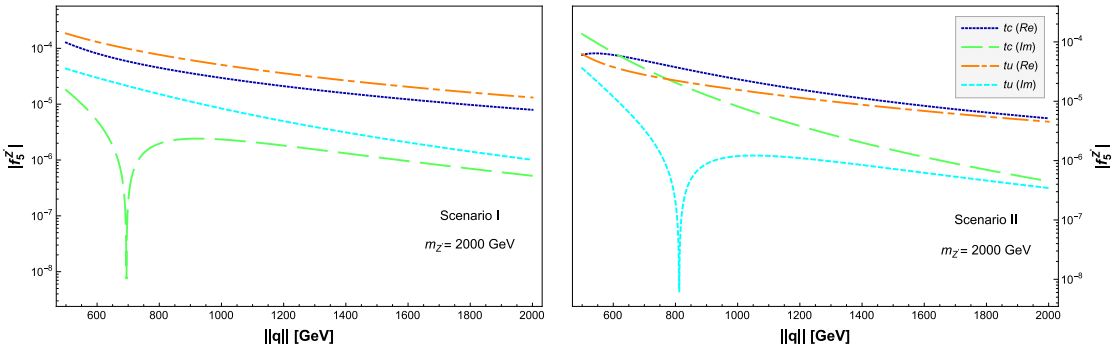

Figure 4.9: Behavior of the $f_5^{Z'}$ form factor in the non-diagonal case as a function of the transfer momentum $|q|$ of the Z' gauge boson.

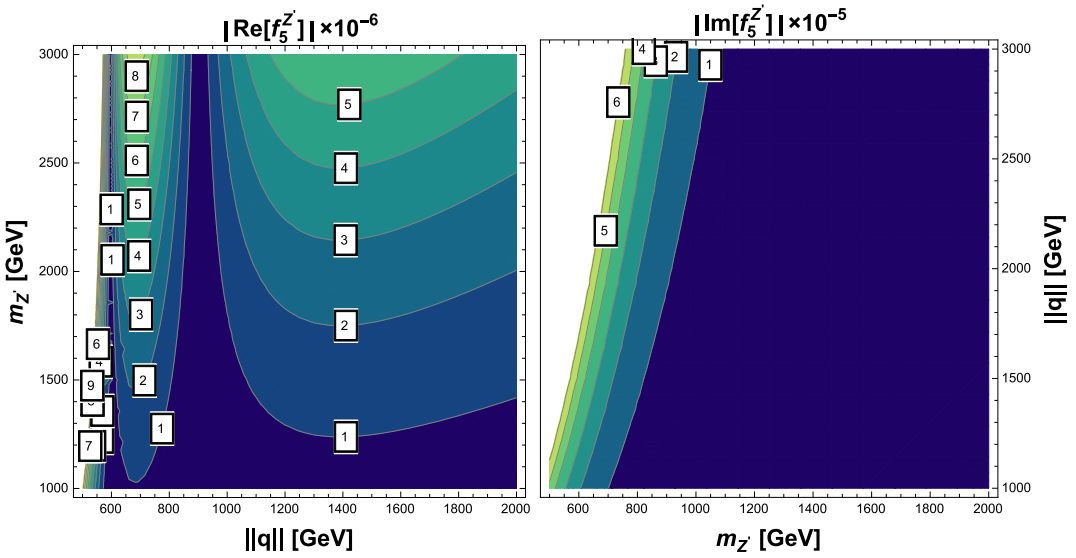

Figure 4.10: Contour lines in the $|q|$ vs $m_{Z'}$ plane of the real and imaginary parts of the $f_5^{Z'}$ form factor in the non-diagonal case and scenario II.

note that at high energy $f_4^{Z'}$ can be of the order of $10^{-7} - 10^{-8}$, though it can be one order of magnitude larger at low energy and for an ultra heavy Z' gauge boson. In our numerical analysis we did not extract the complex phases as in the ZZZ^* case, since the $f_4^{Z'}$ factors depends on five distinct combinations of all of the involved phases [see Eq. (4.35)].

4.6 Remarks

We have presented a calculation of the TNGBCs ZZV^* ($V = \gamma$, Z, Z') in models where FCNCs couplings mediated by the Z and Z' gauge bosons are allowed. These TNGBCs are given in terms of one CP-conserving form factor f_5^V and another CP-violating one f_4^V, for which we present analytical results in terms of Passarino-Veltman scalar functions. Such results reduce to the contributions with diagonal Z couplings already studied in the literature. To asses the behavior

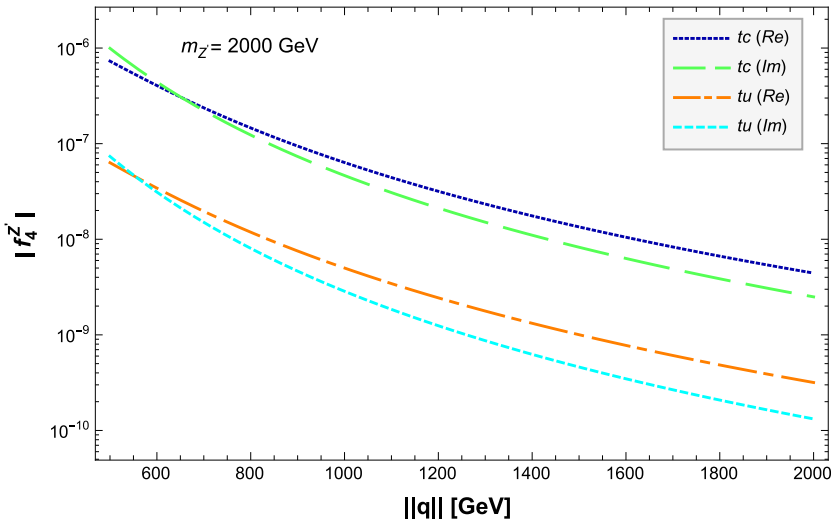

Figure 4.11: Behavior of the $f_4^{Z'}$ form factor as a function of $|q|$ in the non-diagonal case and scenario I.

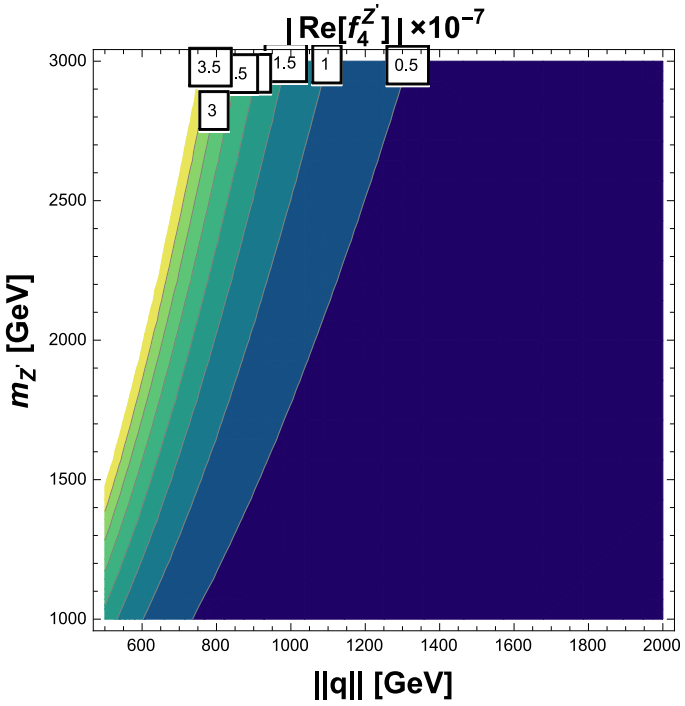

Figure 4.12: Contour lines of the real part of $f_4^{Z'}$ in the q vs $m_{Z'}$ plane in the non-diagonal case and scenario I.

of f_4^V and f_5^V, for the numerical analysis we obtain constraints on the FCNCs couplings of the Z gauge boson to up quarks, which are the less constrained by experimental data: it is found that the current constraints on the $t \to qZ$ branching ratios obtained at the LHC translate into the following constraints on the vector and axial Z couplings $\left|g_{VZ}^{tu}\right| < 0.0096$ and $\left|g_{VZ}^{tc}\right| < 0.011$.

As far as the $ZZ\gamma^*$ coupling is concerned, it is found that the only non-vanishing form factor is the CP-conserving one f_5^γ, whose real and imaginary parts are of the order of 10^{-3}, with the dominant contributions arising from the heavier up and down quarks. On the other hand, as for the ZZZ^* coupling, both the CP-conserving and the CP violating form factors are non-vanishing. We consider two scenarios for the FCNC Z couplings (scenario I and scenario II) and find that the magnitude of the real and imaginary parts of these form factors are of the order of $|f_5^Z| \sim 10^{-6}$ and $|f_4^Z| \sim |\mathrm{Im}\left(g_{AZ}^{tc*} g_{VZ}^{tc}\right)| \times 10^{-5}$, with the dominant contributions arising from the non-diagonal top quark couplings. Our estimates for the FCNC contributions to the CP-conserving f_5^γ and f_5^Z form factors are smaller than the prediction of the SM, whereas the f_4^Z form factor is not induced in the SM up to the one loop level.

We also consider the case of a new heavy neutral Z' gauge boson with FCNCs and obtain the TNGBC ZZZ'^*, for which we present analytical results in the case of both diagonal and non-diagonal Z' couplings in terms of Passarino-Veltman scalar functions. In the diagonal case we find the following numerical estimate for the CP-conserving $f_5^{Z'}$ form factor, which is the only non-vanishing, $|\mathrm{Re}f_5^{Z'}| \sim 10^{-1} - 10^{-2}$ and $|\mathrm{Im}f_5^{Z'}| \sim 10^{-2} - 10^{-3}$, with the dominant contributions arising from the light quarks and leptons. In the non-diagonal case we also consider two scenarios for the FCNC couplings of the Z gauge boson (scenario I and scenario II). It is found that both the real and imaginary parts of $f_5^{Z'}$ are of the order of 10^{-4} in scenario I, whereas in scenario II $|\mathrm{Re}f_5^{Z'}| \sim 10^{-6}$ and $|\mathrm{Im}f_5^{Z'}| \sim 10^{-5}$. In general, in the non-diagonal case the magnitude of both real and imaginary parts of the $f_5^{Z'}$ form factor are one order of magnitude larger for moderate energies and an ultra heavy Z' gauge boson than for high energies, with the dominant contributions arising from the $Z'tu$ and $Z'tc$ couplings. The real (imaginary) part of the non-diagonal contributions to $f_5^{Z'}$ are at least two (one) orders of magnitude smaller than the real (imaginary) parts of the diagonal contributions.

As far as the CP-violating form factor $f_4^{Z'}$ is concerned, we obtain similar estimates for its real and imaginary parts, of the order of $10^{-7} - 10^{-8}$ in both scenarios of the FCNC couplings of the Z gauge boson. In closing we would like to stress that FCNC couplings can also yield CP violation in the TNGBCs of a new neutral gauge boson, which may be on interest.

Apenddix A

Appendix

A.1 Analytic results for the loop functions

We now present the results for the loop functions appearing in the contributions to the CMDM of quarks discussed in Sec. 1.1 in term of Feynman parameter integrals, Passarino-Veltman scalar functions, and closed form functions. For sake of completeness we also include the results for $q^2 = 0$.

A.1.1 Feynman parameter integrals

We note that this calculation was done via the unitary gauge as the result are gauge independent, which was explicitly verified via the Passarino-Veltman reduction scheme. Therefore, in the EW sector we only computed by this method the Feynman diagrams (a) through (c) of Fig. 1.3.

We introduce the definition $r_{a,b} = m_a/m_b$ and present the loop functions for the QCD contributions to the CMDM of quarks. Feynman diagram 1.2(a) yields the loop function [Eq. (1.11)]:

$$\mathscr{F}_q^{\mathrm{QCD}_1}\left(q^2\right) = m_q^2 \int_0^1 \int_0^{1-u} \frac{(u-1)u}{m_q^2(u-1)^2 + q^2 v(u+v-1)} dv du, \tag{A.1}$$

whereas Feynman diagram 1.2(b) gives [Eq. (1.16)]:

$$\mathscr{F}_q^{\mathrm{QCD}_2}\left(q^2\right) = m_q^2 \int_0^1 \int_0^{1-u} \frac{(u-1)u}{m_q^2 u^2 - q^2 v(1-u-v)} dv du, \tag{A.2}$$

which for $q^2 = 0$ reduces to

$$\mathscr{F}_q^{\mathrm{QCD}_2}(0) = \int_0^1 \frac{(1-u)^2}{u} du. \tag{A.3}$$

As far as the EW contributions to the CMDM of quarks are concerned, the Feynman diagram

with photon exchange of Fig. 1.3(a) gives [Eq. (1.19)]:

$$\mathscr{F}_q^A\left(q^2\right) = m_q^2 \int_0^1 \int_0^{1-u} \frac{(u-1)u}{m_q^2(u-1)^2 + q^2 v(u+v-1)} dvdu, \tag{A.4}$$

whereas the Z boson exchange diagram gives [Eq. (1.25)]

$$\mathscr{A}_q^Z\left(q^2\right) = \int_0^1 \int_0^{1-u} \frac{dudv}{\Delta_Z}\left((3u-1)\Delta_Z \log\left(\frac{\Delta_Z}{\mu^2}\right) + 2\left(m_q^2(u-1)^3 - 2m_Z^2 u\right) + 2q^2 uv(u+v-1)\right), \tag{A.5}$$

and

$$\mathscr{V}_q^Z\left(q^2\right) = -\int_0^1 \int_0^{1-u} \frac{dudv}{\Delta_Z} m_Z^2 (u-1)u, \tag{A.6}$$

where $\Delta_Z = m_q^2(u-1)^2 + m_Z^2 u + q^2 v(u+v-1)$ and μ is the scale of dimensional regularization, which cancels out after integration.

For $q^2 = 0$, the last two loop functions give:

$$\mathscr{A}_q^Z(0) = \int_0^1 du \frac{u\left(2u^2 + r_{Z,q}^2(u-4)(u-1)\right)}{r_{Z.q}^2(u-1) - u^2}, \tag{A.7}$$

and

$$\mathscr{V}_q^Z(0) = \int_0^1 du \frac{{g_V^q}^2 r_{Z,q}^2 (u-1)u^2}{r_{Z.q}^2(u-1) - u^2}. \tag{A.8}$$

As for the W boson exchange contribution of diagram 1.3(b), it is given by [Eq. (1.30)]:

$$\mathscr{F}_{qq'}^W\left(q^2\right) = \int_0^1 \int_0^{1-u} \frac{dudv}{\Delta_W}\Bigg(-(1-3u)\log\left(\frac{\Delta_W}{\mu^2}\right)\Delta_W - 2m_{q'}^2(u-1)^2 + u\big(2m_q^2(u-1)^2 - m_W^2(u+3) + 2q^2 v(u+y-1)\big)\Bigg), \tag{A.9}$$

with the following result for $q^2 = 0$:

$$\mathscr{F}_{qq'}^W(0) = \int_0^1 \frac{u\left[u\left((u-1) + r_{q',q}^2(u+1)\right) + 2r_{W,q}^2(u-2)(u-1)\right]}{r_{W,q}^2(u-1) - u\left((u-1) + r_{q',q}^2\right)} du, \tag{A.10}$$

where $\Delta_W = u\left(m_q^2(u-1) + m_W^2\right) - m_{q'}^2(u-1) + q^2 v(u+v-1)$. Again this calculation was done via the unitary gauge.

Finally, for the Higgs contribution [Eq. (1.32)] we obtain:

$$\mathscr{F}_q^h\left(q^2\right) = m_q^2 \int_0^1 \int_0^{1-u} \frac{(u^2-1)}{m_q^2(u-1)^2 + um_h^2 + q^2 v(u+v-1)} dvdu, \tag{A.11}$$

which for $q^2 = 0$ reduces to

$$\mathscr{F}_q^h(0) = -\int_0^1 du \frac{(1+u)(1-u)^2}{(1-u)^2 + ur_{h,q}^2}. \tag{A.12}$$

A.1.2 Passarino-Veltman results

We now present the above results in terms of Passarino-Veltman scalar integrals, where we use the standard notation for the two- and three-point scalar functions. Our calculation was done via a renormalizable linear R_ξ gauge and the BFM to verify that the dependence on the ξ gauge parameter drops out. The loop functions are thus gauge independent and read

$$\mathscr{F}_q^{\mathrm{QCD}_1}\left(q^2\right) = \frac{m_q^2}{\eta^2(\|q\|, m_q)}\Big\{\mathbf{B}_0(0; m_q, m_q) - \mathbf{B}_0\left(q^2; m_q, m_q\right) + 2\Big\}, \tag{A.13}$$

where we define $\eta(x,y) = \sqrt{x^2 - 4y^2}$. Also

$$\begin{aligned}\mathscr{F}_q^{\mathrm{QCD}_2}\left(q^2\right) = \frac{m_q^2}{\eta^4(\|q\|, m_q)}\Big\{ &\left(8m_q^2 + q^2\right)\left(\mathbf{B}_0(0; m_q, m_q) - \mathbf{B}_0\left(q^2; 0, 0\right)\right) \\ &- 6m_q^2\left(q^2\mathbf{C}_0\left(m_q^2, m_q^2, q^2; 0, m_q, 0\right) - 4\right)\Big\},\end{aligned} \tag{A.14}$$

$$\mathscr{F}_q^{\mathrm{QCD}_2}(0) = \frac{1}{2}\Big\{\mathbf{B}_0(0; m_q, m_q) + 3\Big\}, \tag{A.15}$$

$$\mathscr{F}_q^{A}\left(q^2\right) = \frac{m_q^2}{\eta^2(\|q\|, m_q)}\Big\{\mathbf{B}_0\left(0; m_q, m_q\right) - \mathbf{B}_0\left(q^2; m_q, m_q\right) + 2\Big\}, \tag{A.16}$$

$$\begin{aligned}\mathscr{A}_q^{Z}\left(q^2\right) = \frac{m_Z^2}{m_q^2\eta^4(\|q\|, m_q)}\Bigg\{ &\left(q^2\left(m_Z^2 - 8m_q^2\right) + 10m_q^2\left(2m_q^2 - m_Z^2\right)\right)\mathbf{B}_0\left(m_q^2; m_q, m_Z\right) \\ &+ \frac{m_q^2}{m_Z^2}\left(q^2\left(9m_Z^2 - 2m_q^2\right) + \left(8m_q^4 - 24m_q^2m_Z^2 + 6m_Z^4\right)\right)\mathbf{B}_0\left(q^2; m_q, m_q\right) \\ &+ \frac{\left(2m_q^2 + m_Z^2\right)\eta^2(\|q\|, m_q)}{m_Z^2}\left(m_q^2\mathbf{B}_0(0; m_q, m_q) - m_Z^2\mathbf{B}_0(0; m_Z, m_Z)\right) \\ &+ 2\Big(2q^2\left(3m_Z^2 - 7m_q^2\right) + 2q^4 + 3\left(8m_q^4 - 6m_q^2m_Z^2 + m_Z^4\right)\Big)m_q^2\mathbf{C}_0\left(m_q^2, m_q^2, q^2; m_q, m_Z, m_q\right) \\ &+ \frac{(4m_q^4 - m_Z^4)\eta^2(\|q\|, m_q)}{m_Z^2}\Bigg\},\end{aligned} \tag{A.17}$$

$$\begin{aligned}\mathscr{V}_q^{Z}\left(q^2\right) = \frac{m_Z^2}{m_q^2\eta^4(\|q\|, m_q)}\Bigg\{ &\left(q^2\left(m_Z^2 - 2m_q^2\right) + 2m_q^2\left(4m_q^2 - 5m_Z^2\right)\right)\mathbf{B}_0\left(m_q^2; m_q, m_Z\right) \\ &+ m_q^2\Big(2\left(3m_Z^2 - 2m_q^2\right) + q^2\Big)\mathbf{B}_0\left(q^2; m_q, m_q\right) + \eta^2(\|q\|, m_q)\left(m_q^2\mathbf{B}_0(0; m_q, m_q) - m_Z^2\mathbf{B}_0(0; m_Z, m_Z)\right) \\ &+ \left(4q^2 + 2\left(3m_Z^2 - 8m_q^2\right)\right)m_q^2m_Z^2\mathbf{C}_0\left(m_q^2, m_q^2, q^2; m_q, m_Z, m_q\right) + (2m_q^2 - m_Z^2)\eta^2(\|q\|, m_q)\Bigg\},\end{aligned} \tag{A.18}$$

$$\mathscr{A}_q^Z(0) = \frac{m_Z^2}{8m_q^4}\Bigg\{\Big(10m_q^2 - 5m_Z^2\Big)\mathbf{B}_0\left(m_q^2; m_q, m_Z\right) + \Big(3m_Z^2 - 14m_q^2\Big)\mathbf{B}_0(0; m_q, m_q)$$
$$+ 2\Big(2m_q^2 + m_Z^2\Big)\mathbf{B}_0(0; m_Z, m_Z) + 3\Big(m_Z^4 - 6m_q^2m_Z^2 + 8m_q^4\Big)\mathbf{C}_0\left(m_q^2, m_q^2, 0; m_q, m_Z, m_q\right)$$
$$+ \frac{2}{m_Z^2}\left(m_Z^4 - 4m_q^4\right)\Bigg\}, \tag{A.19}$$

$$\mathscr{V}_q^Z(0) = \frac{m_Z^2}{8m_q^4}\Bigg\{\Big(4m_q^2 - 5m_Z^2\Big)\mathbf{B}_0\left(m_q^2; m_q, m_Z\right) + \Big(3m_Z^2 - 4m_q^2\Big)\mathbf{B}_0(0; m_q, m_q)$$
$$+ 2m_Z^2\mathbf{B}_0(0; m_Z, m_Z) + \Big(3m_Z^2 - 8m_q^2\Big)m_Z^2\mathbf{C}_0\left(m_q^2, m_q^2, 0; m_q, m_Z, m_q\right) + 2\left(m_Z^2 - 2m_q^2\right)\Bigg\}, \tag{A.20}$$

$$\mathscr{F}_{qq'}^W\left(q^2\right) = \frac{1}{m_q^2\eta^4(\|q\|, m_q)}\Big\{\eta^2(\|q\|, m_q)\left(m_q^2 + m_{q'}^2 + 2m_W^2\right)\left(m_{q'}^2\mathbf{B}_0(0; m_{q'}, m_{q'}) - m_W^2\mathbf{B}_0(0; m_W, m_W)\right)$$
$$- \Big[q^2\left(m_q^4 + m_q^2\left(9m_W^2 - 2m_{q'}^2\right) + m_{q'}^4 + m_{q'}^2m_W^2 - 2m_W^4\right) + 2m_q^2\Big(m_q^4 + m_q^2\left(4m_{q'}^2 - 9m_W^2\right)$$
$$- 5\left(m_{q'}^4 + m_{q'}^2m_W^2 - 2m_W^4\right)\Big)\Big]\mathbf{B}_0\left(m_q^2; m_{q'}, m_W\right) + m_q^2\Big[q^2\left(m_q^2 - 3m_{q'}^2 + 10m_W^2\right)$$
$$+ 2\left(m_q^4 + m_q^2\left(6m_{q'}^2 - 11m_W^2\right) - 3\left(m_{q'}^4 + m_{q'}^2m_W^2 - 2m_W^4\right)\right)\Big]\mathbf{B}_0\left(q^2; m_{q'}, m_{q'}\right)$$
$$- 2m_q^2\Big[m_q^2\left(m_q^4 - m_q^2\left(5m_{q'}^2 + 12m_W^2\right) + \left(7m_{q'}^4 - 12m_{q'}^2m_W^2 + 17m_W^4\right)\right) - 3\left(m_{q'}^6 - 3m_{q'}^2m_W^4 + 2m_W^6\right)$$
$$- q^2\left(m_q^4 - 2m_q^2\left(m_{q'}^2 + 4m_W^2\right) + m_{q'}^4 - 6m_{q'}^2m_W^2 + 8m_W^4\right) - 2m_W^2\left(q^2\right)^2\Big]\mathbf{C}_0\left(m_q^2, m_q^2, q^2; m_{q'}, m_W, m_{q'}\right)$$
$$+ \eta^2(\|q\|, m_q)\left(m_q^2 + m_{q'}^2 - m_W^2\right)\left(m_q^2 + m_{q'}^2 + 2m_W^2\right)\Big\}, \tag{A.21}$$

$$\mathscr{F}_{qq'}^W(0) = \frac{1}{8m_q^4}\Big\{2m_W^2\left(m_q^2 + m_{q'}^2 + 2m_W^2\right)\mathbf{B}_0(0; m_W, m_W) + \Big[m_q^4 + m_q^2\left(4m_{q'}^2 - 11m_W^2\right)$$
$$- 5m_{q'}^4 - 7m_{q'}^2m_W^2 + 6m_W^4\Big]\mathbf{B}_0(0; m_{q'}, m_{q'}) - \Big[m_q^4 + m_q^2\left(4m_{q'}^2 - 9m_W^2\right)$$
$$- 5\left(m_{q'}^4 + m_{q'}^2m_W^2 - 2m_W^4\right)\Big]\mathbf{B}_0\left(m_q^2; m_{q'}, m_W\right) + \Big[12m_q^2m_W^2\left(m_q^2 + m_{q'}^2\right)$$
$$- m_W^4\left(17m_q^2 + 9m_{q'}^2\right) - \left(m_q^2 - 3m_{q'}^2\right)\left(m_q^2 - m_{q'}^2\right)^2 + 6m_W^6\Big]\mathbf{C}_0\left(m_q^2, m_q^2, 0; m_{q'}, m_W, m_{q'}\right)$$
$$- 2\left(m_q^2 + m_{q'}^2 - m_W^2\right)\left(m_q^2 + m_{q'}^2 + 2m_W^2\right)\Big\}, \tag{A.22}$$

$$\mathscr{F}_q^h\left(q^2\right) = \frac{1}{\eta^4(\|q\|,m_q)}\Big\{\eta^2(\|q\|,m_q)\left(m_h^2\mathbf{B}_0(0;m_h,m_h) - m_q^2\mathbf{B}_0(0;m_q,m_q)\right) + \left(4m_q^2\eta^2(\|q\|,m_q) + m_h^2(10m_q^2 - q^2)\right)\mathbf{B}_0\left(m_q^2;m_q,m_h\right) - 3m_q^2\left(\eta^2(\|q\|,m_q) - 2m_h^2\right)\mathbf{B}_0\left(q^2;m_q,m_q\right) - 6m_h^2m_q^2\left(\eta^2(\|q\|,m_q) + m_h^2\right)\mathbf{C}_0\left(m_q^2,m_q^2,q^2;m_q,m_h,m_q\right) + (m_h^2 - 2m_q^2)\eta^2(\|q\|,m_q)\Big\}, \tag{A.23}$$

and

$$\mathscr{F}_q^h(0) = -\frac{1}{8m_q^2}\Big\{\left(3m_h^2 - 8m_q^2\right)\mathbf{B}_0(0;m_q,m_q) + \left(8m_q^2 - 5m_h^2\right)\mathbf{B}_0\left(m_q^2;m_q,m_h\right) + 2m_h^2\mathbf{B}_0(0;m_h,m_h) + 3m_h^2\left(m_h^2 - 4m_q^2\right)\mathbf{C}_0\left(m_q^2,m_q^2,0;m_q,m_h,m_q\right) + 2(m_h^2 - 2m_q^2)\Big\}. \tag{A.24}$$

A.1.3 Closed form results

We also present the explicit solutions for the two-point scalar functions in terms of closed form functions. Below $C_0\left(m_i^2,m_j^2,q^2;m_k,m_l,m_n\right)$ stands for a three-point Passarino-Veltman scalar function.

$$\mathscr{F}_q^{\mathrm{QCD}_1}\left(q^2\right) = -\frac{m_q^2}{\|q\|\eta(\|q\|,m_q)}\log\left(\frac{\|q\|\eta(\|q\|,m_q) + 2m_q^2 - q^2}{2m_q^2}\right), \tag{A.25}$$

$$\mathscr{F}_q^{\mathrm{QCD}_2}\left(q^2\right) = -\frac{m_q^2}{\eta^4(\|q\|,m_q)}\left\{q^2\left[6m_q^2C_0\left(m_q^2,m_q^2,q^2;0,m_q,0\right) + \log\left(\frac{m_q^2}{q^2}\right) + 2 + i\pi\right] + 8m_q^2\left[\log\left(\frac{m_q^2}{q^2}\right) - 1 + i\pi\right]\right\}, \tag{A.26}$$

$$\mathscr{F}_q^{\mathrm{QCD}_2}(0) = \frac{1}{2}\left\{\frac{1}{\epsilon} + \log\left(\frac{\mu^2}{m_q^2}\right) + 3\right\}, \tag{A.27}$$

$$\mathscr{F}_q^A\left(q^2\right) = -\frac{m_q^2}{\|q\|\eta(\|q\|,m_q)}\log\left(\frac{\|q\|\eta(\|q\|,m_q) + 2m_q^2 - q^2}{2m_q^2}\right), \tag{A.28}$$

$$\mathscr{A}_q^Z\left(q^2\right) = \frac{m_Z^2}{2m_q^2\eta^4(\|q\|,m_q)}\Bigg\{\left(20m_Z\left(2m_q^2-m_Z^2\right)+\frac{2m_Z\left(m_Z^2-8m_q^2\right)q^2}{m_q^2}\right)\eta(m_Z,m_q)\log\left(\frac{m_Z+\eta(m_Z,m_q)}{2m_q}\right)$$
$$+2\left(\frac{\left(9m_Z^2-2m_q^2\right)}{m_Z^2}+\frac{\left(8m_q^4-24m_Z^2m_q^2+6m_Z^4\right)}{m_Z^2q^2}\right)m_q^2\|q\|\eta(\|q\|,m_q)\log\left(\frac{2m_q^2-q^2+\|q\|\eta(\|q\|,m_q)}{2m_q^2}\right)$$
$$+\left(2\left(8m_q^4+14m_Z^2m_q^2-5m_Z^4\right)+\frac{\left(-4m_q^4-10m_Z^2m_q^2+m_Z^4\right)q^2}{m_q^2}\right)\log\left(\frac{m_q^2}{m_Z^2}\right)$$
$$+\left(8\left(q^2\right)^2+12\left(8m_q^4-6m_Z^2m_q^2+m_Z^4\right)+8\left(3m_Z^2-7m_q^2\right)q^2\right)m_q^2C_0\left(m_q^2,m_q^2,q^2;m_q,m_Z,m_q\right)$$
$$+2\left(2m_q^2+m_Z^2\right)\eta^2(\|q\|,m_q)\Bigg\}, \tag{A.29}$$

$$\mathscr{V}_q^Z\left(q^2\right) = \frac{m_Z^2}{2m_q^2\eta^4(\|q\|,m_q)}\Bigg\{2m_Z^2\Big(\left(3m_Z^2-8m_q^2\right)+2q^2\Big)m_q^2C_0\left(m_q^2,m_q^2,q^2;m_q,m_Z,m_q\right)$$
$$+\left(\frac{4\left(3m_Z^2-2m_q^2\right)}{q^2}+2\right)m_q^2\|q\|\eta^2(\|q\|,m_q)\log\left(\frac{2m_q^2-q^2+\|q\|\eta(\|q\|,m_q)}{2m_q^2}\right)$$
$$+2m_Z^2\eta(\|q\|,m_q)+\left(2m_Z^2\left(8m_q^2-5m_Z^2\right)+\frac{m_Z^2\eta^2(m_Z,m_q)q^2}{m_q^2}\right)\log\left(\frac{m_q^2}{m_Z^2}\right)$$
$$+\left(4m_Z\left(4m_q^2-5m_Z^2\right)+\frac{2m_Z\left(m_Z^2-2m_q^2\right)q^2}{m_q^2}\right)\eta(m_Z,m_q)\log\left(\frac{m_Z+\eta(m_Z,m_q)}{2m_q}\right)\Bigg\}, \tag{A.30}$$

$$\mathscr{A}_q^Z(0) = \frac{m_Z^2}{2m_q^6}\Bigg\{-\frac{m_q^2\left(m_q^2-2m_Z^2\right)\left(2m_q^2-m_Z^2\right)}{m_Z^2}+\left(-2m_q^4+4m_q^2m_Z^2-m_Z^4\right)\log\left(\frac{m_q^2}{m_Z^2}\right)$$
$$-\frac{2\left(8m_q^4-6m_q^2m_Z^2+m_Z^4\right)m_Z}{\eta(m_Z,m_q)}\log\left(\frac{m_Z+\eta(m_Z,m_q)}{2m_q}\right)\Bigg\}, \tag{A.31}$$

$$\mathscr{V}_q^Z(0) = \frac{m_Z^2}{2m_q^6}\Bigg\{m_q^2\left(m_q^2-2m_Z^2\right)-m_Z^2\left(m_Z^2-2m_q^2\right)\log\left(\frac{m_q^2}{m_Z^2}\right)$$
$$-\frac{2\left(2m_q^4-4m_q^2m_Z^2+m_Z^4\right)}{\eta(m_Z,m_q)}\log\left(\frac{\eta(m_Z,m_q)+m_Z}{2m_q}\right)\Bigg\}, \tag{A.32}$$

$$
\begin{aligned}
\mathscr{F}^{W}_{qq'}\left(q^2\right) = \frac{1}{2m_q^2\eta^4(\|q\|,m_q)}\Bigg\{ & -4m_q^2\Big(m_q^6 - m_q^4\left(5m_{q'}^2+12m_W^2\right) + m_q^2\left(7m_{q'}^4 - 12m_{q'}^2m_W^2 + 17m_W^4\right) \\
& - q^2\left(m_q^4 - 2m_q^2\left(m_{q'}^2+4m_W^2\right) + m_{q'}^4 - 6m_{q'}^2m_W^2 + 8m_W^4\right) - 3\left(m_{q'}^6 - 3m_{q'}^2m_W^4 + 2m_W^6\right) \\
& - 2m_W^2\left(q^2\right)^2\Big)C_0\left(m_q^2,m_q^2,q^2;m_{q'},m_W,m_{q'}\right) + 2\eta^2(\|q\|,m_q)\big(m_q^4 + 3m_q^2m_W^2 - m_{q'}^4 - m_{q'}^2m_W^2 + 2m_W^4\big) \\
& + \frac{2m_q^2}{q^2}\|q\|\eta(\|q\|,m_q')\Big(2\left(m_q^4 + m_q^2\left(6m_{q'}^2 - 11m_W^2\right) - 3\left(m_{q'}^4 + m_{q'}^2m_W^2 - 2m_W^4\right)\right) \\
& + q^2\big(-3m_{q'}^2 + m_q^2 + 10m_W^2\big)\Big)\log\left(\frac{\|q\|\eta(\|q\|,m_q') + 2m_{q'}^2 - q^2}{2m_{q'}^2}\right) \\
& - \frac{2}{m_q^2}\sqrt{((m_q-m_q')^2 - m_W^2)((m_q+m_q')^2 - m_W^2)}\Big(q^2\big(m_q^4 + m_q^2\left(9m_W^2 - 2m_{q'}^2\right) + m_{q'}^4 + m_{q'}^2m_W^2 \\
& - 2m_W^4\big) + 2m_q^2\left(m_q^4 + m_q^2\left(4m_{q'}^2 - 9m_W^2\right) - 5\left(m_{q'}^4 + m_{q'}^2m_W^2 - 2m_W^4\right)\right)\Big) \\
& \times \log\left(\frac{\sqrt{((m_q-m_q')^2 - m_W^2)((m_q+m_q')^2 - m_W^2)} + m_{q'}^2 - m_q^2 + m_W^2}{2m_{q'}m_W}\right) \\
& - \frac{1}{m_q^2}\Big(q^2\big(m_q^6 - 3m_q^4\left(m_{q'}^2 - 4m_W^2\right) + m_q^2\left(3m_{q'}^4 - 8m_{q'}^2m_W^2 + 11m_W^4\right) \\
& - m_{q'}^6 + 3m_{q'}^2m_W^4 - 2m_W^6\big) + 2m_q^2\big(m_q^6 + 3m_q^4\left(m_{q'}^2 - 4m_W^2\right) + m_q^2\left(-9m_{q'}^4 + 4m_{q'}^2m_W^2 - 7m_W^4\right) \\
& + 5\left(m_{q'}^6 - 3m_{q'}^2m_W^4 + 2m_W^6\right)\big)\Big)\log\left(\frac{m_{q'}^2}{m_W^2}\right)\Bigg\}, \qquad \text{(A.33)}
\end{aligned}
$$

$$
\begin{aligned}
\mathscr{F}^{W}_{qq'}(0) = \frac{1}{2m_q^6}\Bigg\{ & m_q^2\Big(-m_q^4 - m_q^2\left(3m_{q'}^2 - 4m_W^2\right) + 2\left(m_{q'}^4 + m_{q'}^2m_W^2 - 2m_W^4\right)\Big) \\
& - \left(m_q^4m_{q'}^2 + m_q^2\left(-2m_{q'}^4 + 2m_{q'}^2m_W^2 - 3m_W^4\right) + m_{q'}^6 - 3m_{q'}^2m_W^4 + 2m_W^6\right)\log\left(\frac{m_{q'}^2}{m_W^2}\right) \\
& - \frac{2}{\sqrt{((m_q-m_q')^2 - m_W^2)((m_q+m_q')^2 - m_W^2)}}\Big(m_q^6m_{q'}^2 + m_q^4\left(-3m_{q'}^4 + m_{q'}^2m_W^2 + 3m_W^4\right) \\
& + m_q^2\left(3m_{q'}^6 - 2m_{q'}^4m_W^2 + 4m_{q'}^2m_W^4 - 5m_W^6\right) - \left(m_{q'}^2 - m_W^2\right)^3\left(m_{q'}^2 + 2m_W^2\right)\Big) \\
& \times \log\left(\frac{\sqrt{((m_q-m_q')^2 - m_W^2)((m_q+m_q')^2 - m_W^2)} + m_{q'}^2 - m_q^2 + m_W^2}{2m_{q'}m_W}\right)\Bigg\}, \qquad \text{(A.34)}
\end{aligned}
$$

$$\mathscr{F}_q^h\left(q^2\right) = -\frac{1}{2m_q^2\eta^4(\|q\|,m_q)}\Bigg\{12m_q^4m_h^2\left(\eta(\|q\|,m_q)+m_h^2\right)C_0\left(m_q^2,m_q^2,q^2;m_q,m_h,m_q\right)$$
$$+2m_q^2m_h^2\eta(\|q\|,m_q)+\frac{6m_q^4}{q^2}\|q\|\eta(\|q\|,m_q)\left(\eta^2(\|q\|,m_q)+2m_h^2\right)\log\left(\frac{\|q\|\eta(\|q\|,m_q)+2m_q^2-q^2}{2m_q^2}\right)$$
$$+m_h^2\left(24m_q^4+q^2\left(m_h^2-6m_q^2\right)-10m_q^2m_h^2\right)\log\left(\frac{m_q^2}{m_h^2}\right)$$
$$-2m_h\eta(m_h,m_q)\left(-16m_q^4-q^2\eta(m_h,m_q)+10m_q^2m_h^2\right)\log\left(\frac{\eta(m_h,m_q)+m_h}{2m_q}\right)\Bigg\}, \tag{A.35}$$

and

$$\mathscr{F}_q^h(0) = -\frac{1}{2m_q^4}\Bigg\{m_q^2(3m_q^2-2m_h^2)+2m_h\left(m_q^2-m_h^2\right)\eta(m_h,m_q)\log\left(\frac{\eta(m_h,m_q)+m_h}{2m_q}\right)$$
$$+m_h^2\left(3m_q^2-m_h^2\right)\log\left(\frac{m_q^2}{m_h^2}\right)\Bigg\}. \tag{A.36}$$

A.2 Feynman rules

We now present in Tables A.1 and A.2 the coupling constants that enter into the Feynman rules [91, 95, 77] that follow from Eqs. (3.13) and (3.16) and are necessary for the evaluation of the CMDM and CEDM of the top quark in the RM331.

Table A.1: Coupling constants for the interactions between gauge bosons and quarks in the RM331. We follow the notation of Lagrangian (3.13). Here $(K_L)_{tq}$ are entries of the complex mixing matrix $\mathbf{K}_L$, where the subscript q runs over u and c. This matrix is given in terms of the unitary complex matrix $\mathbf{V}_L^u$ that diagonalizes the mass matrix of up quarks, and can be written as $(K_L)_{tq} = (V_L^u)^*_{tq}(V_L^u)_{qt}$. Here $h_W = 1 - 4s_W^2$.

Coupling	$g_V^{Vqq'}$	$g_A^{Vqq'}$
$Z'\bar{t}t$	$\frac{1-2s_W^2}{2\sqrt{12h_W}}$	$\frac{1-2s_W^2}{2\sqrt{12h_W}}$
$Z\bar{t}q$	$\frac{s_W^2}{\sqrt{12h_W}}(K_L)_{tq}$	$\frac{s_W^2}{\sqrt{12h_W}}(K_L)_{tq}$
$V^-\bar{t}J_3$	$\sqrt{2}c_W(V_L^u)_{33}$	$\sqrt{2}c_W(V_L^u)_{33}$

Table A.2: Coupling constants for the interactions between scalar bosons and quarks necessary for the evaluation of the one-loop contributions to the CMDM and CEDM in the RM331. We follow the notation of Lagrangian (3.16). Here $(\eta^u)_{tq}$ are entries of the complex mixing matrix $\boldsymbol{\eta}^u$, where the subscript q runs over u and c. This matrix is given in terms of the unitary complex matrices $\mathbf{V}_L^u$ and $\mathbf{V}_L^d$ that diagonalize the mass matrix of up quarks, and can be written as $(\eta^u)_{tq} = (V_L^u)_{qq}(V_R^u)^*_{tq}$ and $(\eta^u)^*_{qt} = (V_L^u)^*_{tq}(V_R^u)_{qq}$ since the matrix $\boldsymbol{\eta}^u$ is not symmetric.

	$G_S^{Sqq'}$	$G_P^{Sqq'}$
$h_1\bar{t}t$	$\frac{m_t}{m_W}\left(c_\beta - \frac{v_\rho}{v_\chi}s_\beta\right)$	-
$h_1\bar{t}q$	$-\frac{s_\beta v_\rho m_{33}}{v_\chi m_W}\left((\eta^u)_{tq} + (\eta^u)^*_{qt}\right)$	$-\frac{s_\beta v_\rho m_{33}}{v_\chi m_W}\left((\eta^u)_{tq} - (\eta^u)^*_{qt}\right)$
$h_2\bar{t}t$	$\frac{m_t}{m_W}\left(s_\beta - \frac{v_\rho}{v_\chi}c_\beta\right)$	-
$h_2\bar{t}q$	$\frac{c_\beta v_\rho m_{33}}{v_\chi m_W}\left((\eta^u)_{tq} + (\eta^u)^*_{qt}\right)$	$\frac{c_\beta v_\rho m_{33}}{v_\chi m_W}\left((\eta^u)_{tq} - (\eta^u)^*_{qt}\right)$

A.3 Analytical results for the loop integrals

In this appendix we present the loop integrals appearing in Eqs. (3.14), (3.15), (3.17), and (3.18) in terms of Feynman parameter integrals and Passarino-Veltman scalar functions both for non-zero and zero q^2. We have verified that all the ultraviolet divergences cancel out. Furthermore, contrary to the QCD contribution, all the contribution of the RM331 are finite for $q^2 = 0$.

A.3.1 Feynman parameter integrals

The $\mathscr{V}^V_{qq'}(q^2)$ function of Eq. (3.14) can be written as

$$\mathscr{V}^V_{qq'}(q^2) = \int_0^1 \int_0^{1-u} \frac{dudv}{\Delta_V}\Big[2(u-1)^2u + (1-r_{q'})\left(2\hat{q}^2uv(u+v-1) + (3u-1)\Delta_V \log(\Delta_V)\right) - r_{q'}(u-1)^2(2u-1) - \left(2r^2_{q'}(u-1)^2 + r^2_V u(u+3)\right) + r_{q'}\left(r^2_{q'}(u-1)^2 - r^2_V(u-5)u\right)\Big], \tag{A.37}$$

where $\Delta_V = u\left((u-1)+r^2_V\right) - r^2_{q'}(u-1) + \hat{q}^2v(u+v-1)$, with $\hat{q}^2 = q^2/m^2_q$ and $r_a = m_a/m_q$.

For $q^2 = 0$ we obtain

$$\mathscr{V}^V_{qq'}(0) = \int_0^1 \frac{udu}{r^2_V(u-1) - u\left((u-1)+r^2_{q'}\right)}\Big[u^2\left((1-r_{q'})^2 + 2r^2_V\right) - u\left(2r^2_V(3-2r_{q'}) + (1+r_{q'})(1-r_{q'})^2\right) + 4r^2_V(1-r_{q'})\Big]. \tag{A.38}$$

As far as the $\widetilde{\mathscr{D}}^V_{qq'}(q^2)$ function of Eq. (3.15) is concerned, it is given by

$$\widetilde{\mathscr{D}}^V_{qq'}(q^2) = r_{q'}\int_0^1 \int_0^{1-u} \frac{dudv}{\Delta_V}\Big[(3u-1)\Delta_V \log(\Delta_V) + (2u+1)(u-1)^2 - r^2_{q'}(u-1)^2 + u\left(r^2_V(u-5) + 2\hat{q}^2v(u+v-1)\right)\Big], \tag{A.39}$$

which leads to

$$\widetilde{\mathscr{D}}^V_{qq'}(0) = r_{q'}\int_0^1 \frac{u\left(u(1-r^2_{q'}) + 4r^2_V(u-1)\right)}{u\left((u-1)+r^2_{q'}\right) - r^2_V(u-1)}du. \tag{A.40}$$

The $\mathscr{P}^S_{qq'}(q^2)$ function of Eq. (3.17) is

$$\mathscr{P}^S_{qq'}(q^2) = \int_0^1 \int_0^{1-u} \frac{(u-1)(u-r_{q'})}{u\left((u-1)+r^2_S\right) - r^2_{q'}(u-1) + \hat{q}^2v(u+v-1)}dudv, \tag{A.41}$$

which for $q^2 =$ simplifies to

$$\mathscr{P}^S_{qq'}(0) = \int_0^1 \frac{u^2((1-u)-r_{q'})}{u\left((u-1)+r^2_{q'}\right) - r^2_S(u-1)}du. \tag{A.42}$$

Finally, the loop function of Eq. (3.18) reads

$$\widetilde{\mathscr{D}}^S_{qq'}(q^2) = \int_0^1 \int_0^{1-u} \frac{r_{q'}(u-1)}{u\left((u-1)+r^2_S\right) - r^2_{q'}(u-1) + \hat{q}^2v(u+v-1)}dudv, \tag{A.43}$$

which yields

$$\widetilde{\mathscr{D}}^S_{qq'}(0) = \int_0^1 \frac{r_{q'}(1-u)^2}{(1-u)\left(r^2_{q'}-u\right) + r^2_S u}du. \tag{A.44}$$

A.3.2 Passarino-Veltman results

We now present the results for the loop functions in terms of Passarino-Veltman scalar functions, which can be numerically evaluated by either LoopTools [46] or Collier [47], which allows one to cross-check the results. We introduce the following notation for the two- and three-point scalar functions in the customary notation used in the literature:

$$B_a = B_0(0, m_a^2, m_a^2), \tag{A.45}$$
$$B_{q'b} = B_0(m_q^2, m_{q'}^2, m_b^2), \tag{A.46}$$
$$B_{\hat{q}q'} = B_0(\hat{q}^2, m_{q'}^2, m_{q'}^2), \tag{A.47}$$
$$C_a = m_q^2 C_0(m_q^2, m_q^2, q^2, m_{q'}^2, m_a^2, m_{q'}^2). \tag{A.48}$$

for $a = V, S, q'$ and $b = V, S$. We also define $\delta_b = 1 - r_b$ and $\chi_b = 1 + r_b$.

For non-zero q^2, the loop functions of Eqs. (3.14) and (3.15) are given by

$$\begin{aligned}\mathscr{V}^V_{qq'}(q^2) = \frac{1}{\left(\hat{q}^2-4\right)^2}\Big[&\left(\hat{q}^2-4\right)\left(r_{q'}^2 - r_V^2 + 1\right)\left(\delta_{q'}^2 + 2r_V^2\right) + \left(\hat{q}^2-4\right)\left(\delta_{q'}^2 + 2r_V^2\right)\left(r_{q'}^2 B_{q'} - r_V^2 B_V\right)\\
&- \Big(\delta_{q'}^2\chi_{q'}\left(\left(\hat{q}^2-10\right)r_{q'} + \hat{q}^2 + 2\right) + r_V^2\left(\hat{q}^2\left(r_{q'}-3\right)^2 - 2r_{q'}\left(5r_{q'}-6\right) - 18\right) - 2\left(\hat{q}^2-10\right)r_V^4\Big)B_{q'V}\\
&+ \Big(\delta_{q'}^2\left(2\hat{q}^2 r_{q'} - 2r_{q'}\left(3r_{q'}+4\right) + \hat{q}^2 + 2\right) - 2r_V^2\left(\hat{q}^2\left(4r_{q'}-5\right) + r_{q'}\left(3r_{q'}-10\right) + 11\right) + 12r_V^4\Big)B_{\hat{q}q'}\\
&+ 2\Big(\delta_{q'}^3\chi_{q'}^2\left(3r_{q'} - \hat{q}^2 + 1\right) + \delta_{q'}r_V^2\left(\left(5\hat{q}^2-8\right)r_{q'}^2 - \left(\hat{q}^2-4\right)r_{q'} - 2\left(\left(\hat{q}^2-4\right)\hat{q}^2 + 6\right)\right)\\
&- r_V^4\left(4\hat{q}^2\left(r_{q'}-2\right) - \left(10 - 9r_{q'}\right)r_{q'} - 17\right) + 6r_V^6\Big)C_{q'V}\Big],\end{aligned} \tag{A.49}$$

and

$$\widetilde{\mathscr{D}}^V_{qq'}(q^2) = \frac{r_{q'}}{\hat{q}^2-4}\Big[\left(r_{q'}^2 - 4r_V^2 - 1\right)\left(B_{q'V} - B_{\hat{q}q'}\right) + \left(r_V^2\left(2\hat{q}^2 - 5r_{q'}^2 - 3\right) + \left(r_{q'}^2-1\right)^2 + 4r_V^4\right)C_{q'V}\Big]. \tag{A.50}$$

As far as the results for $q^2 = 0$ are concerned, they read

$$\begin{aligned}\mathscr{V}^V_{qq'}(0) = \frac{1}{r_V^2 - \chi_{q'}^2}\Big[&8r_V^6 - 4\left(r_{q'}\left(3r_{q'}+2\right)+2\right)r_V^4 + 2\left(r_{q'}\left(r_{q'}\left(2r_{q'}+7\right)+4\right)-5\right)r_V^2\\
&+ 2\left(r_{q'}^2-1\right)^2\left(2r_{q'}\chi_{q'}+1\right) - \left(4\delta_{q'}^2 r_{q'}\chi_{q'}^3 + 4r_{q'}\chi_{q'}^2 r_V^2 - 4\left(r_{q'}\left(3r_{q'}+2\right)+3\right)r_V^4 + 8r_V^6\right)B_{q'V}\\
&- \left(4\delta_{q'}r_{q'}\chi_{q'}^2 r_V^2 + 4\left(r_{q'}\left(r_{q'}+2\right)+3\right)r_V^4 - 8r_V^6\right)B_V + 4r_{q'}\left(\delta_{q'}^2\chi_{q'}^3 + r_{q'}\chi_{q'}^2 r_V^2 - 2r_{q'}r_V^4\right)B_{q'}\Big],\end{aligned} \tag{A.51}$$

and

$$\widetilde{\mathscr{D}}^{V}_{qq'}(0) = \frac{r_{q'}}{(1-(r_{q'}-r_V)^2)(1-(r_{q'}+r_V)^2)}\Big[\left(r_{q'}^2-r_V^2-1\right)\left(4r_V^4-\left(5r_{q'}^2+3\right)r_V^2+\left(r_{q'}^2-1\right)^2\right)$$
$$+\left(4r_{q'}^2r_V^4+\left(-5r_{q'}^4+4r_{q'}^2+1\right)r_V^2+\left(r_{q'}^2-1\right)^3\right)B_{q'}+\left(\left(5r_{q'}^2+3\right)r_V^4-\left(r_{q'}^2-1\right)^2r_V^2-4r_V^6\right)B_V$$
$$-\left(3\left(3r_{q'}^2+1\right)r_V^4-6r_{q'}^2\left(r_{q'}^2-1\right)r_V^2+\left(r_{q'}^2-1\right)^3-4r_V^6\right)B_{q'V}\Big]. \tag{A.52}$$

The loop functions of Eqs. (3.17) and (3.18) are given by

$$\mathscr{P}^{S}_{qq'}(q^2) = \frac{1}{\left(\hat{q}^2-4\right)^2}\Big[\left(4-\hat{q}^2\right)\left(r_{q'}^2-r_S^2+1\right)+\left(\hat{q}^2\left(2r_{q'}-1\right)+6r_{q'}^2-8r_{q'}-6r_S^2-2\right)B_{\hat{q}q'}$$
$$+\left(2\delta_{q'}^2\chi_{q'}\left(1-3r_{q'}-\hat{q}^2\right)+2r_S^2\left(\hat{q}^2\left(r_{q'}-2\right)+6r_{q'}^2-4r_{q'}+2\right)-6r_S^4\right)C_{q'S}$$
$$+\left(\delta_{q'}\left(\left(\hat{q}^2-10\right)r_{q'}-\hat{q}^2-2\right)-\left(\hat{q}^2-10\right)r_S^2\right)B_{q'S}+\left(\hat{q}^2-4\right)\left(r_S^2B_S-r_{q'}^2B_{q'}\right)\Big], \tag{A.53}$$

and

$$\mathscr{D}^{S}_{qq'}(q^2) = \frac{r_{q'}}{\hat{q}^2-4}\Big[B_{q'S}-B_{\hat{q}q'}+\left(r_{q'}^2-r_S^2-1\right)C_{q'S}\Big]. \tag{A.54}$$

For $q^2 = 0$ we obtain

$$\mathscr{P}^{S}_{qq'}(0) = \frac{1}{2\left(\chi_{q'}-r_S\right)\left(r_{q'}+\chi_S\right)}\Big[\left(4r_{q'}^2+2r_{q'}-1\right)r_S^2-2r_{q'}^4-2r_{q'}^3+r_{q'}^2-2r_S^4-1$$
$$+2\left(\delta_{q'}r_{q'}\chi_{q'}^2-r_{q'}\left(2r_{q'}+1\right)r_S^2+r_S^4\right)B_{q'S}+2r_{q'}\left(r_{q'}r_S^2-\delta_{q'}\chi_{q'}^2\right)B_{q'}+2r_S^2\left(r_{q'}^2+r_{q'}-r_S^2\right)B_S\Big], \tag{A.55}$$

and

$$\mathscr{D}^{S}_{qq'}(0) = \frac{1}{(1-(r_{q'}-r_S)^2)(1-(r_{q'}+r_S)^2)}\Big[\left(1-r_{q'}^2+r_S^2\right)^2+\left(r_S^2\left(1-r_{q'}^2+r_S^2\right)\right)\left(B_S-B_{q'S}\right)$$
$$+\left(2r_S^2-\left(1-r_{q'}^2+r_S^2\right)\left(1-r_{q'}^2\right)\right)\left(B_{q'S}-B_{q'}\right)\Big]. \tag{A.56}$$

A.3.3 Two-point scalar functions

In closing we present the closed form solutions for the two-point Passarino-Veltman scalar functions appearing in the calculation. The three-point scalar functions are too lengthy to be shown

here.

$$B_0(0, m_a^2, m_a^2) = -\log\left(\frac{m_a^2}{\mu^2}\right) + \frac{1}{\epsilon} + \log(4\pi) - \gamma_E, \tag{A.57}$$

$$B_0(\hat{q}^2, m_{q'}^2, m_{q'}^2) = \frac{\sqrt{\hat{q}^2 - 4r_{q'}^2}}{|\hat{q}|}\log\left(\frac{|\hat{q}|\sqrt{\hat{q}^2 - 4r_{q'}^2} - \hat{q}^2 + 2r_{q'}^2}{2r_{q'}^2}\right) + 2 - \log\left(\frac{m_{q'}^2}{\mu^2}\right) + \frac{1}{\epsilon} + \log(4\pi) - \gamma_E, \tag{A.58}$$

$$B_0(m_q^2, m_{q'}^2, m_b^2) = \sqrt{\lambda\left(x_q^2, x_b^2, x_{q'}^2\right)}\log\left(\frac{\sqrt{\lambda\left(x_q^2, x_b^2, x_{q'}^2\right)} + \left(r_b^2 + r_{q'}^2 - 1\right)}{2r_b r_{q'}}\right) + \frac{1}{2}\left(1 - r_b^2 + r_{q'}^2\right)\log\left(\frac{r_b^2}{r_{q'}^2}\right)$$
$$+ 2 - \log\left(\frac{m_b^2}{\mu^2}\right) + \frac{1}{\epsilon} + \log(4\pi) - \gamma_E, \tag{A.59}$$

where $\lambda(x, y, z) = x^2 + y^2 + z^2 - 2(xy - xz - yz)$. The scale μ and the pole ϵ of dimensional regularization cancel out in the final result.

A.4 Analytical form of the TNGBCs ZZV^* ($V = \gamma, Z, Z'$)

In this appendix we present the analytical expressions for the loop functions appearing in the contributions to the TNGBCs ZZV^* ($V = \gamma, Z, Z'$) arising from the FCNC couplings mediated by the Z gauge boson and a new heavy neutral gauge boson Z'. For the calculation we use the Passarino-Veltman reduction scheme.

A.4.1 Passarino-Veltman results

$ZZ\gamma^*$ coupling

There are only contribution to the f_5^γ form factor, which is given in Eq. (4.27), where R_{ij} reads

$$\begin{aligned}
R_{ij} &= 4\left(q^2 - m_Z^2\right)\left(m_j^2 - m_i^2\right)\left(B_{ii}\left(q^2\right) - B_{jj}\left(q^2\right)\right) + 2\left(q^2 - 2m_Z^2\right)\left(q^2 - 4m_Z^2\right) \\
&\quad + 2m_Z^2\left(q^2 + 2m_Z^2\right)\left(B_{ii}\left(q^2\right) + B_{jj}\left(q^2\right) - 2B_{ij}\left(m_Z^2\right)\right) \\
&\quad + 4\left(q^2 - m_Z^2\right)\left(m_i^4 + m_j^4 + m_Z^4 - 2m_i^2m_j^2 - 2m_i^2m_Z^2 - 2m_j^2m_Z^2\right)\left(C_{iji}\left(q^2\right) + C_{jij}\left(q^2\right)\right) \\
&\quad + 2q^2\left(q^2 + 2m_Z^2\right)\left(m_j^2 C_{iji}\left(q^2\right) + m_i^2 C_{jij}\left(q^2\right)\right),
\end{aligned} \tag{A.60}$$

where we have introduced the shorthand notation

$$\begin{aligned}
B_{ij}(c^2) &= B_0\left(c^2, m_i^2, m_j^2\right), \\
C_{ijk}\left(q^2\right) &= C_0\left(m_Z^2, m_Z^2, q^2, m_i^2, m_j^2, m_k^2\right),
\end{aligned} \tag{A.61}$$

with B_0 and C_0 being the usual two- and three-point Passarino-Veltman scalar functions. It is useful observe the following symmetry relations

$$\begin{aligned}
B_{ij}(c^2) &= B_{ji}(c^2), \\
C_{ijk}\left(q^2\right) &= C_{kji}\left(q^2\right), \\
C_{iij}\left(q^2\right) &= C_{jji}\left(q^2\right), \\
C_{iji}\left(q^2\right) &= C_{jij}\left(q^2\right).
\end{aligned} \tag{A.62}$$

In Eq. (A.60) it is evident that ultraviolet divergences cancel out. We have also verified that R_{ij} vanishes for an on-shell photon.

ZZZ^* coupling

There are contributions to both the CP-conserving form factor f_5^Z and the CP-violating one f_4^Z. They are given in Eqs. (4.31) and (4.29), with the R_{kij}, and S_{ij} functions given in terms of Passarino-Veltman scalar functions as follows

$$
\begin{aligned}
R_{1ij} =& 1 + \frac{2\left(m_i^2 - m_j^2\right)\left(2m_Z^2 + q^2\right)}{q^2\left(q^2 - 4m_Z^2\right)}\left(B_{ij}\left(m_Z^2\right) - B_{ii}\left(m_Z^2\right)\right) \\
&- \frac{1}{\left(q^2 - 4m_Z^2\right)\left(q^2 - m_Z^2\right)}\Bigg[\frac{1}{q^2}C_{iij}\left(q^2\right)\Big(-q^4\left(m_i^2\left(m_i^2 - m_j^2\right) - m_Z^2\left(7m_i^2 + 3m_j^2 - 4m_Z^2\right)\right) \\
&+4q^2m_Z^2\left(m_i^2m_j^2 - 2m_i^2m_Z^2 - m_j^4 + m_Z^4\right) + 4m_Z^4\left(m_i^2 - m_j^2\right)^2 - 2q^6m_i^2\Big) \\
&- C_{iji}\left(q^2\right)\Big(q^2\left(-3m_i^2m_j^2 - 3m_i^2m_Z^2 + m_i^4 - 2m_j^2m_Z^2 + 2m_j^4 + 2m_Z^4\right) \\
&+2m_Z^2\left(m_i^4 + 2m_j^2m_Z^2 - m_j^4 - m_Z^4\right) + q^4m_j^2\Big) \\
&+ \left(B_{ii}\left(q^2\right) - B_{ii}\left(m_Z^2\right)\right)\left(\left(m_i^2 - m_Z^2\right)\left(2m_Z^2 + q^2\right) - 2m_j^2\left(q^2 - m_Z^2\right)\right) \\
&+ \left(B_{ij}\left(q^2\right) - B_{ij}\left(m_Z^2\right)\right)\left(\left(m_j^2 - 2m_Z^2\right)\left(2m_Z^2 + q^2\right) - 3m_i^2\left(q^2 - 2m_Z^2\right)\right)\Bigg],
\end{aligned} \tag{A.63}
$$

$$
\begin{aligned}
R_{2ij} =& \frac{m_i^2}{q^2 - m_Z^2}\Big[\left(m_i^2 - m_j^2 - m_Z^2\right)\left(C_{iij}\left(q^2\right) - C_{iji}\left(q^2\right)\right) + \left(q^2 - m_Z^2\right)C_{iij}\left(q^2\right) \\
&+ B_{ii}\left(q^2\right) - B_{ii}\left(m_Z^2\right) + 2\left(B_{ij}\left(q^2\right) - B_{ij}\left(m_Z^2\right)\right)\Big],
\end{aligned} \tag{A.64}
$$

$$
\begin{aligned}
R_{3ij} =& \frac{m_im_j}{q^2 - m_Z^2}\Big[\left(2m_i^2 - 2m_j^2 + q^2\right)\left[C_{iij}\left(q^2\right) - C_{iji}\left(q^2\right)\right] + 2\left(q^2 - m_Z^2\right)C_{iji}\left(q^2\right) \\
&+ 2\left[B_{ii}\left(q^2\right) - B_{ii}\left(m_Z^2\right)\right] + 4\left[B_{ij}\left(q^2\right) - B_{ij}\left(m_Z^2\right)\right]\Big],
\end{aligned} \tag{A.65}
$$

and

$$
\begin{aligned}
S_{ij} =& \left(4m_Z^2 - 2q^2\right)\left[B_{ii}\left(m_Z^2\right) - B_{jj}\left(m_Z^2\right)\right] \\
&- 2q^2\left[B_{ii}\left(q^2\right) - B_{jj}\left(q^2\right)\right] - \left(2m_Z^2 - q^2\right)\left(2m_i^2 - 2m_j^2 + q^2\right)C_{iij}\left(q^2\right) \\
&- q^2\left[q^2 - 2\left(m_i^2 - m_j^2 + m_Z^2\right)\right]C_{iji}\left(q^2\right) + \left(q^2 - 2m_Z^2\right)\left(2m_i^2 - 2m_j^2 - q^2\right)C_{jji}\left(q^2\right) \\
&+ q^2\left[q^2 - 2\left(m_j^2 - m_i^2 + m_Z^2\right)\right]C_{jij}\left(q^2\right).
\end{aligned} \tag{A.66}
$$

$ZZZ^{'*}$ coupling

The contributions to the $f_5^{Z'}$ and $f_4^{Z'}$ form factors are given in Eqs. (4.33)-(4.35), with the L_i T_{kij} and U_{kij} functions given as follows

$$L_{1i} = 2m_Z^2\big(2\left(q^2\left(m_i^2+m_Z^2\right)-m_Z^2\left(4m_i^2+m_Z^2\right)\right)C_{iii}\left(q^2\right) - \left(2m_Z^2+q^2\right)\left(B_{ii}\left(m_Z^2\right)-B_{ii}\left(q^2\right)\right)\big) - 6q^2m_Z^2+8m_Z^4+q^4, \tag{A.67}$$

$$L_{2i} = -4\left(m_Z-q\right)\left(m_Z+q\right)\left(m_i^2\left(q^2-4m_Z^2\right)+m_Z^4\right)C_{iii}\left(q^2\right) - 2\left(4m_i^2\left(q^2-4m_Z^2\right)+m_Z^2\left(2m_Z^2+q^2\right)\right)\left(B_{ii}\left(m_Z^2\right)-B_{ii}\left(q^2\right)\right) - 6q^2m_Z^2+8m_Z^4+q^4, \tag{A.68}$$

$$L_{3i} = 2\big(2\left(m_i^2\left(-6q^2m_Z^2+8m_Z^4+q^4\right)-2m_Z^4\left(m_Z^2-q^2\right)\right)C_{iii}\left(q^2\right) - 2m_Z^2\left(2m_Z^2+q^2\right)\left(B_{ii}\left(m_Z^2\right)-B_{ii}\left(q^2\right)\right) - 6q^2m_Z^2+8m_Z^4+q^4\big). \tag{A.69}$$

$$\begin{aligned} U_{1ij} = -\frac{1}{q^2}\Big[&B_{ii}\left(m_Z^2\right)\big(q^4\left(2m_i\left(m_i-m_j\right)+m_Z^2\right)+2q^2m_Z^2\left(m_Z^2-2\left(m_i-m_j\right)^2\right) \\ &-4m_Z^4\left(m_i^2-m_j^2\right)\big)+q^2\left(B_{ij}\left(m_Z^2\right)-2B_{ij}\left(q^2\right)\right)\big(q^2\left(\left(m_i-m_j\right)^2+m_Z^2\right)-4m_Z^2\left(m_i-m_j\right)^2 \\ &+2m_Z^4\big)+C_{iij}\left(q^2\right)\big(q^6m_i\left(m_j-3m_i\right)+q^4\big(m_Z^2\left(m_i(13m_i-4m_j)+3m_j^2\right)-2m_i\left(m_i-m_j\right)^2\left(m_i+m_j\right) \\ &-4m_Z^4\big)+4q^2m_Z^2\left(\left(m_i-m_j\right)^3\left(m_i+m_j\right)-4m_i^2m_Z^2+m_Z^4\right)+4m_Z^4\left(m_i^2-m_j^2\right)^2\big) \\ &+\left(6q^4m_Z^2-8q^2m_Z^4-q^6\right)\Big]+(i\leftrightarrow j), \end{aligned} \tag{A.70}$$

$$U_{2ij} = U_{1ij}(m_j\to -m_j), \tag{A.71}$$

$$\begin{aligned} U_{3ij} = 2\Big[&B_{ii}\left(q^2\right)\left(q^2\left(2(m_j^2-m_j^2)+m_Z^2\right)+2m_Z^2\left(m_i^2-m_j^2+m_Z^2\right)\right)-m_Z^2\left(2m_Z^2+q^2\right)B_{ij}\left(m_Z^2\right) \\ &+C_{iji}\left(q^2\right)\big(2q^2\left(m_Z^4-m_Z^2\left(2m_i^2+m_j^2\right)+\left(m_i^2-m_j^2\right)^2\right)-2m_Z^2\left((m_i+m_j)^2-m_Z^2\right)\left((m_i-m_j)^2-m_Z^2\right) \\ &+q^4m_j^2\big)-3q^2m_Z^2+4m_Z^4+\frac{1}{2}q^4\Big]+(i\leftrightarrow j), \end{aligned} \tag{A.72}$$

$$\begin{aligned}U_{4ij} = -\frac{1}{q^2}\Big[& m_Z^2 B_{ii}\left(m_Z^2\right)\left(2q^2\left(2m_i^2 - 2m_j^2 + m_Z^2\right) - 4m_Z^2\left(m_i^2 - m_j^2\right) + q^4\right) \\ & + q^2\left(m_Z^2\left(2m_Z^2 + q^2\right)\left(B_{ij}\left(m_Z^2\right) - 2B_{ij}\left(q^2\right)\right) + \left(6q^2 m_Z^2 - 8m_Z^4 + q^4\right)\right) \\ & + C_{iij}\left(q^2\right)\left(q^6 m_i\left(m_j - m_i\right) - q^4 m_Z^2\left(8m_i m_j - m_i^2 - 3m_j^2 + 4m_Z^2\right)\right. \\ & \left. - 4q^2 m_Z^2\left(\left(m_i - m_j\right)^2 - m_Z^2\right)\left(\left(m_i + m_j\right)^2 + m_Z^2\right) + 4m_Z^4\left(m_i^2 - m_j^2\right)^2\right)\Big] + (i \leftrightarrow j),\end{aligned} \tag{A.73}$$

$$U_{5ij} = U_{4ij}(m_j \to -m_j), \tag{A.74}$$

$$\begin{aligned}U_{6ij} = -2\Big[& B_{ii}\left(q^2\right)\left(-q^2\left(2m_j\left(m_i + m_j\right) + m_Z^2\right) + 2m_Z^2\left(m_i + m_j\right)\left(3m_i + m_j\right) - 2m_Z^4\right) \\ & + B_{ij}\left(m_Z^2\right)\left(q^2\left(\left(m_i + m_j\right)^2 + m_Z^2\right) - 4m_Z^2\left(m_i + m_j\right)^2 + 2m_Z^4\right) \\ & + C_{iji}\left(q^2\right)\left(-q^4 m_j\left(m_i + m_j\right) + 2q^2\left(m_Z^2\left(3m_i m_j + m_i^2 + m_j^2\right) + m_j\left(m_i^2 - m_j^2\right)\left(m_i + m_j\right) - m_Z^4\right)\right. \\ & \left. - 2m_Z^2\left(\left(m_i + m_j\right)^2 - m_Z^2\right)\left(\left(m_i - m_j\right)\left(3m_i + m_j\right) + m_Z^2\right)\right) + 3q^2 m_Z^2 - 4m_Z^4 - \frac{1}{2}q^4\Big] + (i \leftrightarrow j),\end{aligned} \tag{A.75}$$

and

$$U_{7ij} = U_{6ij}(m_j \to -m_j). \tag{A.76}$$

$$\begin{aligned}T_{1ij} = \Big[& 3\left(m_i - m_j\right)\left(q^2\left(m_i + m_j\right)\left(B_{ij}\left(q^2\right)\left(q^2 - 2m_Z^2\right) - m_Z^2 B_{ij}\left(m_Z^2\right)\right) + C_{iij}\left(q^2\right)\left(q^4\left(2m_i^2\left(m_i + m_j\right)\right.\right.\right. \\ & \left.\left.\left. - m_Z^2\left(3m_i + m_j\right)\right) - 2q^2 m_Z^2\left(m_i + m_j\right)\left(2m_i\left(m_i + m_j\right) - m_Z^2\right) + 2m_Z^2\left(m_i - m_j\right)^2\left(m_i + m_j\right)^3 + q^6 m_i\right)\right) \\ & + B_{ii}\left(m_Z^2\right)\left(q^2 m_Z^2\left(12m_i m_j + 7m_i^2 - 3m_j^2 - 4m_Z^2\right) - 6m_Z^2\left(m_i^2 - m_j^2\right)^2 + q^4\left(m_Z^2 - 4m_i^2\right)\right) \\ & - 2q^2 B_{ii}(0) m_i^2\left(q^2 - 4m_Z^2\right)\Big] - (i \leftrightarrow j),\end{aligned} \tag{A.77}$$

$$T_{2ij} = T_{1ij}(m_j \to -m_j), \tag{A.78}$$

$$T_{3ij} = 6q^4 m_i m_j\Big[C_{iji}\left(q^2\right)\left(2\left(m_i^2 - m_j^2 + m_Z^2\right) - q^2\right) - 2B_{ii}\left(q^2\right)\Big] - (i \leftrightarrow j), \tag{A.79}$$

$$
\begin{aligned}
T_{4ij} = \Big[& 3\left(m_i + m_j\right)\left(C_{iij}\left(q^2\right)\left(q^4\left(m_Z^2\left(m_i + m_j\right) + 2m_i m_j\left(m_j - m_i\right)\right) - 2q^2 m_Z^2\left(m_i - m_j\right)\right.\right. \\
& \times \left(2m_i\left(m_i - m_j\right) - m_Z^2\right) + 2m_Z^2\left(m_i - m_j\right)\left(m_i^2 - m_j^2\right)^2 - q^6 m_i\Big) \\
& - q^2\left(m_i - m_j\right)\left(B_{ij}\left(q^2\right)\left(2m_Z^2 + q^2\right) + \left(m_Z^2 - q^2\right) B_{ij}\left(m_Z^2\right)\right)\Big) \\
& + B_{ii}\left(m_Z^2\right)\left(q^4\left(2m_i\left(m_i + 3m_j\right) + m_Z^2\right) - q^2 m_Z^2\left(12m_i m_j - 7m_i^2 + 3m_j^2 + 4m_Z^2\right) - 6m_Z^2\left(m_i^2 - m_j^2\right)^2\right) \\
& - 2q^2 B_{ii}(0) m_i^2\left(q^2 - 4m_Z^2\right)\Big] - (i \leftrightarrow j),
\end{aligned} \tag{A.80}
$$

$$
T_{5ij} = T_{4ij}(m_j \to -m_j), \tag{A.81}
$$

A.4.2 Closed form results

We now present the closed form of the TGNBCs presented above. We only expand the two-point scalar functions in terms of transcendental functions as the three-point functions are too cumbersome to be expanded. We first introduce the following auxiliary functions:

$$
\eta\left(x,y\right) = \sqrt{x^4 - 4x^2 y^2}, \tag{A.82}
$$

$$
\beta\left(x,y,z\right) = \sqrt{-2x^2\left(y^2 + z^2\right) + x^4 + \left(y^2 - z^2\right)^2}, \tag{A.83}
$$

$$
\chi\left(x,y\right) = \log\left(\frac{\sqrt{x^4 - 4x^2 y^2} + 2y^2 - x^2}{2y^2}\right), \tag{A.84}
$$

and

$$
\xi\left(x,y,z\right) = \log\left(\frac{\sqrt{-2x^2\left(y^2 + z^2\right) + x^4 + \left(y^2 - z^2\right)^2} + x^2 + y^2 - z^2}{2xy}\right). \tag{A.85}
$$

$ZZ\gamma^*$ coupling

The R_{ij} function of Eq.(4.27) can be written as follows

$$
\begin{aligned}
R_{ij} = -\frac{1}{q^2}\Big[& -q^2\big(2q^2\left(-m_Z^2\left(2m_i^2+m_j^2\right)+\left(m_i^2-m_j^2\right)^2+m_Z^4\right)-2m_Z^2\left(-m_i-m_j+m_Z\right)\left(m_i-m_j+m_Z\right) \\
& \times\left(-m_i+m_j+m_Z\right)\left(m_i+m_j+m_Z\right)+q^2m_j^2\big)C_{iji}\left(q^2\right)-q^2\big(m_i^2\big(-2q^2\left(2m_j^2+m_Z^2\right) \\
& +4m_Z^2\left(m_j^2+m_Z^2\right)+q^4\big)+2m_i^4\left(q^2-m_Z^2\right)-2\left(m_j^2-m_Z^2\right)^2\left(m_Z^2-q^2\right)\big)C_{jij}\left(q^2\right) \\
& +3q^4\log\left(\frac{m_i^2}{m_j^2}\right)\left(m_j^2-m_i^2\right)-\eta\left(q,m_j\right)\log\left(\chi\left(q,m_j\right)\right)\left(q^2\left(2m_i^2-2m_j^2+m_Z^2\right)+2m_Z^2\left(-m_i^2+m_j^2+m_Z^2\right)\right) \\
& +2\eta\left(q,m_i\right)\log\left(\chi\left(q,m_i\right)\right)\left(m_i^2-m_j^2\right)\left(q^2-m_Z^2\right)+6q^4m_Z^2+4\beta\left(m_i,m_j,m_Z\right)q^2m_Z^2\log\left(\xi\left(m_i,m_j,m_Z\right)\right) \\
& -\eta\left(q,m_i\right)q^2m_Z^2\log\left(\chi\left(q,m_i\right)\right)-8q^2m_Z^4-2\eta\left(q,m_i\right)m_Z^4\log\left(\chi\left(q,m_i\right)\right)-q^6+2\beta\left(m_i,m_j,m_Z\right)q^4 \\
& \times\log\left(\xi\left(m_i,m_j,m_Z\right)\right)\Big]. \qquad \text{(A.86)}
\end{aligned}
$$

ZZZ^* coupling

The R_{kij} and S_{ij} functions of Eqs. (4.31) and (4.29) read

$$
\begin{aligned}
R_{1ij} = \frac{1}{\left(q^2-4m_Z^2\right)q^2m_Z^2}\Bigg[& -\frac{1}{\left(q^2-m_Z^2\right)}\Big\{-q^2m_Z^2\big(q^2\left(-3m_i^2\left(m_j^2+m_Z^2\right)+m_i^4+2\left(-m_j^2m_Z^2+m_j^4+m_Z^4\right)\right) \\
& -2m_Z^2\left(\left(m_j^2-m_Z^2\right)^2-m_i^4\right)+q^4m_j^2\big)C_{iji}\left(q^2\right)+m_Z^2\big(q^4\big(m_i^2\left(m_j^2+7m_Z^2\right)-m_i^4+3m_j^2m_Z^2-4m_Z^4\big) \\
& +4q^2m_Z^2\left(m_i^2\left(m_j^2-2m_Z^2\right)-m_j^4+m_Z^4\right)+4m_Z^4\left(m_i^2-m_j^2\right)^2-2q^6m_i^2\big)C_{iij}\left(q^2\right)-m_Z^2q^2\big(q^4-5q^2m_Z^2+m_Z^4\big) \\
& +\eta\left(q,m_i\right)m_Z^2\left(q^2\left(m_i^2-2m_j^2-m_Z^2\right)+2m_Z^2\left(m_i^2+m_j^2-m_Z^2\right)\right)\log\left(\chi\left(q,m_i\right)\right) \\
& +\eta\left(m_Z,m_i\right)\left(m_i^2\left(q^4-4m_Z^4\right)+m_Z^2\left(4m_j^2\left(m_Z^2-q^2\right)+2q^2m_Z^2+q^4\right)\right)\log\left(\chi\left(m_Z,m_i\right)\right) \\
& +\beta\left(m_i,m_j,m_Z\right)\left(q^4\left(m_i^2+m_j^2+2m_Z^2\right)+4m_Z^4\left(m_i^2-m_j^2\right)+4q^2m_Z^2\left(m_Z^2-2m_i^2\right)\right)\log\left(\xi\left(m_i,m_j,m_Z\right)\right) \\
& +\beta\left(m_i,m_j,q\right)m_Z^2\left(m_i^2\left(6m_Z^2-3q^2\right)+\left(m_j^2-2m_Z^2\right)\left(2m_Z^2+q^2\right)\right)\log\left(\xi\left(m_i,m_j,q\right)\right)\Big\} \\
& -\frac{\left(m_i^2-m_j^2\right)}{2}\Big\{m_i^2\left(10m_Z^2-q^2\right)-\left(m_j^2+4m_Z^2\right)\left(2m_Z^2+q^2\right)\Big\}\log\left(\frac{m_i^2}{m_j^2}\right)\Bigg], \qquad \text{(A.87)}
\end{aligned}
$$

$$
\begin{aligned}
R_{2ij} = \frac{m_i^2}{q^2m_Z^2}\Bigg[& -\frac{1}{\left(m_Z^2-q^2\right)}\Big\{q^2m_Z^2\left(m_i^2-m_j^2-2m_Z^2+q^2\right)C_{iij}\left(q^2\right)+q^2m_Z^2\left(-m_i^2+m_j^2+m_Z^2\right)C_{iji}\left(q^2\right) \\
& +m_Z^2\big(2\beta\left(m_i,m_j,q\right)\log\left(\xi\left(m_i,m_j,q\right)\right)+\eta\left(q,m_i\right)\log\left(\chi\left(q,m_i\right)\right)\big) \\
& -q^2\left(2\beta\left(m_i,m_j,m_Z\right)\log\left(\xi\left(m_i,m_j,m_Z\right)\right)+\eta\left(m_Z,m_i\right)\log\left(\chi\left(m_Z,m_i\right)\right)\right)\Big\}+\left(m_i^2-m_j^2\right)\log\left(\frac{m_i^2}{m_j^2}\right)\Bigg], \\
& \qquad \text{(A.88)}
\end{aligned}
$$

$$R_{3ij} = \frac{m_i m_j}{q^2 m_Z^2}\Bigg[- \frac{1}{\left(m_Z^2 - q^2\right)}\Big\{q^2 m_Z^2 \left(2m_i^2 - 2m_j^2 + q^2\right) C_{iij}\left(q^2\right) + q^2 m_Z^2 \left(q^2 - 2\left(m_i^2 - m_j^2 + m_Z^2\right)\right) C_{iji}\left(q^2\right) + 2m_Z^2 \big(2\beta\left(m_i,m_j,q\right)\log\left(\xi\left(m_i,m_j,q\right)\right) + \eta\left(q,m_i\right)\log\left(\chi\left(q,m_i\right)\right)\big) - 2q^2\big(2\beta_1\log\left(\xi\left(m_i,m_j,m_Z\right)\right) + \eta\left(m_Z,m_i\right)\log\left(\chi\left(m_Z,m_i\right)\right)\big)\Big\} + 2\left(m_i^2 - m_j^2\right)\log\left(\frac{m_i^2}{m_j^2}\right)\Bigg], \tag{A.89}$$

and

$$S_{ij} = -C_{iij}\left(q^2\right)\left(2m_Z^2 - q^2\right)\left(2m_i^2 - 2m_j^2 + q^2\right) + q^2 C_{iji}\left(q^2\right)\left(-\left(q^2 - 2\left(m_i^2 - m_j^2 + m_Z^2\right)\right)\right) + C_{ijj}\left(q^2\right)\left(q^2 - 2m_Z^2\right)\left(2m_i^2 - 2m_j^2 - q^2\right) + q^2 C_{jij}\left(q^2\right)\left(2m_i^2 - 2\left(m_j^2 + m_Z^2\right) + q^2\right) - 2\eta\left(q,m_i\right)\log\left(\chi\left(q,m_i\right)\right) + 2\eta\left(q,m_j\right)\log\left(\chi\left(q,m_j\right)\right) + 4\left(q^2 - m_Z^2\right)\log\left(\frac{m_i^2}{m_j^2}\right) + \frac{2\left(2m_Z^2 - q^2\right)}{m_Z^2}\Big\{\eta\left(m_Z,m_i\right)\log\left(\chi\left(m_Z,m_i\right)\right) - \eta\left(m_Z,m_j\right)\log\left(\chi\left(m_Z,m_j\right)\right)\Big\}. \tag{A.90}$$

ZZZ'^* coupling

Finally, the L_i T_{kij} and U_{kij} functions of Eqs. (4.33)-(4.35) are given as follows

$$L_{1i} = \frac{1}{q^2}\Big\{4q^2 m_Z^2 C_{iii}\left(q^2\right)\left(q^2\left(m_i^2 + m_Z^2\right) - m_Z^2\left(4m_i^2 + m_Z^2\right)\right) - 6q^4 m_Z^2 + 2\left(2m_Z^2 + q^2\right)\big(\eta\left(q,m_i\right)m_Z^2\log\left(\chi\left(q,m_i\right)\right) - \eta\left(m_Z,m_i\right)q^2\log\left(\chi\left(m_Z,m_i\right)\right)\big) + 8q^2 m_Z^4 + q^6\Big\}, \tag{A.91}$$

$$L_{2i} = \frac{1}{q^2 m_Z^2}\Big\{ - 4q^2 m_Z^2 C_{iii}\left(q^2\right)\left(m_Z^2 - q^2\right)\left(m_i^2\left(q^2 - 4m_Z^2\right) + m_Z^4\right) + 2\big(4m_i^2\left(q^2 - 4m_Z^2\right) + m_Z^2\left(2m_Z^2 + q^2\right)\big)\left(\eta\left(q,m_i\right)m_Z^2\log\left(\chi\left(q,m_i\right)\right) - \eta\left(m_Z,m_i\right)q^2\log\left(\chi\left(m_Z,m_i\right)\right)\right) + q^6 m_Z^2 - 6q^4 m_Z^4 + 8q^2 m_Z^6\Big\}, \tag{A.92}$$

$$L_{3i} = \frac{2}{q^2}\Big\{2q^2 C_{iii}\left(q^2\right)\left(m_i^2\left(-6q^2m_Z^2+8m_Z^4+q^4\right)-2m_Z^4\left(m_Z^2-q^2\right)\right)-6q^4m_Z^2 + 2\left(2m_Z^2+q^2\right)\left(\eta\left(q,m_i\right)m_Z^2\log\left(\chi\left(q,m_i\right)\right)-\eta\left(m_Z,m_i\right)q^2\log\left(\chi\left(m_Z,m_i\right)\right)\right)+8q^2m_Z^4+q^6\Big\}, \tag{A.93}$$

$$\begin{aligned}U_{1ij} = &-\frac{1}{q^2}\Big\{C_{iij}\left(q^2\right)\left(q^6m_i\left(m_j-3m_i\right)+q^4\left(m_Z^2\left(-4m_im_j+13m_i^2+3m_j^2\right)-2m_i\left(m_i-m_j\right)^2\left(m_i+m_j\right)-4m_Z^4\right)\right.\\ &+4q^2m_Z^2\left(\left(m_i-m_j\right)^3\left(m_i+m_j\right)-4m_i^2m_Z^2+m_Z^4\right)+4m_Z^4\left(m_i^2-m_j^2\right)^2\big)+C_{jji}\left(q^2\right)\left(q^6m_j\left(m_i-3m_j\right)\right.\\ &+q^4\left(m_Z^2\left(-4m_im_j+3m_i^2+13m_j^2\right)-2m_j\left(m_i-m_j\right)^2\left(m_i+m_j\right)-4m_Z^4\right)+4q^2m_Z^2\big(-\left(m_i-m_j\right)^3\left(m_i+m_j\right)\\ &\left.\left.-4m_j^2m_Z^2+m_Z^4\right)+4m_Z^4\left(m_i^2-m_j^2\right)^2\right)-2\left(-6q^4m_Z^2+8q^2m_Z^4+q^6\right)\Big\}-\frac{2}{m_Z^2}\Big\{\beta\left(m_i,m_j,m_Z\right)\\ &\times\log\left(\xi\left(m_i,m_j,m_Z\right)\right)\left(q^2\left(\left(m_i-m_j\right)^2+m_Z^2\right)-4m_Z^2\left(m_i-m_j\right)^2+2m_Z^4\right)\Big\}+\frac{4}{q^2}\Big\{\beta\left(m_i,m_j,q\right)\\ &\times\log\left(\xi\left(m_i,m_j,q\right)\right)\left(q^2\left(\left(m_i-m_j\right)^2+m_Z^2\right)-4m_Z^2\left(m_i-m_j\right)^2+2m_Z^4\right)\Big\}\\ &+\frac{\left(m_i^2-m_j^2\right)\left(2m_Z^2-q^2\right)}{q^2m_Z^2}\log\left(\frac{m_i^2}{m_j^2}\right)\left\{q^2\left(-\left(\left(m_i-m_j\right)^2+2m_Z^2\right)\right)-4m_Z^2\left(m_Z^2-\left(m_i-m_j\right)^2\right)\right\}\\ &+\frac{\eta\left(m_Z,m_i\right)\log\left(\chi\left(m_Z,m_i\right)\right)}{q^2m_Z^2}\Big\{q^4\left(-\left(2m_i\left(m_i-m_j\right)+m_Z^2\right)\right)-2q^2m_Z^2\left(m_Z^2-2\left(m_i-m_j\right)^2\right)\\ &+4m_Z^4\left(m_i^2-m_j^2\right)\Big\}-\frac{\eta\left(m_Z,m_j\right)\log\left(\chi\left(m_Z,m_j\right)\right)}{q^2m_Z^2}\Big\{q^4\left(2m_j\left(m_j-m_i\right)+m_Z^2\right)\\ &+2q^2m_Z^2\left(m_Z^2-2\left(m_i-m_j\right)^2\right)+4m_Z^4\left(m_i^2-m_j^2\right)\Big\},\end{aligned} \tag{A.94}$$

$$U_{2ij} = U_{1ij}(m_j \to -m_j), \tag{A.95}$$

$$\begin{aligned}U_{3ij} = &2\Big\{\big(C_{iji}\left(q^2\right)\left(2q^2\left(-m_Z^2\left(2m_i^2+m_j^2\right)+\left(m_i^2-m_j^2\right)^2+m_Z^4\right)-2m_Z^2\left(-(m_i-m_j)^2+m_Z^2\right)\right.\\ &\left.\times\left(-(m_i+m_j)^2+m_Z^2\right)+q^4m_j^2\right)+C_{jij}\left(q^2\right)\left(m_i^2\left(-2q^2\left(2m_j^2+m_Z^2\right)+4m_Z^2\left(m_j^2+m_Z^2\right)+q^4\right)\right.\\ &\left.+2m_i^4\left(q^2-m_Z^2\right)-2\left(m_j^2-m_Z^2\right)^2\left(m_Z^2-q^2\right)\big)-6q^2m_Z^2+8m_Z^4+q^4\Big\}\\ &+\frac{2\eta\left(q,m_i\right)\log\left(\chi\left(q,m_i\right)\right)}{q^2}\Big\{q^2\left(-2m_i^2+2m_j^2+m_Z^2\right)+2m_Z^2\left(m_i^2-m_j^2+m_Z^2\right)\Big\}\\ &+\frac{2\eta\left(q,m_j\right)\log\left(\chi\left(q,m_j\right)\right)}{q^2}\Big\{q^2\left(2m_i^2-2m_j^2+m_Z^2\right)+2m_Z^2\left(-m_i^2+m_j^2+m_Z^2\right)\Big\}\\ &+6q^2\left(m_i^2-m_j^2\right)\log\left(\frac{m_i^2}{m_j^2}\right)-4\beta\left(m_i,m_j,m_Z\right)\log\left(\xi\left(m_i,m_j,m_Z\right)\right)\left(2m_Z^2+q^2\right),\end{aligned} \tag{A.96, A.97}$$

$$
\begin{aligned}
U_{4ij} = & -\frac{1}{q^2}\Big\{C_{iij}\left(q^2\right)\left(q^6 m_i\left(m_j-m_i\right)+q^4 m_Z^2\left(-8m_i m_j+m_i^2+3m_j^2-4m_Z^2\right)+4q^2 m_Z^2\left(-\left(m_i-m_j\right)^2+m_Z^2\right)\right. \\
& \times\left(\left(m_i+m_j\right)^2+m_Z^2\right)+4m_Z^4\left(m_i^2-m_j^2\right)^2)+C_{jji}\left(q^2\right)\left(q^6 m_j\left(m_i-m_j\right)+q^4 m_Z^2(-8m_i m_j+3m_i^2+m_j^2\right. \\
& -4m_Z^2)+4q^2 m_Z^2\left(-\left(m_i-m_j\right)^2+m_Z^2\right)\left(\left(m_i+m_j\right)^2+m_Z^2\right)+4m_Z^4\left(m_i^2-m_j^2\right)^2)-2(-6q^4 m_Z^2+8q^2 m_Z^4 \\
& \left.+q^6)\Big\}-\frac{\eta\left(m_Z,m_i\right)\log\left(\chi\left(m_Z,m_i\right)\right)}{q^2}\left\{2q^2\left(2m_i^2-2m_j^2+m_Z^2\right)-4m_Z^2\left(m_i^2-m_j^2\right)+q^4\right\} \\
& -\frac{\eta\left(m_Z,m_j\right)\log\left(\chi\left(m_Z,m_j\right)\right)}{q^2}\left\{2q^2\left(-2m_i^2+2m_j^2+m_Z^2\right)+4m_Z^2\left(m_i^2-m_j^2\right)+q^4\right\} \\
& +\frac{\left(m_i^2-m_j^2\right)\left(4q^2 m_Z^2-8m_Z^4+q^4\right)}{q^2}\log\left(\frac{m_i^2}{m_j^2}\right)-2\beta\left(m_i,m_j,m_Z\right)\log\left(\xi\left(m_i,m_j,m_Z\right)\right)\left(2m_Z^2+q^2\right) \\
& +\log\left(\xi\left(m_i,m_j,q\right)\right)\left\{\frac{8\beta\left(m_i,m_j,q\right)m_Z^4}{q^2}+4\beta\left(m_i,m_j,q\right)m_Z^2\right\},
\end{aligned}
\tag{A.98}
$$

$$
U_{5ij} = U_{4ij}(m_j \to -m_j),
\tag{A.99}
$$

$$
\begin{aligned}
U_{6ij} = & 2\Big\{C_{iji}\left(q^2\right)\left(q^4 m_j\left(m_i+m_j\right)-2q^2\left(m_Z^2\left(3m_i m_j+m_i^2+m_j^2\right)+m_j\left(m_i-m_j\right)\left(m_i+m_j\right)^2-m_Z^4\right)\right. \\
& -2m_Z^2\left(-\left(m_i+m_j\right)^2+m_Z^2\right)\left(\left(m_i-m_j\right)\left(3m_i+m_j\right)+m_Z^2\right))+C_{jij}\left(q^2\right)\left(q^4 m_i\left(m_i+m_j\right)\right. \\
& +2q^2\left(-m_Z^2\left(3m_i m_j+m_i^2+m_j^2\right)+m_i\left(m_i-m_j\right)\left(m_i+m_j\right)^2+m_Z^4\right)-2m_Z^2\left(-\left(m_i+m_j\right)^2+m_Z^2\right) \\
& \times\left(m_Z^2-\left(m_i-m_j\right)\left(m_i+3m_j\right)\right))-6q^2 m_Z^2+8m_Z^4+q^4\Big\} \\
& -\frac{4\beta\left(m_i,m_j,m_Z\right)\log\left(\xi\left(m_i,m_j,m_Z\right)\right)}{m_Z^2}\left\{q^2\left(\left(m_i+m_j\right)^2+m_Z^2\right)-4m_Z^2\left(m_i+m_j\right)^2+2m_Z^4\right\} \\
& +\frac{2\eta\left(q,m_i\right)\log\left(\chi\left(q,m_i\right)\right)\left(q^2\left(2m_j\left(m_i+m_j\right)+m_Z^2\right)-2m_Z^2\left(m_i+m_j\right)\left(3m_i+m_j\right)+2m_Z^4\right)}{q^2} \\
& +\frac{2\eta\left(q,m_j\right)\log\left(\chi\left(q,m_j\right)\right)\left(q^2\left(2m_i\left(m_i+m_j\right)+m_Z^2\right)-2m_Z^2\left(m_i+m_j\right)\left(m_i+3m_j\right)+2m_Z^4\right)}{q^2} \\
& -\frac{2\left(m_i^2-m_j^2\right)}{m_Z^2}\log\left(\frac{m_i^2}{m_j^2}\right)\left\{4m_Z^2\left(\left(m_i+m_j\right)^2-m_Z^2\right)-q^2\left(\left(m_i+m_j\right)^2+2m_Z^2\right)\right\},
\end{aligned}
\tag{A.100}
$$

$$
U_{7ij} = U_{6ij}(m_j \to -m_j),
\tag{A.101}
$$

$$
\begin{aligned}
T_{1ij} = {} & \left(m_i - m_j\right)\Big\{3C_{iij}\left(q^2\right)\left(q^4\left(2m_i^2\left(m_i+m_j\right) - m_Z^2\left(3m_i+m_j\right)\right) - 2q^2m_Z^2\left(m_i+m_j\right)\left(2m_i\left(m_i+m_j\right) - m_Z^2\right)\right. \\
& + 2m_Z^2\left(m_i-m_j\right)^2\left(m_i+m_j\right)^3 + q^6m_i\Big) + 3C_{jji}\left(q^2\right)\left(q^4\left(2m_j^2\left(m_i+m_j\right) - m_Z^2\left(m_i+3m_j\right)\right)\right. \\
& - 2q^2m_Z^2\left(m_i+m_j\right)\left(2m_j\left(m_i+m_j\right) - m_Z^2\right) + 2m_Z^2\left(m_i-m_j\right)^2\left(m_i+m_j\right)^3 + q^6m_j\Big) \\
& + 4q^2\left(m_i+m_j\right)\left(q^2 - 4m_Z^2\right)\Big\} + 6\beta\left(m_i,m_j,m_Z\right)q^2\log\left(\xi\left(m_i,m_j,m_Z\right)\right)\left(m_j^2 - m_i^2\right) \\
& - 6\beta\left(m_i,m_j,q\right)\log\left(\xi\left(m_i,m_j,q\right)\right)\left(m_i^2 - m_j^2\right)\left(2m_Z^2 - q^2\right) \\
& + \frac{\eta\left(m_Z,m_i\right)\log\left(\chi\left(m_Z,m_i\right)\right)}{m_Z^2}\Big\{q^2m_Z^2\left(12m_im_j + 7m_i^2 - 3m_j^2 - 4m_Z^2\right) - 6m_Z^2\left(m_i^2 - m_j^2\right)^2 + q^4\left(m_Z^2 - 4m_i^2\right)\Big\} \\
& + \frac{\eta\left(m_Z,m_j\right)\log\left(\chi\left(m_Z,m_j\right)\right)}{m_Z^2}\Big\{q^2m_Z^2\left(-12m_im_j + 3m_i^2 - 7m_j^2 + 4m_Z^2\right) + 6m_Z^2\left(m_i^2 - m_j^2\right)^2 + q^4\left(4m_j^2 - m_Z^2\right)\Big\} \\
& + \log\left(\frac{m_i^2}{m_j^2}\right)\Big\{q^4\left(3\left(m_i^2+m_j^2\right) - m_Z^2\right) - 2q^2m_Z^2\left(3\left(m_i+m_j\right)^2 - 2m_Z^2\right) + 12m_Z^2\left(m_i^2 - m_j^2\right)^2\Big\},
\end{aligned}
\tag{A.102}
$$

$$
T_{2ij} = T_{1ij}(m_j \to -m_j), \tag{A.103}
$$

$$
\begin{aligned}
T_{3ij} = {} & 6q^4m_im_j\Big\{C_{iji}\left(q^2\right)\left(2\left(m_i^2 - m_j^2 + m_Z^2\right) - q^2\right) + C_{jij}\left(q^2\right)\left(2m_i^2 - 2\left(m_j^2+m_Z^2\right) + q^2\right)\Big\} \\
& + 12q^4m_im_j\log\left(\frac{m_i^2}{m_j^2}\right) - 12\eta\left(q,m_i\right)q^2m_im_j\log\left(\chi\left(q,m_i\right)\right) + 12\eta\left(q,m_j\right)q^2m_im_j\log\left(\chi\left(q,m_j\right)\right),
\end{aligned}
\tag{A.104}
$$

$$
\begin{aligned}
T_{4ij} = {} & \left(m_i + m_j\right)\Big\{3C_{iij}\left(q^2\right)\left(q^4\left(m_Z^2\left(m_i + m_j\right) + 2m_i m_j\left(m_j - m_i\right)\right) - 2q^2 m_Z^2\left(m_i - m_j\right)\left(2m_i\left(m_i - m_j\right) - m_Z^2\right)\right. \\
& + 2m_Z^2\left(m_i - m_j\right)^3\left(m_i + m_j\right)^2 + q^6\left(-m_i\right)\Big) + 3C_{jji}\left(q^2\right)\Big(-q^4\left(m_Z^2\left(m_i + m_j\right) + 2m_i m_j\left(m_i - m_j\right)\right) \\
& + 2q^2 m_Z^2\left(m_i - m_j\right)\left(2m_j\left(m_i - m_j\right) + m_Z^2\right) + 2m_Z^2\left(m_i - m_j\right)^3\left(m_i + m_j\right)^2 + q^6 m_j\Big) \\
& \left. + 4q^2\left(m_i - m_j\right)\left(q^2 - 4m_Z^2\right)\right\} + \frac{6\beta\left(m_i, m_j, m_Z\right) q^2 \log\left(\xi\left(m_i, m_j, m_Z\right)\right)}{m_Z^2}\left(m_i^2 - m_j^2\right)\left(q^2 - m_Z^2\right) \\
& - 6\beta\left(m_i, m_j, q\right)\log\left(\xi\left(m_i, m_j, q\right)\right)\left(m_i^2 - m_j^2\right)\left(2m_Z^2 + q^2\right) + \frac{\eta\left(m_Z, m_i\right)\log\left(\chi\left(m_Z, m_i\right)\right)}{m_Z^2}\Big\{q^4\big(2m_i\left(m_i + 3m_j\right) + r \\
& - q^2 m_Z^2\left(12m_i m_j - 7m_i^2 + 3m_j^2 + 4m_Z^2\right) - 6m_Z^2\left(m_i^2 - m_j^2\right)^2\Big\} + \frac{\eta\left(m_Z, m_j\right)\log\left(\chi\left(m_Z, m_j\right)\right)}{m_Z^2}\Big\{q^4\big(-\big(2m_j \\
& \times\left(3m_i + m_j\right) + m_Z^2\big)\big) + q^2 m_Z^2\left(12m_i m_j + 3m_i^2 - 7m_j^2 + 4m_Z^2\right) + 6m_Z^2\left(m_i^2 - m_j^2\right)^2\Big\} \\
& + \frac{1}{m_Z^2}\log\left(\frac{m_i^2}{m_j^2}\right)\Big\{q^4\left(-\left(6m_i m_j m_Z^2 + 3\left(m_i^2 - m_j^2\right)^2 + m_Z^4\right)\right) + 2q^2 m_Z^2\big(-3m_Z^2\left(m_i - m_j\right)^2 + 3\left(m_i^2 - m_j^2\right)^2 \\
& + 2m_Z^4\big) + 12m_Z^4\left(m_i^2 - m_j^2\right)^2\Big\}, \qquad \text{(A.105)}
\end{aligned}
$$

and

$$
T_{5ij} = T_{4ij}(m_j \to -m_j), \qquad \text{(A.106)}
$$

Bibliography

[1] S. Laporta and E. Remiddi. The Analytical value of the electron (g-2) at order alpha**3 in QED. *Phys. Lett.*, B379:283–291, 1996.

[2] S. R. Moore, K. Whisnant, and Bing-Lin Young. Second Order Corrections to the Muon Anomalous Magnetic Moment in Alternative Electroweak Models. *Phys. Rev.*, D31:105, 1985.

[3] Fred Jegerlehner. The Muon g-2 in Progress. *Acta Phys. Polon.*, B49:1157, 2018.

[4] Andrzej Czarnecki and Maciej Skrzypek. The Muon anomalous magnetic moment in QED: Three loop electron and tau contributions. *Phys. Lett.*, B449:354–360, 1999.

[5] Manfred Lindner, Moritz Platscher, and Farinaldo S. Queiroz. A Call for New Physics : The Muon Anomalous Magnetic Moment and Lepton Flavor Violation. *Phys. Rept.*, 731:1–82, 2018.

[6] Maxim Pospelov and Adam Ritz. Electric dipole moments as probes of new physics. *Annals Phys.*, 318:119–169, 2005.

[7] Andrzej Czarnecki and William J. Marciano. Electromagnetic dipole moments and new physics. *Adv. Ser. Direct. High Energy Phys.*, 20:11–67, 2009.

[8] A. Moyotl, A. Rosado, and G. Tavares-Velasco. Lepton electric and magnetic dipole moments via lepton flavor violating spin-1 unparticle interactions. *Phys. Rev.*, D84:073010, 2011.

[9] H. Novales-Sánchez, M. Salinas, J. J. Toscano, and O. Vázquez-Hernández. Electric dipole moments of charged leptons at one loop in the presence of massive neutrinos. *Phys. Rev.*, D95(5):055016, 2017.

[10] Chia-Feng Chang, P. Q. Hung, Chrisna Setyo Nugroho, Van Que Tran, and Tzu-Chiang Yuan. Electron Electric Dipole Moment in Mirror Fermion Model with Electroweak Scale Non-sterile Right-handed Neutrinos. *Nucl. Phys.*, B928:21–37, 2018.

[11] Venus Keus, Niko Koivunen, and Kimmo Tuominen. Singlet scalar and 2HDM extensions of the Standard Model: CP-violation and constraints from $(g-2)_\mu$ and eEDM. *JHEP*, 09:059, 2018.

[12] Hector Gisbert and Joan Ruiz Vidal. Improved bounds on heavy quark electric dipole moments. *Phys. Rev. D*, 101(11):115010, 2020.

[13] A.I. Hernández-Juárez, A. Moyotl, and G. Tavares-Velasco. Chromomagnetic and chromoelectric dipole moments of the top quark in the fourth-generation THDM. *Phys. Rev. D*, 98(3):035040, 2018.

[14] R. Martinez, M. A. Perez, and N. Poveda. Chromomagnetic Dipole Moment of the Top Quark Revisited. *Eur. Phys. J. C*, 53:221–230, 2008.

[15] R. Gaitan, E.A. Garces, J. H. Montes de Oca, and R. Martinez. Top quark Chromoelectric and Chromomagnetic Dipole Moments in a Two Higgs Doublet Model with CP violation. *Phys. Rev. D*, 92(9):094025, 2015.

[16] Qing-Hong Cao, Chuan-Ren Chen, F. Larios, and C. P. Yuan. Anomalous gtt couplings in the Littlest Higgs Model with T-parity. *Phys. Rev. D*, 79:015004, 2009.

[17] Li Ding and Chong-Xing Yue. Top quark chromomagnetic dipole moment in the littlest Higgs model with T-parity. *Commun. Theor. Phys.*, 50:441–444, 2008.

[18] Amin Aboubrahim, Tarek Ibrahim, Pran Nath, and Anas Zorik. Chromoelectric Dipole Moments of Quarks in MSSM Extensions. *Phys. Rev. D*, 92(3):035013, 2015.

[19] R. Martinez, M. A. Perez, and O. A. Sampayo. Constraints on unparticle physics from the gt $\bar{t}$ anomalous coupling. *Int. J. Mod. Phys. A*, 25:1061–1067, 2010.

[20] Tarek Ibrahim and Pran Nath. The Chromoelectric Dipole Moment of the Top Quark in Models with Vector Like Multiplets. *Phys. Rev. D*, 84:015003, 2011.

[21] V. Khachatryan et al. Measurements of t t-bar spin correlations and top quark polarization using dilepton final states in pp collisions at sqrt(s) = 8 TeV. *Phys. Rev.*, D93(5):052007, 2016.

[22] Andrzej Czarnecki and Bernd Krause. Neutron electric dipole moment in the standard model: Valence quark contributions. *Phys. Rev. Lett.*, 78:4339–4342, 1997.

[23] I. B. Khriplovich. Quark Electric Dipole Moment and Induced θ Term in the Kobayashi-Maskawa Model. *Phys. Lett. B*, 173:193–196, 1986.

[24] E. P. Shabalin. Electric Dipole Moment of Quark in a Gauge Theory with Left-Handed Currents. *Sov. J. Nucl. Phys.*, 28:75, 1978.

[25] Ishita Dutta Choudhury and Amitabha Lahiri. Anomalous chromomagnetic moment of quarks. *Mod. Phys. Lett. A*, 30(23):1550113, 2015.

[26] J.I. Aranda, D. Espinosa-Gómez, J. Montaño, B. Quezadas-Vivian, F. Ramírez-Zavaleta, and E.S. Tututi. Flavor violation in chromo- and electromagnetic dipole moments induced by Z' gauge bosons and a brief revisit of the Standard Model. *Phys. Rev. D*, 98(11):116003, 2018.

[27] Albert M Sirunyan et al. Search for new physics in top quark production in dilepton final states in proton-proton collisions at $\sqrt{s} = 13$ TeV. *Eur. Phys. J. C*, 79(11):886, 2019.

[28] Albert M Sirunyan et al. Measurement of the top quark polarization and $\mathrm{t\bar{t}}$ spin correlations using dilepton final states in proton-proton collisions at $\sqrt{s} = 13$ TeV. *Phys. Rev. D*, 100(7):072002, 2019.

[29] Andrei I. Davydychev, P. Osland, and L. Saks. Quark gluon vertex in arbitrary gauge and dimension. *Phys. Rev. D*, 63:014022, 2001.

[30] John M. Cornwall. Dynamical Mass Generation in Continuum QCD. *Phys. Rev. D*, 26:1453, 1982.

[31] John M. Cornwall and Joannis Papavassiliou. Gauge Invariant Three Gluon Vertex in QCD. *Phys. Rev. D*, 40:3474, 1989.

[32] Daniele Binosi and Joannis Papavassiliou. Pinch Technique: Theory and Applications. *Phys. Rept.*, 479:1–152, 2009.

[33] Ansgar Denner, Georg Weiglein, and Stefan Dittmaier. Application of the background field method to the electroweak standard model. *Nucl. Phys. B*, 440:95–128, 1995.

[34] Apostolos Pilaftsis. Generalized pinch technique and the background field method in general gauges. *Nucl. Phys. B*, 487:467–491, 1997.

[35] Vladyslav Shtabovenko, Rolf Mertig, and Frederik Orellana. New Developments in FeynCalc 9.0. *Comput. Phys. Commun.*, 207:432–444, 2016.

[36] Hiren H. Patel. Package-X: A Mathematica package for the analytic calculation of one-loop integrals. *Comput. Phys. Commun.*, 197:276–290, 2015.

[37] W. Hollik, Jose I. Illana, S. Rigolin, C. Schappacher, and D. Stockinger. Top dipole formfactors and loop induced CP violation in supersymmetry. *Nucl. Phys. B*, 551:3–40, 1999. [Erratum: Nucl.Phys.B 557, 407–409 (1999)].

[38] Zenro Hioki and Kazumasa Ohkuma. Search for anomalous top-gluon couplings at LHC revisited. *Eur. Phys. J. C*, 65:127–135, 2010.

[39] Jernej F. Kamenik, Michele Papucci, and Andreas Weiler. Constraining the dipole moments of the top quark. *Phys. Rev. D*, 85:071501, 2012. [Erratum: Phys.Rev.D 88, 039903 (2013)].

[40] Werner Bernreuther and Zong-Guo Si. Top quark spin correlations and polarization at the LHC: standard model predictions and effects of anomalous top chromo moments. *Phys. Lett. B*, 725:115–122, 2013. [Erratum: Phys.Lett.B 744, 413–413 (2015)].

[41] King-man Cheung. Probing the chromoelectric and chromomagnetic dipole moments of the top quark at hadronic colliders. *Phys. Rev. D*, 53:3604–3615, 1996.

[42] P. Haberl, O. Nachtmann, and A. Wilch. Top production in hadron hadron collisions and anomalous top - gluon couplings. *Phys. Rev. D*, 53:4875–4885, 1996.

[43] S.A. Larin and J.A.M. Vermaseren. The Three loop QCD Beta function and anomalous dimensions. *Phys. Lett. B*, 303:334–336, 1993.

[44] G.M. Prosperi, M. Raciti, and C. Simolo. On the running coupling constant in QCD. *Prog. Part. Nucl. Phys.*, 58:387–438, 2007.

[45] M. Tanabashi et al. Review of Particle Physics. *Phys. Rev.*, D98(3):030001, 2018.

[46] T. Hahn and M. Perez-Victoria. Automatized one loop calculations in four-dimensions and D-dimensions. *Comput. Phys. Commun.*, 118:153–165, 1999.

[47] Ansgar Denner, Stefan Dittmaier, and Lars Hofer. Collier: a fortran-based Complex One-Loop LIbrary in Extended Regularizations. *Comput. Phys. Commun.*, 212:220–238, 2017.

[48] A. I. Hernández-Juárez, A. Moyotl, and G. Tavares-Velasco. New estimate of the chromomagnetic dipole moment of quarks in the standard model. *Eur. Phys. J. Plus*, 136(2):262, 2021.

[49] A. I. Hernández-Juárez, A. Moyotl, and G. Tavares-Velasco. Chromomagnetic and chromoelectric dipole moments of quarks in the reduced 331 model. *Chinese Physics C*, 12 2021.

[50] D. Atwood, A. Kagan, and T.G. Rizzo. Constraining anomalous top quark couplings at the Tevatron. *Phys. Rev. D*, 52:6264–6270, 1995.

[51] Cen Zhang and Scott Willenbrock. Effective-Field-Theory Approach to Top-Quark Production and Decay. *Phys. Rev. D*, 83:034006, 2011.

[52] Celine Degrande, Jean-Marc Gerard, Christophe Grojean, Fabio Maltoni, and Geraldine Servant. Non-resonant New Physics in Top Pair Production at Hadron Colliders. *JHEP*, 03:125, 2011.

[53] Christoph Englert, Ayres Freitas, Michael Spira, and Peter M. Zerwas. Constraining the Intrinsic Structure of Top-Quarks. *Phys. Lett. B*, 721:261–268, 2013.

[54] Alper Hayreter and German Valencia. Constraints on anomalous color dipole operators from Higgs boson production at the LHC. *Phys. Rev. D*, 88:034033, 2013.

[55] Juan A. Aguilar-Saavedra, Benjamin Fuks, and Michelangelo L. Mangano. Pinning down top dipole moments with ultra-boosted tops. *Phys. Rev. D*, 91:094021, 2015.

[56] D. Barducci, M. Fabbrichesi, and A. Tonero. Constraints on top quark nonstandard interactions from Higgs and $t\bar{t}$ production cross sections. *Phys. Rev. D*, 96(7):075022, 2017.

[57] Malihe Malekhosseini, Mehrdad Ghominejad, Hamzeh Khanpour, and Mojtaba Mohammadi Najafabadi. Constraining top quark flavor violation and dipole moments through three and four-top quark productions at the LHC. *Phys. Rev. D*, 98(9):095001, 2018.

[58] Christoph Englert, Dorival Goncalves, and Michael Spannowsky. Nonstandard top substructure. *Phys. Rev. D*, 89(7):074038, 2014.

[59] Diogo Buarque Franzosi and Cen Zhang. Probing the top-quark chromomagnetic dipole moment at next-to-leading order in QCD. *Phys. Rev. D*, 91(11):114010, 2015.

[60] D. Barducci et al. Interpreting top-quark LHC measurements in the standard-model effective field theory. 2 2018.

[61] Albert M Sirunyan et al. Measurement of the top quark forward-backward production asymmetry and the anomalous chromoelectric and chromomagnetic moments in pp collisions at $\sqrt{s} = 13$ TeV. *JHEP*, 06:146, 2020.

[62] R. E. Cutkosky. Singularities and discontinuities of feynman amplitudes. *Journal of Mathematical Physics*, 1(5):429–433, sep 1960.

[63] Yong Zhou. Imaginary part of Feynman amplitude, cutting rules and optical theorem. 12 2004.

[64] M. Gluck, J. F. Owens, and E. Reya. Gluon Contribution to Hadronic J/psi Production. *Phys. Rev. D*, 17:2324, 1978.

[65] Georges Aad et al. Measurement of the $t\bar{t}$ production cross-section in the lepton+jets channel at $\sqrt{s} = 13$ TeV with the ATLAS experiment. *Phys. Lett. B*, 810:135797, 2020.

[66] J. Alwall, R. Frederix, S. Frixione, V. Hirschi, F. Maltoni, O. Mattelaer, H. S. Shao, T. Stelzer, P. Torrielli, and M. Zaro. The automated computation of tree-level and next-to-leading order differential cross sections, and their matching to parton shower simulations. *JHEP*, 07:079, 2014.

[67] Adam Alloul, Neil D. Christensen, Céline Degrande, Claude Duhr, and Benjamin Fuks. FeynRules 2.0 - A complete toolbox for tree-level phenomenology. *Comput. Phys. Commun.*, 185:2250–2300, 2014.

[68] P. A. Zyla et al. Review of Particle Physics. *PTEP*, 2020(8):083C01, 2020.

[69] Eric Conte, Benjamin Fuks, and Guillaume Serret. MadAnalysis 5, A User-Friendly Framework for Collider Phenomenology. *Comput. Phys. Commun.*, 184:222–256, 2013.

[70] Ilja Dorsner, Svjetlana Fajfer, Jernej F. Kamenik, and Nejc Kosnik. Light colored scalars from grand unification and the forward-backward asymmetry in t t-bar production. *Phys. Rev. D*, 81:055009, 2010.

[71] Paul H. Frampton, Jing Shu, and Kai Wang. Axigluon as Possible Explanation for p anti-p —> t anti-t Forward-Backward Asymmetry. *Phys. Lett. B*, 683:294–297, 2010.

[72] J. G. Ferreira, Jr, P. R. D. Pinheiro, C. A. de S. Pires, and P. S. Rodrigues da Silva. The Minimal 3-3-1 model with only two Higgs triplets. *Phys. Rev. D*, 84:095019, 2011.

[73] Benjamin W. Lee and Steven Weinberg. SU(3) x U(1) Gauge Theory of the Weak and Electromagnetic Interactions. *Phys. Rev. Lett.*, 38:1237, 1977.

[74] F. Pisano and V. Pleitez. An SU(3) x U(1) model for electroweak interactions. *Phys. Rev. D*, 46:410–417, 1992.

[75] P. H. Frampton. Chiral dilepton model and the flavor question. *Phys. Rev. Lett.*, 69:2889–2891, 1992.

[76] J. D. Ruiz-Alvarez, C. A. de S. Pires, Farinaldo S. Queiroz, D. Restrepo, and P. S. Rodrigues da Silva. On the Connection of Gamma-Rays, Dark Matter and Higgs Searches at LHC. *Phys. Rev. D*, 86:075011, 2012.

[77] Chris Kelso, C. A. de S. Pires, Stefano Profumo, Farinaldo S. Queiroz, and P. S. Rodrigues da Silva. A 331 WIMPy Dark Radiation Model. *Eur. Phys. J. C*, 74(3):2797, 2014.

[78] E. Ramirez Barreto, Y. A. Coutinho, and J. Sa Borges. Vector- and Scalar-Bilepton Pair Production in Hadron Colliders. *Phys. Rev. D*, 83:075001, 2011.

[79] E. Ramirez Barreto, Y. A. Coutinho, and J. Sa Borges. Searching for an Extra Neutral Gauge Boson from Muon Pair Production at LHC. *Phys. Lett. B*, 689:36–41, 2010.

[80] E. Ramirez Barreto, Y. A. Coutinho, and J. Sa Borges. Charged Bilepton Pair Production at LHC Including Exotic Quark Contribution. *Nucl. Phys. B*, 810:210–225, 2009.

[81] Vo Quoc Phong, Vo Thanh Van, and Hoang Ngoc Long. Electroweak phase transition in the reduced minimal 3-3-1 model. *Phys. Rev. D*, 88:096009, 2013.

[82] P. V. Dong, N. T. K. Ngan, and D. V. Soa. Simple 3-3-1 model and implication for dark matter. *Phys. Rev. D*, 90(7):075019, 2014.

[83] Arindam Das, Kazuki Enomoto, Shinya Kanemura, and Kei Yagyu. Radiative generation of neutrino masses in a 3-3-1 type model. *Phys. Rev. D*, 101(9):095007, 2020.

[84] D. Cogollo, H. Diniz, C. A. de S. Pires, and P. S. Rodrigues da Silva. The Seesaw mechanism at TeV scale in the 3-3-1 model with right-handed neutrinos. *Eur. Phys. J. C*, 58:455–461, 2008.

[85] F. Queiroz, C. A. de S. Pires, and P. S. Rodrigues da Silva. A minimal 3-3-1 model with naturally sub-eV neutrinos. *Phys. Rev. D*, 82:065018, 2010.

[86] W. Caetano, C. A. de S. Pires, P. S. Rodrigues da Silva, D. Cogollo, and Farinaldo S. Queiroz. Explaining ATLAS and CMS Results Within the Reduced Minimal 3-3-1 model. *Eur. Phys. J. C*, 73(10):2607, 2013.

[87] A. G. Dias, P. R. D. Pinheiro, C. A. de S. Pires, and P. S. Rodrigues da Silva. A compact 341 model at TeV scale. *Annals Phys.*, 349:232–252, 2014.

[88] J. G. Ferreira, C. A. de S. Pires, P. S. Rodrigues da Silva, and A. Sampieri. Higgs sector of the supersymmetric reduced 331 model. *Phys. Rev. D*, 88(10):105013, 2013.

[89] V. V. Vien and H. N. Long. The D_4 flavor symmery in 3-3-1 model with neutral leptons. *Int. J. Mod. Phys. A*, 28:1350159, 2013.

[90] Vu Thi Ngoc Huyen, Hoang Ngoc Long, Tran Thanh Lam, and Vo Quoc Phong. Neutral Current in Reduced Minimal 3-3-1 Model. *Commun. in Phys.*, 24(2):97, 2014.

[91] D. Cogollo, Farinaldo S. Queiroz, and P. Vasconcelos. Flavor Changing Neutral Current Processes in a Reduced Minimal Scalar Sector. *Mod. Phys. Lett. A*, 29(32):1450173, 2014.

[92] Chris Kelso, H. N. Long, R. Martinez, and Farinaldo S. Queiroz. Connection of $g-2_\mu$, electroweak, dark matter, and collider constraints on 331 models. *Phys. Rev. D*, 90(11):113011, 2014.

[93] G. De Conto and V. Pleitez. Electron and muon anomalous magnetic dipole moment in a 3–3–1 model. *JHEP*, 05:104, 2017.

[94] P. A. Zyla et al. Review of Particle Physics. *PTEP*, 2020(8):083C01, 2020.

[95] A. C. B. Machado, J. C. Montero, and V. Pleitez. Flavor-changing neutral currents in the minimal 3-3-1 model revisited. *Phys. Rev. D*, 88(11):113002, 2013.

[96] Stanislaw Tatur and Jan Bartelski. Mass matrices for quarks and leptons in triangular form. *Acta Phys. Polon. B*, 39:2903–2920, 2008.

[97] Georges Aad et al. Search for a heavy charged boson in events with a charged lepton and missing transverse momentum from pp collisions at $\sqrt{s} = 13$ TeV with the ATLAS detector. *Phys. Rev. D*, 100(5):052013, 2019.

[98] Albert M Sirunyan et al. Search for high-mass resonances in final states with a lepton and missing transverse momentum at $\sqrt{s} = 13$ TeV. *JHEP*, 06:128, 2018.

[99] Georges Aad et al. Search for new resonances in mass distributions of jet pairs using 139 fb^{-1} of pp collisions at $\sqrt{s} = 13$ TeV with the ATLAS detector. *JHEP*, 03:145, 2020.

[100] Albert M Sirunyan et al. Search for high mass dijet resonances with a new background prediction method in proton-proton collisions at $\sqrt{s} = 13$ TeV. *JHEP*, 05:033, 2020.

[101] Georges Aad et al. Search for high-mass dilepton resonances using 139 fb^{-1} of pp collision data collected at $\sqrt{s}$ =13 TeV with the ATLAS detector. *Phys. Lett. B*, 796:68–87, 2019.

[102] Albert M Sirunyan et al. Search for resonant and nonresonant new phenomena in high-mass dilepton final states at $\sqrt{s} = 13$ TeV. 3 2021.

[103] E. R. Barreto, A. G. Dias, J. Leite, C. C. Nishi, R. L. N. Oliveira, and W. C. Vieira. Hierarchical fermions and detectable Z' from effective two-Higgs-triplet 3-3-1 model. *Phys. Rev. D*, 97(5):055047, 2018.

[104] H. N. Long, N. V. Hop, L. T. Hue, and N. T. T. Van. Constraining heavy neutral gauge boson Z' in the 3 - 3 - 1 models by weak charge data of Cesium and proton. *Nucl. Phys. B*, 943:114629, 2019.

[105] H. N. Long, N. V. Hop, L. T. Hue, N. H. Thao, and A. E. Cárcamo Hernández. Some phenomenological aspects of the 3-3-1 model with the Cárcamo-Kovalenko-Schmidt mechanism. *Phys. Rev. D*, 100(1):015004, 2019.

[106] Albert M Sirunyan et al. Search for vector-like quarks in events with two oppositely charged leptons and jets in proton-proton collisions at $\sqrt{s} = 13$ TeV. *Eur. Phys. J. C*, 79(4):364, 2019.

[107] Albert M Sirunyan et al. Search for single production of vector-like quarks decaying to a top quark and a W boson in proton-proton collisions at $\sqrt{s} = 13$ TeV. *Eur. Phys. J. C*, 79:90, 2019.

[108] Morad Aaboud et al. Search for pair production of heavy vector-like quarks decaying into high-p_T W bosons and top quarks in the lepton-plus-jets final state in pp collisions at $\sqrt{s} = 13$ TeV with the ATLAS detector. *JHEP*, 08:048, 2018.

[109] Stanislaw Tatur and Jan Bartelski. Triangular mass matrices for quarks and leptons. *Phys. Rev. D*, 74:013007, 2006.

[110] E. O. Iltan. Top quark electric and chromo electric dipole moments in the general two Higgs doublet model. *Phys. Rev. D*, 65:073013, 2002.

[111] David Atwood, Shaouly Bar-Shalom, Gad Eilam, and Amarjit Soni. CP violation in top physics. *Phys. Rept.*, 347:1–222, 2001.

[112] M. Acciarri et al. Study of neutral current four fermion and Z Z production in e+ e- collisions at S**(1/2) = 183-GeV. *Phys. Lett.*, B450:281–293, 1999.

[113] G. Abbiendi et al. Search for trilinear neutral gauge boson couplings in Z^- gamma production at $S^{(1/2)}$ = 189-GeV at LEP. *Eur. Phys. J.*, C17:553–566, 2000.

[114] J. Abdallah et al. Study of triple-gauge-boson couplings ZZZ, ZZgamma and Zgamma gamma LEP. *Eur. Phys. J.*, C51:525–542, 2007.

[115] F. Abe et al. Measurement of $W - \gamma$ couplings with CDF in $p\bar{p}$ collisions at $\sqrt{s} = 1.8$ TeV. *Phys. Rev. Lett.*, 74:1936–1940, 1995.

[116] S. Abachi et al. Studies of gauge boson pair production and trilinear couplings. *Phys. Rev.*, D56:6742–6778, 1997.

[117] T. Aaltonen et al. Limits on Anomalous Trilinear Gauge Couplings in $Z\gamma$ Events from $p\bar{p}$ Collisions at $\sqrt{s} = 1.96$ TeV. *Phys. Rev. Lett.*, 107:051802, 2011.

[118] Vardan Khachatryan et al. Measurement of the $pp \to ZZ$ production cross section and constraints on anomalous triple gauge couplings in four-lepton final states at $\sqrt{s}$ =8 TeV. *Phys. Lett.*, B740:250–272, 2015. [erratum: Phys. Lett.B757,569(2016)].

[119] Vardan Khachatryan et al. Measurements of the Z Z production cross sections in the 2l2ν channel in proton–proton collisions at $\sqrt{s} = 7$ and 8 TeV and combined constraints on triple gauge couplings. *Eur. Phys. J.*, C75(10):511, 2015.

[120] Morad Aaboud et al. Measurement of the ZZ production cross section in proton-proton collisions at $\sqrt{s} = 8$ TeV using the $ZZ \to \ell^-\ell^+\ell'^-\ell'^+$ and $ZZ \to \ell^-\ell^+\nu\bar{\nu}$ channels with the ATLAS detector. *JHEP*, 01:099, 2017.

[121] Morad Aaboud et al. $ZZ \to \ell^+\ell^-\ell'^+\ell'^-$ cross-section measurements and search for anomalous triple gauge couplings in 13 TeV pp collisions with the ATLAS detector. *Phys. Rev.*, D97(3):032005, 2018.

[122] Albert M Sirunyan et al. Measurements of the pp $\rightarrow$ ZZ production cross section and the Z $\rightarrow 4\ell$ branching fraction, and constraints on anomalous triple gauge couplings at $\sqrt{s} = 13\,\text{TeV}$. *Eur. Phys. J.*, C78:165, 2018. [Erratum: Eur. Phys. J.C78,no.6,515(2018)].

[123] Albert M Sirunyan et al. Measurements of pp $\rightarrow$ ZZ production cross sections and constraints on anomalous triple gauge couplings at $\sqrt{s} = 13\,\text{TeV}$. *Eur. Phys. J. C*, 81(3):200, 2021.

[124] G.J. Gounaris, J. Layssac, and F.M. Renard. New and standard physics contributions to anomalous Z and gamma selfcouplings. *Phys. Rev. D*, 62:073013, 2000.

[125] Debajyoti Choudhury, Sukanta Dutta, Subhendu Rakshit, and Saurabh Rindani. Trilinear neutral gauge boson couplings. *Int. J. Mod. Phys.*, A16:4891–4910, 2001.

[126] G. J. Gounaris. Contrasting the anomalous and the SM-MSSM couplings at the colliders. *Acta Phys. Polon.*, B37:1111–1126, 2006.

[127] Tyler Corbett, Matthew J. Dolan, Christoph Englert, and Karl Nordström. Anomalous neutral gauge boson interactions and simplified models. *Phys. Rev.*, D97(11):115040, 2018.

[128] Hermès Bélusca-Maïto, Adam Falkowski, Duarte Fontes, Jorge. C. Romão, and João P. Silva. CP violation in 2HDM and EFT: the ZZZ vertex. *JHEP*, 04:002, 2018.

[129] B. Grzadkowski, O. M. Ogreid, and P. Osland. CP-Violation in the ZZZ and ZWW vertices at e^+e^- colliders in Two-Higgs-Doublet Models. *JHEP*, 05:025, 2016. [Erratum: JHEP11,002(2017)].

[130] A. Moyotl, J. J. Toscano, and G. Tavares-Velasco. CP-odd contributions to the $ZZ^*\gamma$, $ZZ\gamma^*$, and ZZZ^* vertices induced by nondiagonal charged scalar boson couplings. *Phys. Rev.*, D91:093005, 2015.

[131] F. Larios, M. A. Perez, G. Tavares-Velasco, and J. J. Toscano. Trilinear neutral gauge boson couplings in effective theories. *Phys. Rev.*, D63:113014, 2001.

[132] G. J. Gounaris, J. Layssac, and F. M. Renard. Signatures of the anomalous Z_γ and ZZ production at the lepton and hadron colliders. *Phys. Rev.*, D61:073013, 2000.

[133] U. Baur and Edmond L. Berger. Probing the weak boson sector in $Z\gamma$ production at hadron colliders. *Phys. Rev.*, D47:4889–4904, 1993.

[134] J. Alcaraz. On the experimental effects of the off-shell structure in anomalous neutral triple gauge vertices. *Phys. Rev.*, D65:075020, 2002.

[135] R. Walsh and A. J. Ramalho. Probing the anomalous z $\gamma\gamma$ and z γ z vertices in radiative moller scattering at next linear collider energies. *Phys. Rev.*, D65:055011, 2002.

[136] S. Atag and I. Sahin. ZZ gamma and Z gamma gamma couplings at linear e+ e- collider energies with the effects of Z polarization and initial state radiation. *Phys. Rev.*, D70:053014, 2004.

[137] G. Moortgat-Pick et al. The Role of polarized positrons and electrons in revealing fundamental interactions at the linear collider. *Phys. Rept.*, 460:131–243, 2008.

[138] A. Gutierrez-Rodriguez, M. A. Hernandez-Ruiz, and M. A. Perez. Probing the ZZgamma and Z gamma gamma Couplings Through the Process e+ e- -¿gt; nu anti-nu gamma. *Phys. Rev.*, D80:017301, 2009.

[139] B. Ananthanarayan, Sumit K. Garg, Monalisa Patra, and Saurabh D. Rindani. Isolating CP-violating γ ZZ coupling in $e^+e^- \to \gamma$ Z with transverse beam polarizations. *Phys. Rev.*, D85:034006, 2012.

[140] A. Senol. $ZZ\gamma$ and $Z\gamma\gamma$ anomalous couplings in γp collision at the LHC. *Phys. Rev.*, D87:073003, 2013.

[141] B. Ananthanarayan, Jayita Lahiri, Monalisa Patra, and Saurabh D. Rindani. New physics in $e^+e^- \to Z\gamma$ at the ILC with polarized beams: explorations beyond conventional anomalous triple gauge boson couplings. *JHEP*, 08:124, 2014.

[142] John Ellis, Shao-Feng Ge, Hong-Jian He, and Rui-Qing Xiao. Probing the scale of new physics in the $ZZ\gamma$ coupling at e^+e^- colliders. *Chin. Phys. C*, 44(6):063106, 2020.

[143] Rafiqul Rahaman and Ritesh K. Singh. On the choice of beam polarization in $e^+e^- \to ZZ/Z\gamma$ and anomalous triple gauge-boson couplings. *Eur. Phys. J.*, C77(8):521, 2017.

[144] Rafiqul Rahaman and Ritesh K. Singh. On polarization parameters of spin-1 particles and anomalous couplings in $e^+e^- \to ZZ/Z\gamma$. *Eur. Phys. J.*, C76(10):539, 2016.

[145] Subhasish Behera, Rashidul Islam, Mukesh Kumar, Poulose Poulose, and Rafiqul Rahaman. Fingerprinting the Top quark FCNC via anomalous Ztq couplings at the LHeC. *Phys. Rev.*, D100(1):015006, 2019.

[146] Rafiqul Rahaman and Ritesh K. Singh. Anomalous triple gauge boson couplings in ZZ production at the LHC and the role of Z boson polarizations. *Nucl. Phys. B*, 948:114754, 2019.

[147] Ali Yilmaz. Search for the limits on anomalous neutral triple gauge couplings via ZZ production in the $\ell\ell\nu\nu$ channel at FCC-hh. 2 2021.

[148] G. J. Gounaris, J. Layssac, and F. M. Renard. Off-shell structure of the anomalous Z and γ selfcouplings. *Phys. Rev.*, D65:017302, 2002. [Phys. Rev.D62,073012(2000)].

[149] Celine Degrande. A basis of dimension-eight operators for anomalous neutral triple gauge boson interactions. *JHEP*, 02:101, 2014.

[150] A. D. Sakharov. Violation of CP Invariance, C asymmetry, and baryon asymmetry of the universe. *Pisma Zh. Eksp. Teor. Fiz.*, 5:32–35, 1967. [Usp. Fiz. Nauk161,no.5,61(1991)].

[151] A. Moyotl. New sources of CP violation. *J. Phys. Conf. Ser.*, 912(1):012019, 2017.

[152] Gerhard Buchalla, Gudrun Hiller, and Gino Isidori. Phenomenology of nonstandard Z couplings in exclusive semileptonic $b \to s$ transitions. *Phys. Rev. D*, 63:014015, 2000.

[153] R. Mohanta. Implications of the non-universal Z boson in FCNC mediated rare decays. *Phys. Rev.*, D71:114013, 2005.

[154] Albert M Sirunyan et al. A multi-dimensional search for new heavy resonances decaying to boosted WW, WZ, or ZZ boson pairs in the dijet final state at 13 TeV. *Eur. Phys. J. C*, 80(3):237, 2020.

[155] Maxim Perelstein. Little Higgs models and their phenomenology. *Prog. Part. Nucl. Phys.*, 58:247–291, 2007.

[156] Francisco del Aguila, Jose I. Illana, and Mark D. Jenkins. Lepton flavor violation in the Simplest Little Higgs model. *JHEP*, 03:080, 2011.

[157] P. V. Dong, D. T. Huong, Farinaldo S. Queiroz, and N. T. Thuy. Phenomenology of the 3-3-1-1 model. *Phys. Rev.*, D90(7):075021, 2014.

[158] R. N. Mohapatra and Jogesh C. Pati. A Natural Left-Right Symmetry. *Phys. Rev.*, D11:2558, 1975.

[159] Abdesslam Arhrib, Kingman Cheung, Cheng-Wei Chiang, and Tzu-Chiang Yuan. Single top-quark production in flavor-changing Z' models. *Phys. Rev.*, D73:075015, 2006.

[160] I. Cortes Maldonado, A. Fernandez Tellez, and G. Tavares-Velasco. Radiative decays $Z_H \to V_i Z (V_i = \gamma, Z)$ in little Higgs models. *J. Phys.*, 39:015003, 2012.

[161] I. Cortes-Maldonado and G. Tavares-Velasco. Radiative Decay $Z_H - > gt; \gamma A_H$ in the Little Higgs Model with T-parity. *Int. J. Mod. Phys.*, A26:5349–5368, 2011.

[162] M. Clements, C. Footman, Andreas S. Kronfeld, S. Narasimhan, and D. Photiadis. Flavor Changing Decays of the Z0. *Phys. Rev.*, D27:570, 1983.

[163] Wei-Shu Hou, N. G. Deshpande, G. Eilam, and A. Soni. CP Nonconservation in Decays of W and Z Bosons. *Phys. Rev. Lett.*, 57:1406, 1986.

[164] J. Bernabeu, A. Pich, and A. Santamaria. Gamma (Z —¿ B anti-B): A Signature of Hard Mass Terms for a Heavy Top. *Phys. Lett.*, B200:569–574, 1988.

[165] J. A. Aguilar-Saavedra. Top flavor-changing neutral interactions: Theoretical expectations and experimental detection. *Acta Phys. Polon.*, B35:2695–2710, 2004.

[166] Dennis Silverman. Z mediated B - anti-B mixing and B meson CP violating asymmetries in the light of new FCNC bounds. *Phys. Rev.*, D45:1800–1803, 1992.

[167] Ashutosh Kumar Alok and Shireen Gangal. b -¿ s Decays in a model with Z-mediated flavor changing neutral current. *Phys. Rev.*, D86:114009, 2012.

[168] Rukmani Mohanta. Effect of FCNC mediated Z boson on lepton flavor violating decays. *Eur. Phys. J.*, C71:1625, 2011.

[169] J. Bernabeu, J. G. Korner, A. Pilaftsis, and K. Schilcher. Universality breaking effects in leptonic Z decays. *Phys. Rev. Lett.*, 71:2695–2698, 1993.

[170] Andrzej J. Buras and Luca Silvestrini. Upper bounds on K —¿ pi neutrino anti-neutrino and K(L) —¿ pi0 e+ e- from epsilon-prime / epsilon and K(L) —¿ mu+ mu-. *Nucl. Phys.*, B546:299–314, 1999.

[171] G. Colangelo and G. Isidori. Supersymmetric contributions to rare kaon decays: Beyond the single mass insertion approximation. *JHEP*, 09:009, 1998.

[172] Yosef Nir and Dennis J. Silverman. Z Mediated Flavor Changing Neutral Currents and Their Implications for CP Asymmetries in B^0 Decays. *Phys. Rev.*, D42:1477–1484, 1990.

[173] Anjan K. Giri and Rukmani Mohanta. New physics effects on the CP asymmetries in B —¿ phi K(S) and B —¿ eta-prime K(S) decays. *Phys. Rev.*, D68:014020, 2003.

[174] M. Aaboud et al. Search for flavour-changing neutral current top-quark decays $t \to qZ$ in proton-proton collisions at $\sqrt{s} = 13$ TeV with the ATLAS detector. *JHEP*, 07:176, 2018.

[175] Paul Langacker and Ming-xing Luo. Constraints on additional Z bosons. *Phys. Rev.*, D45:278–292, 1992.

[176] O. Cakir, I.T. Cakir, A. Senol, and A.T. Tasci. Search for Top Quark FCNC Couplings in Z' Models at the LHC and CLIC. *Eur. Phys. J. C*, 70:295–303, 2010.

[177] J. I. Aranda, F. Ramirez-Zavaleta, J. J. Toscano, and E. S. Tututi. Bounding the $Z'tc$ coupling from $D^0 - \overline{D^0}$ mixing and single top production at the ILC. *J. Phys.*, G38:045006, 2011.

[178] Sudhir Kumar Gupta and G. Valencia. Flavor changing Z' couplings at the LHC. *Phys. Rev.*, D82:035017, 2010.

[179] Xiao-Gang He and German Valencia. Ansatz for small FCNC with a non-universal Z-prime. *Phys. Lett.*, B680:72–75, 2009.

[180] Cheng-Wei Chiang, Takaaki Nomura, and Jusak Tandean. Effects of Family Nonuniversal Z' Boson on Leptonic Decays of Higgs and Weak Bosons. *Phys. Rev.*, D87:075020, 2013.

[181] Wei-Shu Hou, Masaya Kohda, and Tanmoy Modak. Search for tZ' associated production induced by tcZ' couplings at the LHC. *Phys. Rev.*, D96(1):015037, 2017.

[182] J. I. Aranda, J. Montano, F. Ramirez-Zavaleta, J. J. Toscano, and E. S. Tututi. Study of the lepton flavor-violating $Z' \to \tau\mu$ decay. *Phys. Rev.*, D86:035008, 2012.

[183] Ying Li, Wen-Long Wang, Dong-Shuo Du, Zuo-Hong Li, and Hong-Xia Xu. Impact of family-non-universal Z' boson on pure annihilation $B_s \to \pi^+\pi^-$ and $B_d \to K^+K^-$ decays. *Eur. Phys. J.*, C75(7):328, 2015.

[184] Georges Aad et al. A search for flavour changing neutral currents in top-quark decays in pp collision data collected with the ATLAS detector at $\sqrt{s} = 7$ TeV. *JHEP*, 09:139, 2012.

[185] Morad Aaboud et al. A search for lepton-flavor-violating decays of the Z boson into a τ-lepton and a light lepton with the ATLAS detector. *Phys. Rev.*, D98:092010, 2018.

[186] Alexander Nehrkorn. Search for Lepton Flavor Violation in Z and Higgs decays with the CMS Experiment. *Nucl. Part. Phys. Proc.*, 287-288:160–163, 2017.

[187] Georges Aad et al. Search for the lepton flavor violating decay Zâ†'eÎ¼ in pp collisions at $\sqrt{s}$ TeV with the ATLAS detector. *Phys. Rev.*, D90(7):072010, 2014.